Energy Storage as Enabling Technology for Smart Grid

(Article begins on next page)

04 August 2020

Energy Storage as Enabling Technology for Smart Grid:

Modeling, Simulation and Prototyping of a Modular Workbench

Candidate: Dario Gandini

Advisor: Marcello Chiaberge

Mechatronics PhD, XVIII cycle, Year 2016

Table of Contents

ii

Table of Figures

List of Tables

Abstract

Awareness about human impact on mighty climatic changes is radically changing our concept of energy. The thoughtless use of energy slowly leaves our habits and good use of energy is certain the way of a better future. CO_2 emission reduction and carbon fossil fuel limitation are the main targets of governmental actions: this is possible thanks to technology improvement as efficient generation from renewable sources and good management of the electricity network. In recent years distributed generation, also of small size, grew up causing new management problems, indeed production from renewable energy sources (RES) is intermittent and unprogrammable.

Energy storage systems can be a solution to these problems and pave the way to completely active users, grid parity and smart grid, moreover can be an useful tool to increase electricity access in rural areas. Research on energy storage is intrinsically a multidisciplinary field: storage types, power stages, technologies, topologies, weather, forecast, control algorithms, regulatory, safety and business cases to mention the most importants.

In the present work is described the whole design of an energy storage system. First chapters are dedicated to a description of energy storage context, chapters 1 and 2; indeed, it is a matter of fact that in the last years, energy storage became more and more interesting from explicit mention as a tool against climatic changes to first options on the market. The general approach was the realization of a modular energy storage system for residential application, hardware and software design steps are deeply described in chapters 3 and 4. Simulations and tests on the prototype are reported in chapter 5. Finally conclusion and future works are given. At the end of the document some appendices are included to cover specific aspects touched during the work thesis.

Chapter 1.   Introduction

In this chapter will be provided an overview on electricity from the born to its future. Historical electricity generation statics are presented in the first section. Different sources trends are shown to understand recent year evolution. Climate changes and pollution are an effective problem and renewable energies can be a resonable solution to limit them. Second section is dedicated to electricity evolution. Electricity generation and network are evolving very fast and the 'smart' era of electricity network is near, but there are necessary new equipment installed inside the network. Research on energy storage system and industrial product present on market are illustrated in the last section of the chapter.

Transmission lines

1.1 Electricity: production and consumption

Electricity is produced as a primary or secondary product in power plants. The total amount of electricity produced is referred to as gross electricity production. However, power plants consume some electricity for their own use (in plant auxiliaries and in other transformers) and net electricity production is obtained by deducting this amount from gross production. The net production is distributed

through national transmission and distribution grids to final consumers, transformed to heat in boilers or heat pumps, stored using pumped storage, or traded (exported or imported).

Final consumption of electricity covers the electricity delivered to the consumer's door (industry, transport, households and other sectors); it excludes deliveries for transformation and own use of energy producing activities, as well as network losses.

World electricity production is constantly increasing. Figure 1 shows world historical electricity generation statics from 2000 to 2014. In 2000, the total electricity generation was 14720 TWh and, in fourteen years, is more than double, reaching 22433 TWh in 2014. Today, the most important source is still coal, but also nuclear, gas and hydroelectric give a wide contribution to production. Even if renewable sources[1] are rapidly increasing all together are, without hydroelectric generation, only 7% of the total production in 2014.
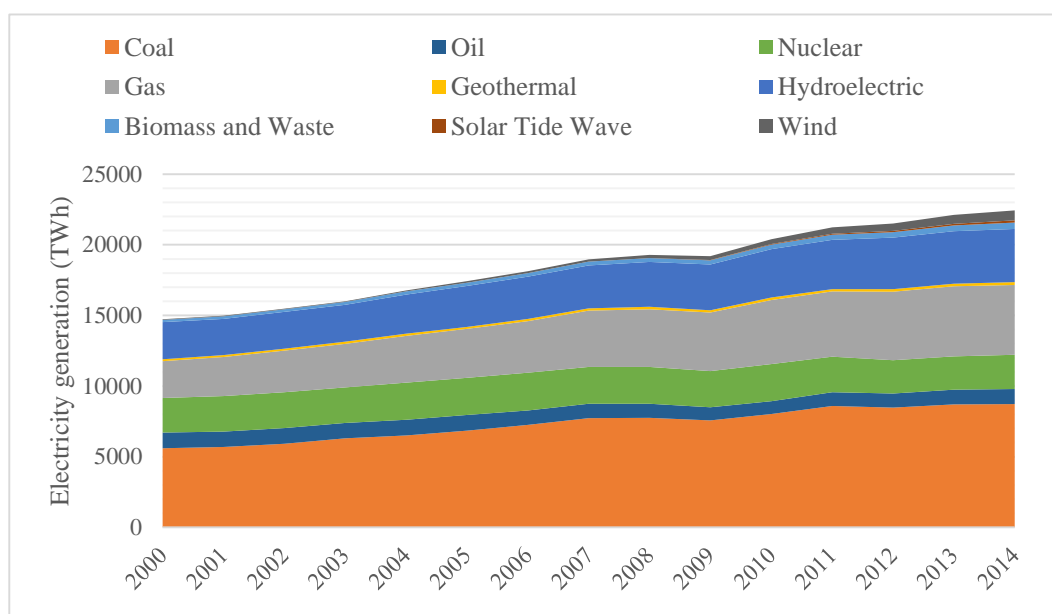
Figure 1 – World historical electricity generation statics by source, from 2000 to 2014 (source: The World Bank – World Development Indicators)

[1] Renewable energy represents the energy resources that are naturally replenishing but flow-limited. They are virtually inexhaustible in duration but limited in the amount of energy that is available per unit of time. Renewable energy resources include: hydro (conventional hydroelectric power), geothermal, solar, tidal action, ocean thermal, wave action, wind and biomass.

In Figure 2 and Figure 3 are shown growth rates, from 2000 to 2014, of all sources: growth is referred to 1999 value. Solar and wind growth are very different form the other, hence sources are graphically displayed separated in order to improve visualization. During this period nuclear production is stable with an increase of only 1%, while production from oil is decreased of 6.5%.
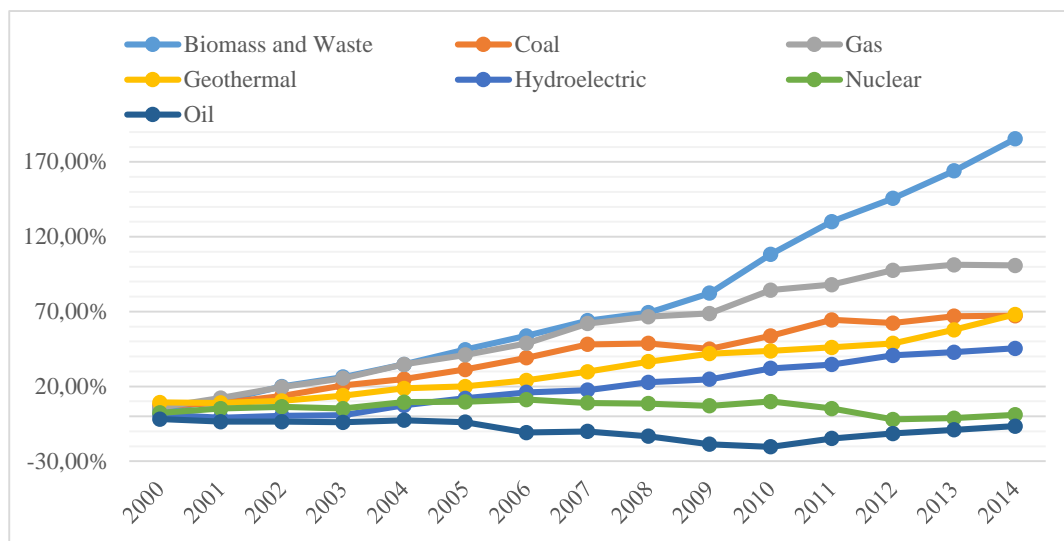
Figure 2 – Growth rate of electricity production by source (from 2000 to 2014) related to year 1999 (source: The World Bank – World Development Indicators)

Electricity generation from coal is increased of 67%, gas of 100%. Renewable sources had the biggest growths: production from hydroelectric increase of 45%, from geothermal increase of 68% and from biomass and waste growth rate is 185%. The highest growth rate are of wind, 3226%, and solar that is 11688%, Figure 3. These last trends are, surely, influeced by government founding, but also from climatic changes fear and cost reduction.

Growths of solar and wind electricity production are displayed, in Figure 4, related to the value of the year before; in 2000 electricity from wind production is among 50% higher than in 1999 and in 2001 is 22% higher than 2000.

Growth production from solar constantly increase from 2000 to 2011 where reach the peak of 93% increase. Then the growth decrease and in the last two years is stable at 32%. Production from wind constantly decrease over this period with little oscillations: starting from 48% in 2000, it is 10% in 2014. Again, these trends are influeced by different government founding.
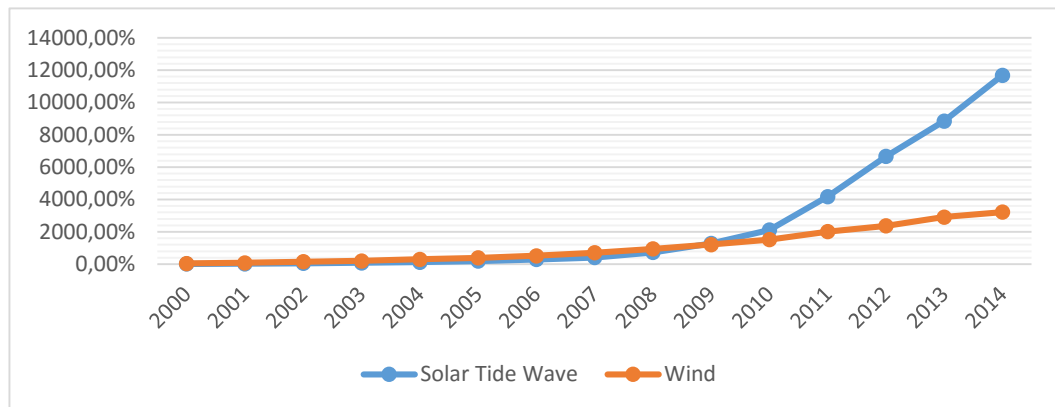
Figure 3– Growth rate of electricity production by source, solar and wind (from 2000 to 2014), related to year 1999 (source: The World Bank – World Development Indicators)

Trend of last years are caused by founding reduction but it also mark a saturation of the market. Unfortunately even if, production from renewable sources is increased, production from these sources is minority.
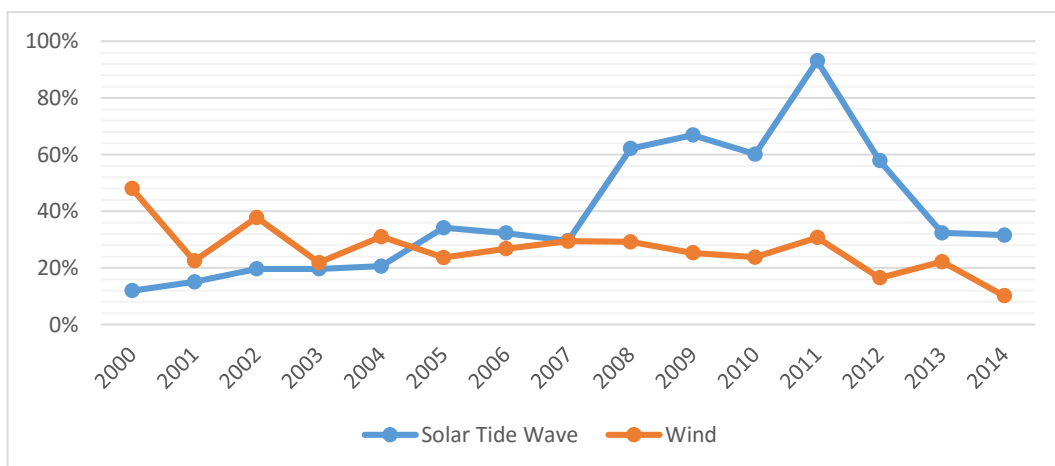
Figure 4 – Growth rate of electricity production by source, solar and wind (from 2000 to 2014), related to year before (source: The World Bank – World Development Indicators)

Figure 5 shows the world breakdown of electricity generation by source in 2014. Coal is the first source with 39% and second is gas, 22% of the total. Nuclear is 11% and all renewable sources are 24%. Hydroelectric is the most used renewable source and it is 71% of all renewables, followed by Wind, 13%, and Biomass and Waste at 8%. Solar is only 1% of total production. Observing statics of specific region the picture is different, in the next section will be shown statics about Europe.
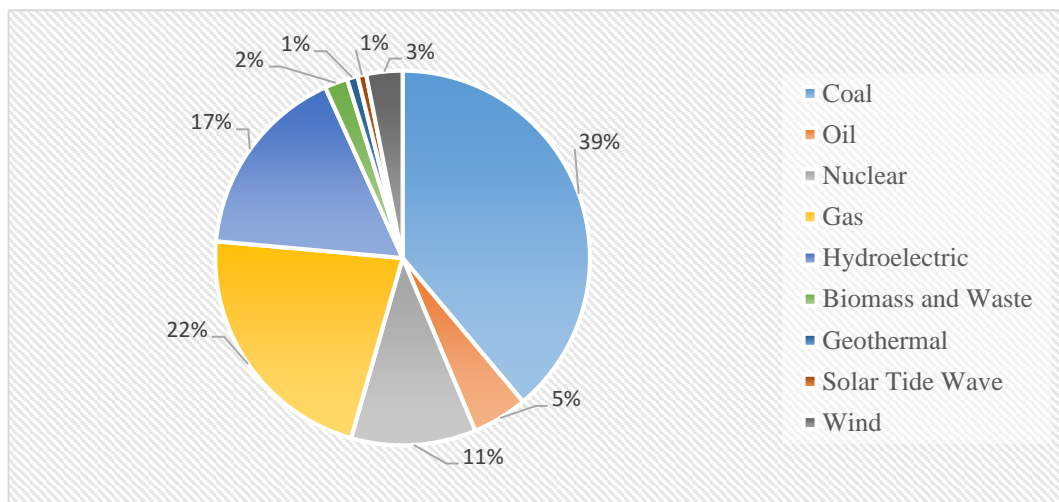
Figure 5 – World breakdown of electricity generation by energy source in 2014 (source: The World Bank – World Development Indicators)

Focus on Europe

European trend is different. Figure 6 shows the Europe electricity production evolution in the same period. In 2000 electricity production was 3220 TWh (among 22% of world production), while in 2014 is 3568 TWh (among 16% of world production), a growth of only 11%. European production slowly growth until 2008 then, in 2009, it fall down due to economic crisis, afterward it is stable.

Overall, there is a reduction of non-renewable sources utilization. Production from coal is reduced of 8% and from oil of 60%, at the same time, production from biomass and waste is increased of 256%, from wind of 1175% and from solar of

14816%. In 2014 the most significant sources are: coal (25%), nuclear (24%), gas (16%) and hydroelectric (17%). This statics are influenced by government policy that promote renewable growth and the European economic situation during this period, as a reduction of industry electricity require. An other important aspect is that European countries electricity networks (production, consumption and management) are strictly connected each other.To figure it out in Figure 7 are presented countries contribution to total European production, while Figure 9 shows European countries electricity consumption per capita.
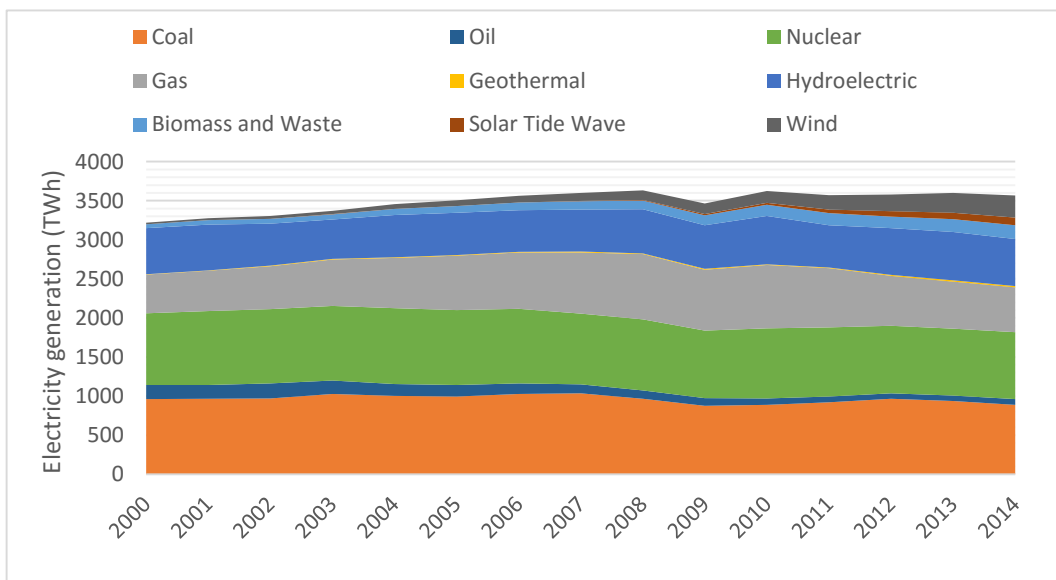
Figure 6 – Europe historical electricity generation statics by source, from 2000 to 2014 (source: The World Bank – World Development Indicators)

More than 65% of total European production is done by five countries: Germany, France, UK, Spain and Italy. In effect they are the European most populated countries, but the sum of countries population is considerably lower, among 40% of total Europe population. Figure 9 shows European countries electricity consumption per capita: from consumption point of view Finland has the highest yearly consumption pro capita, 15.7 MWh, Romania has the lowest with 2.6 MWh, while the European average is 6.5 MWh.
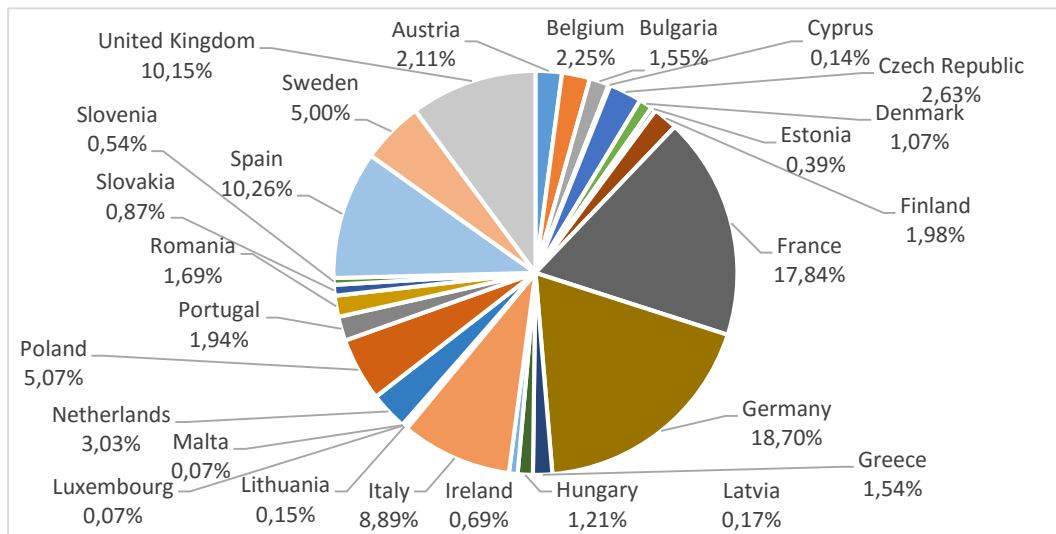
Figure 7– Europe electricity production, countries contribution, 2014
(source: US EIA The World Bank – World Development Indicators)

Countries with highest production have not always the highst consumption: electricity is imported and exported among countries, neighbor could use electricity production from other countries thanks to a complex and reliable transmission and distribution networks built during years.

An analysis of the final end use of energy in the EU-28 in 2013 shows three dominant categories: transport (31.6%), households(26.8%) and industry (25.1%). Improve consumption or management of one of these categories can give an important push to all grid improvement.
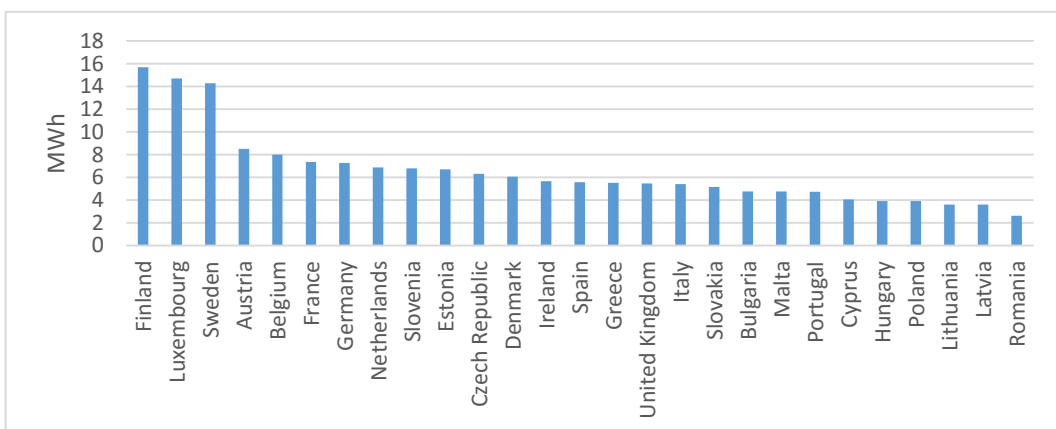
Figure 8 – Final energy consumption , EU-28, 2013 (%of total, based on tonnes of oil equivalent), source Eurostat.
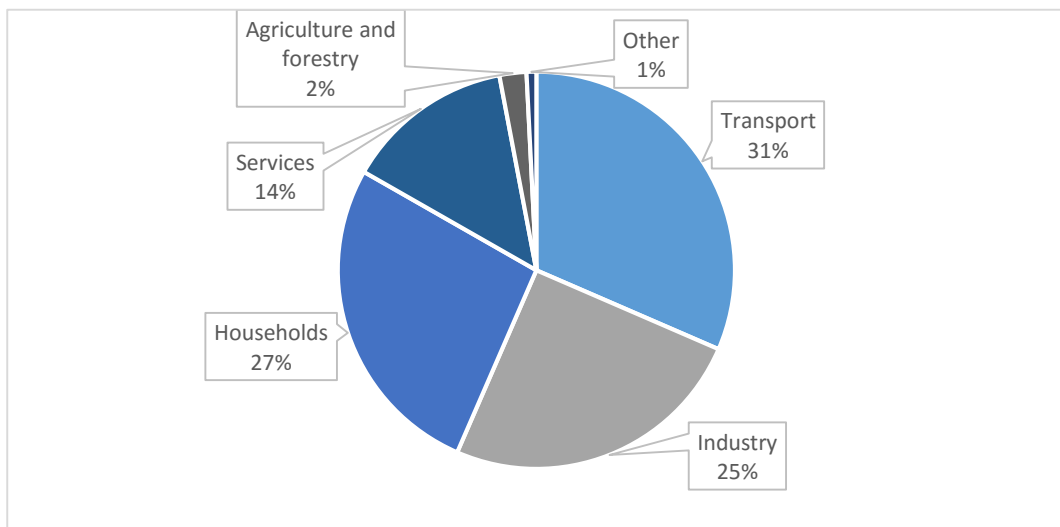
Figure 9 - European electricity consumption per capita, 2014
(source: US EIA The World Bank – World Development Indicators)

1.2 Road to Smart and Micro Grid

Electricity production has a relative young story. The world's first power station was designed and built by Lord Armstrong at Cragside, England in 1868. Water from one lake was used to power dynamos. The electricity supplied power to lights, heating, produced hot water, ran an elevator as well as labor-saving devices and farm buildings.

The first public power station was the *Edison Electric Light Station*, built in London at 57, Holborn Viaduct, which started operation in January 1882. The first continental Europe power plant was built in 1883 in Milan, near *Scala Theater*, to power the illumination of the building. Father of the plant was Giuseppe Colombo, engineer and professor of Milan Polytechnic, with the help of Giovanni Battista Pirelli.

Access to electricity change radically industrial world and people habits, today it is almost unimaginable to live without use of electricity. Traditionally big power plant generate electricity and trough transmission and distribution lines it comes to users. Energy flux is unidirectional from power plant to consumer that are

passive player. This structure is going to be outdated. In fact, the arrival of cheaper generators from renewable sources, even of small size, is changing users' behavior. Users are equipped with renewable generators and they are going to be active. This new player is called 'prosumer' from the fusion of words producer and consumer. This new character is changing electricity perception and, slowly, it is changing the electricity network. After the entrance of this new figure energy flux are bidirectional and network management is more complex.
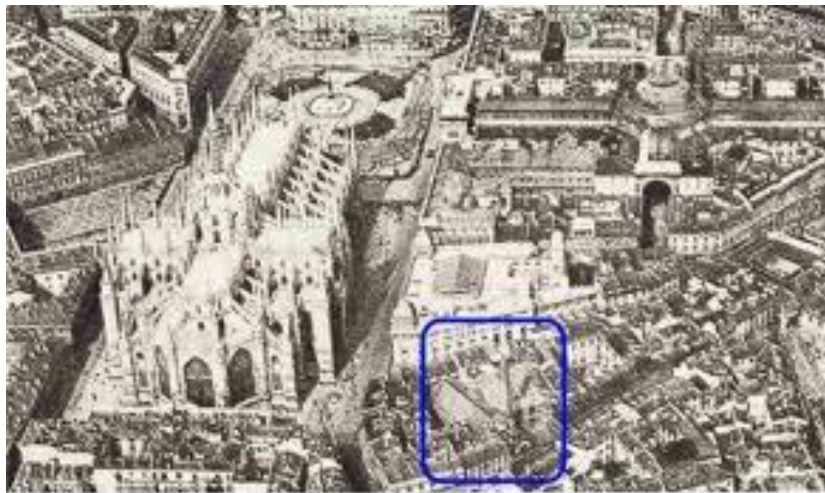
Figure 10 – Power plant of Santa Radegonda, Milan

The future of the electricity network is called 'Smart Grid', but smart grid is today used as a marketing term, rather than a technical definition. For this reason there is no well defined and commonly accepted scope of what 'smart' is and what it is not. The general understanding is that the smart grid is the concept of modernizing the electric grid.

A smart grid employs innovative products and services together with intelligent monitoring, control, communication, and self-healing technologies to:

- facilitate the connection and operation of generators of all sizes and technologies;
- allow consumers to play a part in optimizing the operation of the system;

- provide consumers with greater information and choice of supply;

- significantly reduce the environmental impact of the whole electricity supply system;

- deliver enhanced levels of reliability and security of supply.
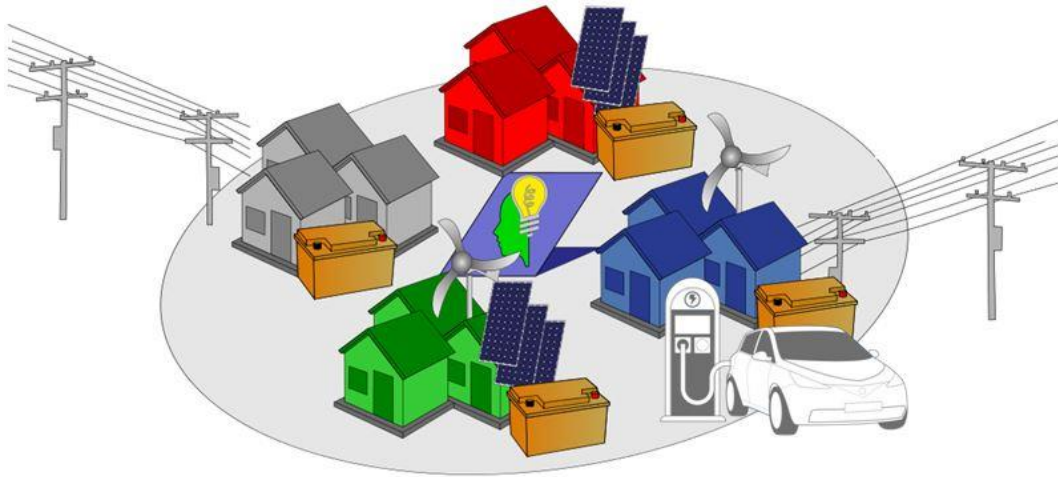
Figure 11 – Micro Grid example scheme

While Smart Grid risk to be a faciful concept without evident technical evolution there are other concepts to describe the new electricity network as 'Micro Grid'. One possible definition of micro grid is:

"A micro grid is an electrical system that includes multiple loads and distributed energy resources that can be operated in parallel with the broader utility grid or as an electrical island."

This definition is less vague and introduces one essential element of our electric future: distributed energy sources. Distributed generation concept is growth together with the growing use of renewable energy sources (RES). Renewable energy sources are the most important ally against climatic changes but they are characterized by non-deterministic and intermittent production profiles and the increased use of RES starts creating electric stability problems in the distribution network.

To realize an evolution of the electricity network need new equipments able to make generation from renewable energies more flexible. Moreover consumers must to be always more active.

Energy Storage System are a possible solution to reduce problems created by renewable energy sources and, at the same time, are an equipment useful to increase consumers capabilities. The follow section is dedicated to energy storage system description. Described research from academic and industrial products are the springboard this work.
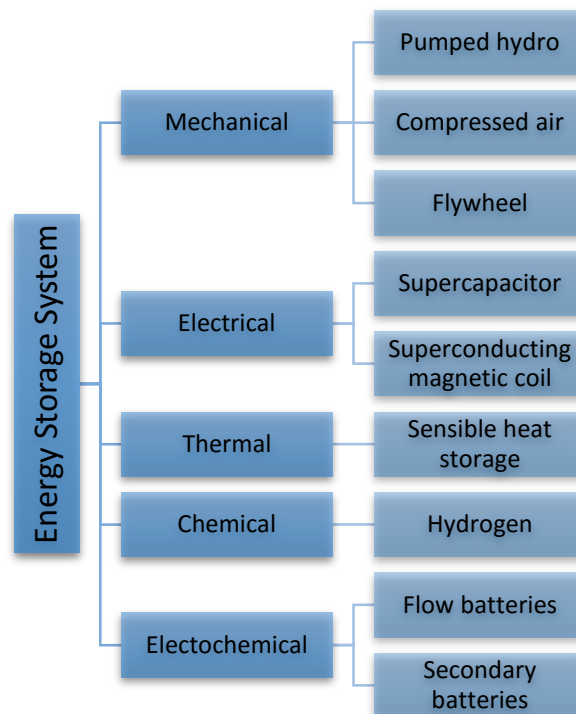
Figure 12 – Classification of energy storage system according to energy form

1.3 Energy Storage

Energy storage is the capture of energy produced at one time for use at a later time. This practice is ancient as first electricity generators. Indeed Lord Armstrong's use an hydroelectric generator: hydroelectric dam stores energy in a resevoir as gravitational potential energy. A widely-used approach for classifying

energy storage system is the determination according to the form of energy used. In Figure 12 energy storage system are classified into mechanical, electrochemical, chemical, electrical and thermal energy storage.

Worldwide, pumped-storage hydroelectricity (PSH) is the largest-capacity form of active grid energy storage available. At times of low electrical demand, excess generation capacity is used to pump water from a lower source into a higher reservoir. When demand grows, water is released back into a lower reservoir (or waterway or body of water) through a turbine, generating electricity. Reversible turbine-generator assemblies act as both pump and turbine. Nearly all facilities use the height difference between two water bodies. Pure pumped-storage plants shift the water between reservoirs, while the "pump-back" approach is a combination of pumped storage and conventional hydroelectric plants that use natural stream-flow.

Compressed air energy storage (CAES) uses surplus energy to compress air for subsequent electricity generation. Small scale systems have long been used in such applications as propulsion of mine locomotives. The compressed air is stored in an underground reservoir. Compression of air creates heat; the air is warmer after compression. Expansion requires heat. If no extra heat is added, the air will be much colder after expansion. If the heat generated during compression can be stored and used during expansion, efficiency improves considerably. A CAES system can deal with the heat in three ways. Air storage can be adiabatic, diabatic, or isothermal.

Flywheel energy storage (FES) works by accelerating a rotor (flywheel) to a very high speed, holding energy as rotational energy. When energy is extracted, the flywheel's rotational speed declines as a consequence of conservation of energy; adding energy correspondingly results in an increase of the flywheel speed. Supercapacitors store the most energy per unit volume or mass among capacitors. They support volts up to 10,000 times that of electrolytic capacitors, but accept less than half as much power per unit time.

Superconducting Magnetic Energy Storage (SMES) systems store energy in a magnetic field. Due to the energy requirements of refrigeration and the high cost of superconducting wire, SMES is currently used for short duration energy storage.

Thermal storage is the temporary storage of heat for later use. An example is the storage of solar heat energy during the day to be used for heating at night. It is also used for cooling through ice made during the cooler night time hours. This ice storage is produced when a standard chiller runs at night to produce an ice pile. Water then circulates through the pile during the day to produce chilled water that would normally be the chiller's daytime output.

Hydrogen is not a primary energy source, but a portable energy storage method, because it first must be manufactured by other energy sources in order to be used.
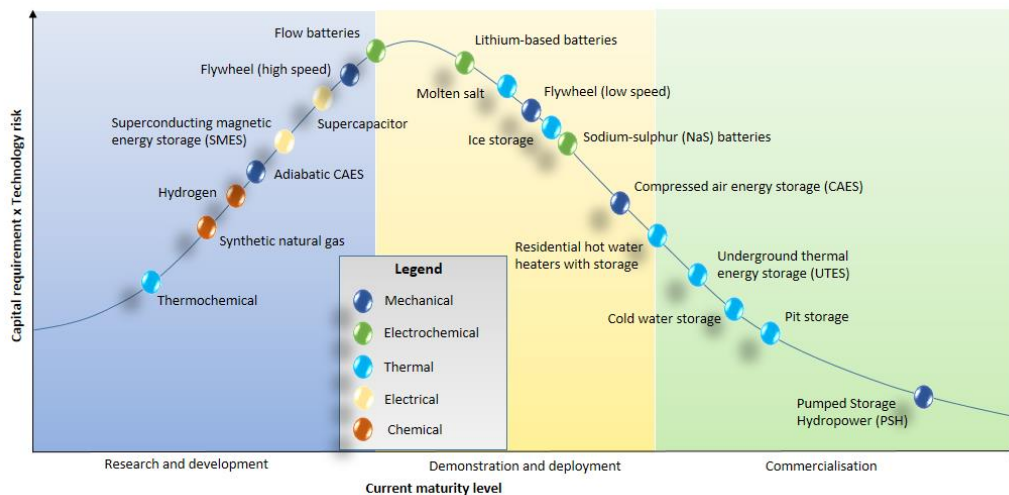
Figure 13 – Energy storage technologies across different stages of their development [49] [50]

A flow battery is a type of rechargeable battery where recharge ability is provided by two chemical components USA), Li-ion (AES Laurel Mountain, USA and Canada) dissolved in liquids contained within the system and separated by a membrane. Ion exchange occurs through the membrane while both liquids circulate in their own respective space.

A rechargeable battery, also called a storage battery or accumulator, comprises one or more electrochemical cells, and is a type of energy accumulator. Accumulators are widely used in comsumer electronics, telecommunications, cars, and, in recent years, also in combination with renewable sources. The foundamental element of an accumulator is called cell. Putting in parallel and/or series more cells it is possible to obtain the desired accumulator electric characteristic. It is possible to realize accumulator with different technologies and it is important to define parameters of classification. Main parameters of accumulators are cell voltage and capacity, but there are many other. [1] [2]

- Cell voltage: expressed in volt (V), it is the nominal voltage of the cell. Cell voltage reaches its maximum at full charge and the minimum at complete discarge.

- Specific energy: usually expressed in watthour per kilogram (Wh/kg), in spite of international system unit for energy is joule (J), express the energy per weight unit

- Energy density: similar to specific energy, it is the energy per volume unit. It is expressed in watthour per cubic meter (Wh/m^3)

- Specific power: expressed in watt per kilogram is the maximum istantaneous discharging power

- Charge/discharge efficiency: ratio between input and output energy, it describes losses from chemical reactions.

- Memory effect (lazy battery): capacity decrease with the increase of charge/discharge cycles. The effect is due to increased size of crystals inside the cell and so a reduction of the surface exposed to the electrolyte.

- Maximum discharge current

- Self – discharge: percentage of montly discarge without utilization.

- Charge time: time to reach the maximum capacity.

- Cycle life: it is the average number of charge/discharge cycles without an efficiency reduction.

- Temperature dependecy: cell chemical reaction velocity and internal resistance are temperature dependent. High temperature cause a degeneration of material inside cell without the possibility to recover.

- Energy/cost ratio: it is the most important parameter to define feasibility of use particular technology for market products.

Nowadays lithium – based batteries are, without a doubt, the most interesting technology even for stationary applications. Due to lightness characteristic lithium-based batteries are used in portable applications and they are always more used in electric vehicle (EV) application, where weight is a key parameter.
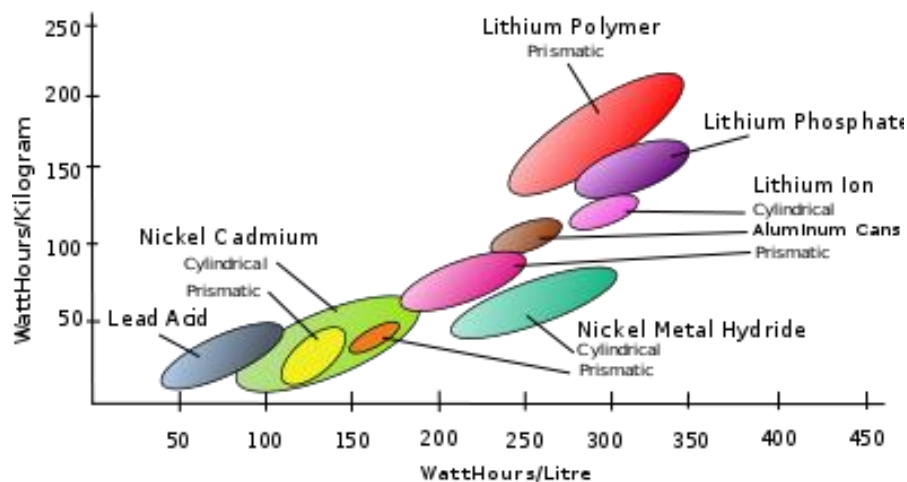
Figure 14 – Graph of mass and volume energy densities of several secondary cells (by direction: down = heavier, up = lighter, right = powerful, left = weaker)

These batteries have an extremely high energy density, needless batteries for the same capacity, and indeed the increasing diffusion of EV could be a catalyzer for their use in stationary application. Lithium batteries cost per kilowatt hours is falling down. This trend is caused by massive production for automotive market,Figure 15. Cell produced can be directly used for stationary application or degradeted batteries used in EV can be reutilized in stationary application.

Lot of studies are evaluating the so called 'second life' of batteries. [3] [4] [5] Batteries used in EV have to supply impulsive power profiles, degraded batteries

cannot supply these pulses but keep a good capacity and can be used in stationary applications.
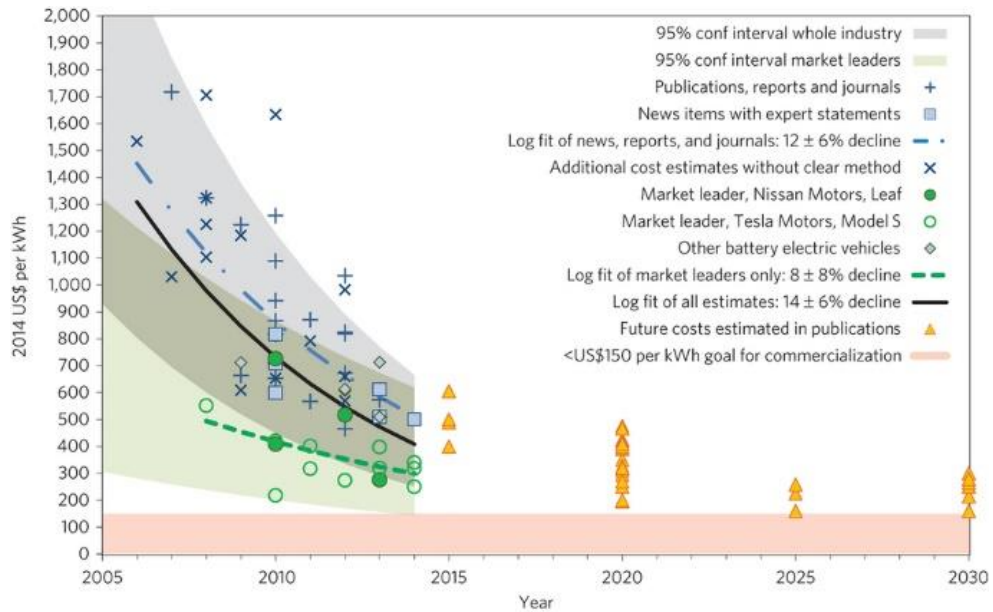
Figure 15 – Lithium-based batteries cost trend

Energy storage systems (ESS) have become increasingly important thanks to renewable energy sources (RES) growth. Renewable energy sources (RES) are characterized by non-deterministic and intermittent production profiles; the presence of self-generation in the residential sector is growing and will certainly become an issue in terms of grid management and reliability. Additionally, the increasing amount of large scale generation from intermittent sources available on the grid is already posing difficulties for the grid management The importance and the opportunities for storage in the electrical system is addressed in several publication. [6] [7] [8] [9] [10] [11] [12]

Figure 16 shows typical photovoltaic (PV) generation and residential consumption profiles. During the day and over the year, there is a large mismatch between the PV generation and the residential consumption profiles. Therefore, a solution is needed to compensate this mismatch in order to reduce additional power flows with the grid, which occur when surplus PV generation is exported to the grid and imported again later to supply the residential consumption.

This aspect could be a source of inefficiency and create difficulties on the electrical grid management. Energy storage is considered as the ultimate solution to solve this issue [13]. Thus, adding local energy storage may become a better option than the PV alone.
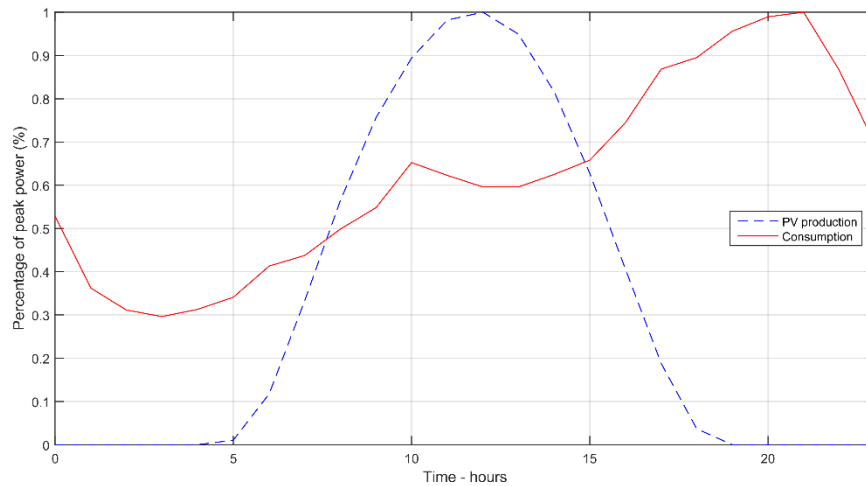
Figure 16 – PV generation and residential consumption profiles. Profiles are average of real behavior and they are expressed in percentage of maximum powers.

Several commercial options are already available for this purpose (Kyocera, Panasonic, SMA, Tesla, Enetelus, Storelio), but these solutions limit the storage purpose to incrementing the self-consumption rates; moreover, these solutions are based on grid connected inverter topologies with added converters with minor changes on the internal control system. It is important to explore different options for the residential energy storage management, both grid interaction and internal power flows, and to perform the evaluation of the impact of distributed energy storage at the residential level on the electricity grid.

Use of energy storage in residential buildings has been addressed in several previous publications. Some publications address the economic benefits from residential storage [14] [15] [16], other works are focused on the distribution grid impact [17]. A comprehensive review of the work done in the topic of PV self-consumption using demand side management (DSM) or energy storage is performed in [18]. The work presented in [19] compares different management

strategies for residential storage. The report [20] gives a perspective on the risks for the grid of drastically reducing of demand from residential customers if an adequate strategy for integrating residential customers with PV is not adopted.

Other works are focused on switchmode converters for storage application. In [21] is presented a trasformerless bidirectional AC/DC converter for storage system; [22] presents a multi-input multi-output DC-DC able to combine supplies with different voltage-current characteristics. In [23] is presented a low power prototype of a grid connected PV system with energy management system, while [24] describe possible circuit configurations and describe best matching power semiconductor devices.Use of wide band gap devices in PV system and energy storage is investigated in many pubblications [25] [26] [27] [28]

Chapter 2.   Analysis

In this chapter is achieved an analysis of different aspects regarding energy storage systems. In the first section are analyzed government action with particular enphasis to Europe action and how energy storage are subsidized in Horizon 2020 calls. Second section is dedicated to world electricity lack. Innovation in storage systems field can be the added value able to bring out from poverty million of people. Finally third section presents different applications of residential energy storage system; using as renewable energy source solar photovotaic panel there are two main classifications stand alone and grid connected, including storage there is a new one: hybrid connection.
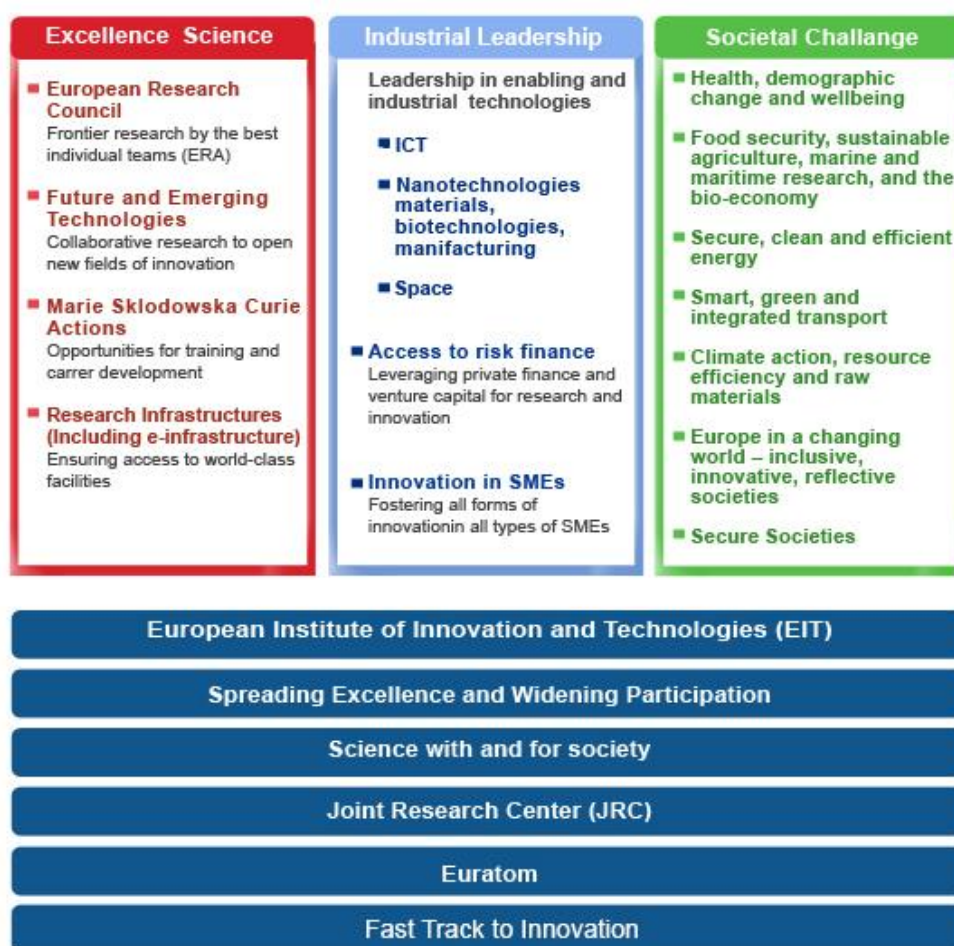
Figure 17 – Horizon 2020 structure: three pillars and five horizontal programmes

2.1 Government actions

Recently energy storage has been getting more attention. Energy storage was specifically cited at the 21st Conference of Parties (COP21), also know as the 2015 Paris Climate Conference[2], as key for global decarbonisation and keep global warning below 2°C. Furthermore there are specific call for energy storage system in Horizon 2020.

Horizon 2020 structure is based on three main pillars and five horizontal programs. Pillar 'Societal Challenge' reflects the policy priorities of the Europe 2020 strategy and addresses major concerns shared by citizens in Europe and elsewhere.

A challenge-based approach will bring together resources and knowledge across different fields, technologies and disciplines, including social sciences and the humanities. This will cover activities from research to market with a new focus on innovation-related activities, such as piloting, demonstration, test-beds, and support for public procurement and market uptake.

The target of the societal challenge 'Secure, clean and efficient energy supports the transition to a reliable, sustainable and competitive energy system. The Energy Challenge is structured around seven specific objectives and research areas:

- Reducing energy consumption and carbon footprint
- Low-cost, low-carbon electricity supply
- Alternative fuels and mobile energy sources
- A single, smart European electricity grid
- New knowledge and technologies
- Robust decision making and public engagement
- Market uptake of energy and ICT innovation.

[2] The first COP took place in Berlin in 1995 and significant meetings since then have included COP3 where the Kyoto Protocol was adopted, COP11 where the Montreal Action Plan was produced, COP15 in Copenhagen where an agreement to success Kyoto Protocol was unfortunately not realised and COP17 in Durban where the Green Climate Fund was created.

A budget of €5 931 million has been allocated to non-nuclear energy research for the period 2014-2020. Out of this figure, more than €200 million is earmarked to support European Institute of Innovation and Technology activities, subject to a mid-term review.

In work programme 2016-2017 is clearly expressed the attention on active consumer and the centrality of storage:

"The work programme 2014-2015 was calling for actions to modernize the electricity grid and to provide the energy system with flexibility through enhanced *storage technologies*. During the SET-Plan conference in December 2014, the stakeholders broadly endorsed a revised structure, not only looking at technologies but at the energy system in its ensemble. In this new approach, the *active consumer* is put at the center of the energy system. […] Unlike the previous call where smart grid and *storage* were separated topics, the new integrated approach of the Set-Plan is reflected through topics which integrate demand response, smart grid, *storage* and links with other networks."

If on the one hand storage is encouraged, on the other hand storage is hindered by existing regulations. In [29] are point out three bottleneck for further development of storage:

- The Renewables Energy Directive (2009/28/EC) defines guarante or priority access for electricity from renewable sources. This implies that large-scale renewables generators (solar fields, wind parks) do not need to take any responsibility to contribute to a more balanced supply of electricity to the grid.
- Incentives for renewable energy production differ widely across Europe. Many of these schemes are variations on feed-in tariffs or net metering. In general, these schemes do not stimulate storage and place all responsibility for net stability on other parties than the operators of the renewable energy sources.

- In many countries, households and small businesses pay (or receive) a flat fee for electricity or use is made of other simple fee structures that don't take actual load profiles into account. This disregards the differences in the value of electricity over time and the value that storage has in bridging the differences in electricity value over time is lost.

First obstacle is a regulatory problem that can be overtaken updating European directive. The second bottleneck highlight a cohesion problem among Eueropean members, a common action of countries is the only way to an Europe develompent. Finally third point

2.2 Electricity access lack

Worldwide 1.3 billion people, equivalent to 17% of the global population, live without access to electricity. [30] Sub-Saharan Africa has more people living without access to electricity than any other world region, more than 620 million people, and nearly half of the global total. It is also the only region in the world where the number of people living without electricity is increasing. Since 2000, the number of people without electricity rose by around 100 million. Nearly 80 % of those lacking access to electricity are in rural. [31]
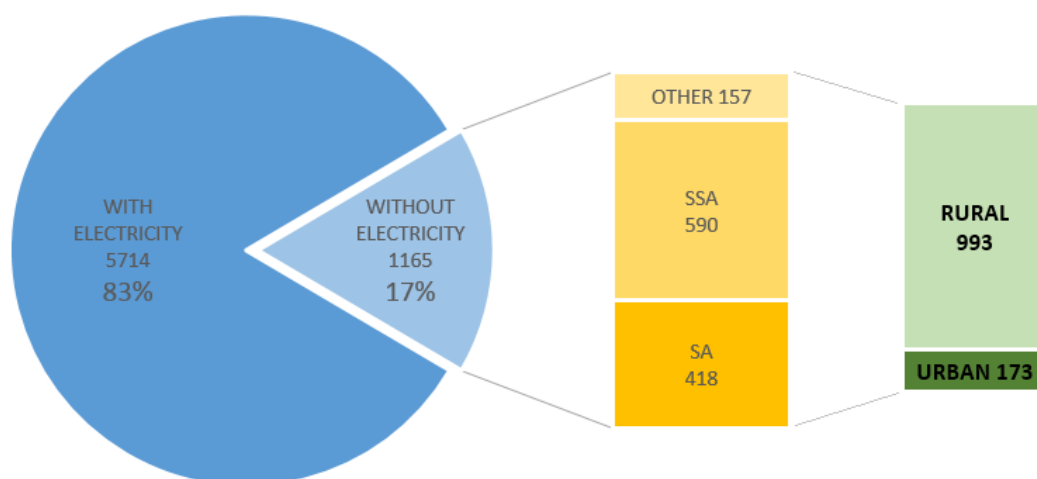
Figure 18 – World electricity access statics. Value in billions of people. SSA: Sub-Sahara Africa. SA: South Asia. Source Sustainable Energy For All, Global Tracking Framework, Vol.3

A lack of access to such services often results in relying on expensive, inefficient and hazardous alternatives. For example, households can typically spend 20-25% of their income on kerosene even though the cost of useful lighting. Each year 4.3 million premature deaths, of which nearly 600 thousands are in Africa, can be attributed to household air pollution resulting from the traditional use of solid fuels, such as fuel wood and charcoal. [32]

Often, the traditional approach to serve these communities is to extend the central grid. This approach is technically and financially inefficient due to a combination of capital scarcity, reduced grid reliability, extended building times and construction challenges to connect remote areas. In principle, adequately financed and operated microgrids based on renewable can overcome many of the challenges faced by traditional electrification strategies. [33]
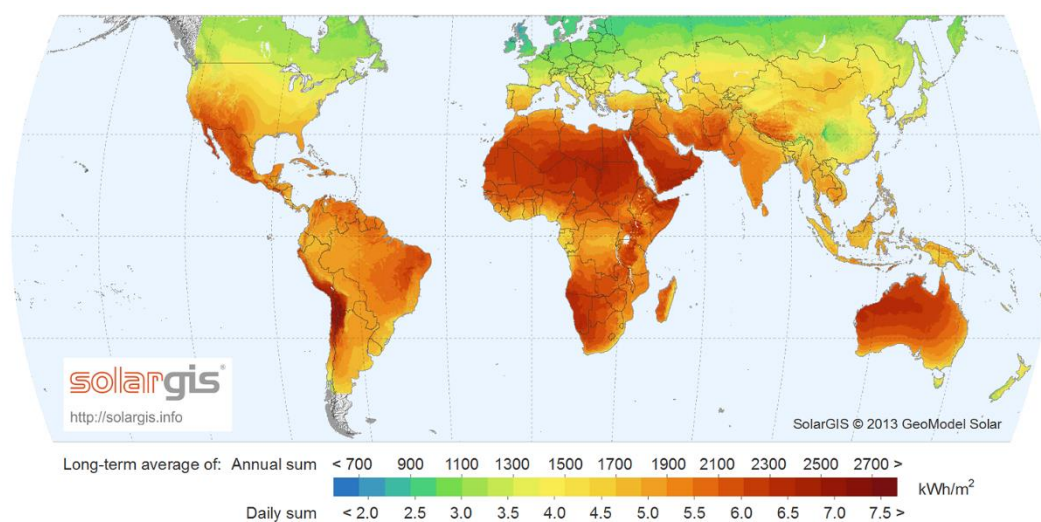
Figure 19 – World irradiance map.

The International Energy Agency (IEA) estimates that more than 50% of those without electricity access could be served by off-grid alternatives. New decentralized models based on renewable generation and innovative payment schemes are gaining ground as a viable alternative. These initiatives are frequently rely on government and donor funds for start-up, scale-up activities, research or development. Some examples of entrepreneurs that are operating in the African

market with these new business models are Azuri technologies, SunnyMoney, SteamaCo and Village Infrastructure, but there are many other.

Sun is most interesting renewable source for this area, because is characterized by high irradiance. Research on energy efficiency, innovative ways for electrification could not forget this part of world population. Electrification is a challenge that it is possible to win. Storage systems are an effective solution and an effort on this research field could change this situation. In Appendix D is given an idea of design for a solar home system for rural application. The design is based on the use of efficient appliances that are a cost effective solution also for rural application and poor areas.

Figure 20 – Rural African villagers holding portable solar charger

2.3 Stand Alone, Grid Connected and Hybrid

Starting from here to the end, as simplified approach, only solar generation are contempleted as renewable energy sources. PV system are widely diffused in residential generation, are modular and simple to integrate in established constructions; anyway all considerations are valid for any generators. There are

two main chategories of PV systems: stand alone and grid connected. It is talking about stand alone PV system in case of absense of electricity network, usually in rural areas. In this case a storage element is necessary to supply loads during the night. In this application a battery charger is conneted to PV panels and an inverter connect the system to loads. When a PV system is connected to an electricity network it is classified as grid connected. In this case all generated power is sent to the grid and storage element is not mandatory.

Figure 21 – An isolated mountain hut with stand-alone PV system

When a storage system is installed in grid connected system it is possible to manage power flows in a smart ways. If storage size is big as household energy consumptions, the household can be indipendent from the electricity network. This situation is called Zero Energy House because there are not power flows between the house and the electricity network. Hence it is possible to disconnect the household from the grid and previous definition is not completely true. A PV system with the storage added value it can be considered an hybrid connection between grid-connected and stand-alone.

From design point of view there are different constrains in case of stand-alone or grid connected applications. Generally grid connected application have more

restrictive regulatory due to safety and reliability problems of the grid. As examples generators must to be stopped if there is a fault on the network, voltage and current harmonic content must to be less than specific values. Considering storage size design in case of grid connected application it could be smaller than total energy consumption according to different power flows management, on the other hand in stand alone application storage size must to be equal or bigger than expected consumptions.

Considering an hybrid application, between stand alone and grid connected, all constrains must to be analyzed. Moreover it is possible to think about the evolution of an household. A storage system born for stand alone application and only recently is insert in grid connected, in the same way a stand alone system could be the settler of new grids if adequately designed.

The approach of this work is based on the idea that an energy storage system can be the base element of new smart micro grid. Equipped in preexisting network can improve energy management while in rural application can be the settler of new smart electricity network without the require of big infrastracture and investment.

Chapter 3.   Design

This chapter is dedicated to power stage design. In the first section are presented costrains, then possible architectures are shown. Defined the choosen hardaware architecture, the second section is adressed to design steps of each module. In the last section main sources of losses are analyzed to estimate total system losses and power stage efficiency.

3.1 Constrains and Structure Definition

Figure 22 shows workbench general block diagram. Renewable source and storage are connected to grid and users through workbench. Control system communicates with each system player and power stage is controlled to reach several targets:

- maximize energy production from renewable source
- maximize energy auto-consumption
- minimization of power grid fluctuation
- minimization of payback time
- Avoid black out events
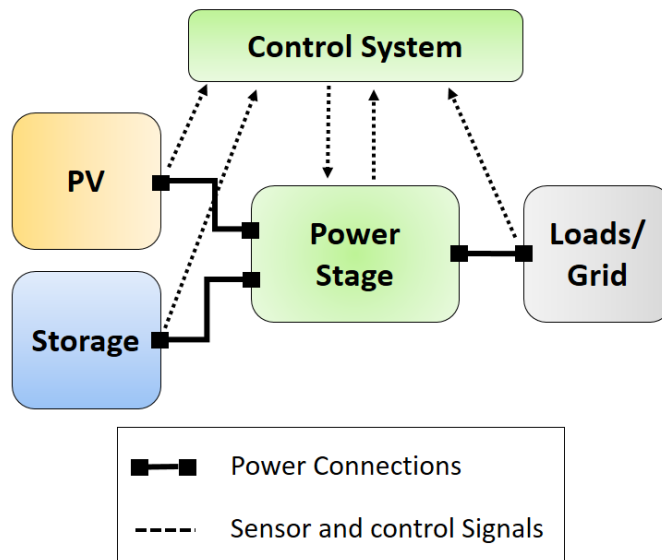
Figure 22 – General workbench block diagram. Control system communicates with each player, while power stage is connected with power connections.

Connection with user and grid are considered together and power stage could be design with only three ports: one in AC and two in DC. Connection with renewable source is only an input, while the other two could be input or output. Below a list of constrains to be comply with electric networks and appliances standards, some others will be shown after the list of possible system structures.

- $V_{grid,rms} = 230\,V \pm 10\%$
- $f_{grid} = 50\,Hz \pm 1\,Hz$

In Figure 23 are reported possible system structures with necessary sub-modules. In (a) is shown the typical connection of a grid connected photovoltaic module. After panels there is a DC-DC power converter that accomplish the maximum power point tracking and stabilize the inverter input voltage, last conversion stage is an inverter. Adding a storage element different configurations are possible: in (b),(c), (d) are shown different topologies with different point of connection of the storage element.
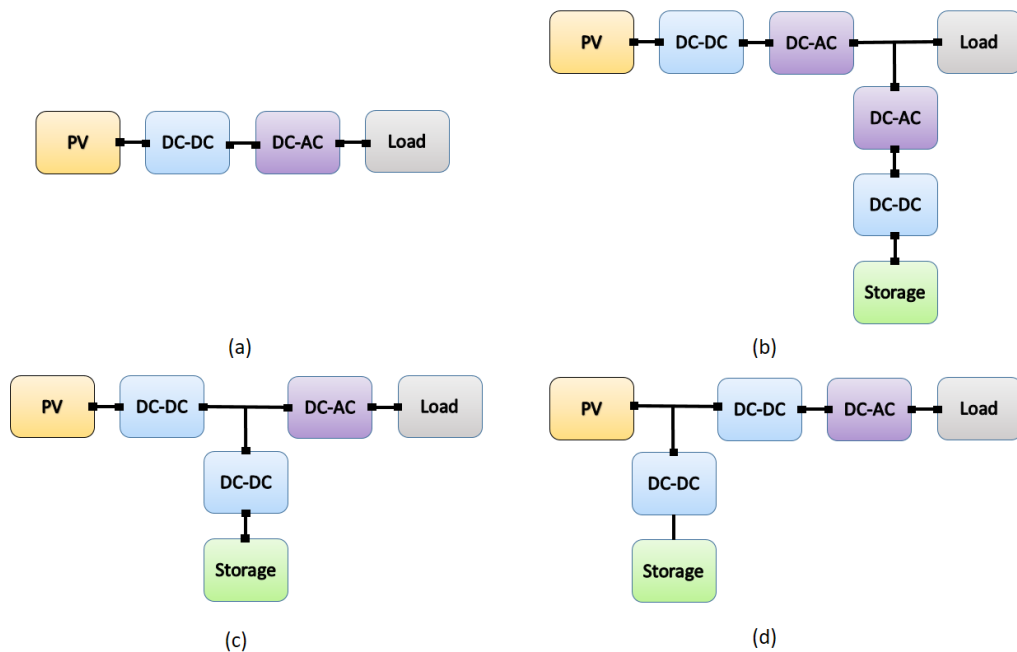
Figure 23 – Energy storage system possible topologies. (a) Simple grid connected PV system. (b) Storage connected near load. (c) Storage connected in middle point. (d) Storage connected near PV source.

From (b) to (d) storage element is connected near load or near PV module, in case (c) storage is in the middle. If storage is collocated between inverter and grid are necessary two conversion stages: this is the worst case considering converter numbers and storage roundtrip efficiency. In the other topologies the system has only three converters. In order to create a common DC bus the selected topology is (c) and the discarghe efficiency is higher (two conversion instead of three), moreover each system player (PV, storage and load) is decouple from the others. Another advantage derived from this topology is the possibility to set an equal voltage of PV module and storage in order to use two identical DC-DC converter reducing realization cost.

Considering trasformerless DC-DC converter multiplying factor limits and in order to increase system efficiency, reducing currents, considering also battery losses, wigth and volume, inputs voltage, PV module and storage, are setted at 100 V [34]. Finally, the last necessary constrain is the output maximum power. A value of 5 kW can guarantee a good option to elaborate multiple control algorithms, furthermore considering typical Italian nominal residential power contract, 3.3 kW, a system able to supply an higher peak power could be a good option for future product users. (Appendix E) Constrains are point out below:

- $V_{PV} \approx 100\ V$
- $V_{storage} \approx 100\ \text{V}$
- $V_{DC,link} = 450\ V$
- $P_{out,MAX} = 5\ \text{kW}$

3.2 Hardware design

The aim of the project is the realization of a system with a high efficiency during every working phase, but it is not correspond to design the system for a particular working power. In fact typical residential consumption and PV production are discontinuous and with high power variation. The base idea is to design a modular system able to adapt its structure with power production and consumption.

A multiphase converter is the best option to reduce current losses at high working power, at the same time monitoring the working power it is possible to enable the
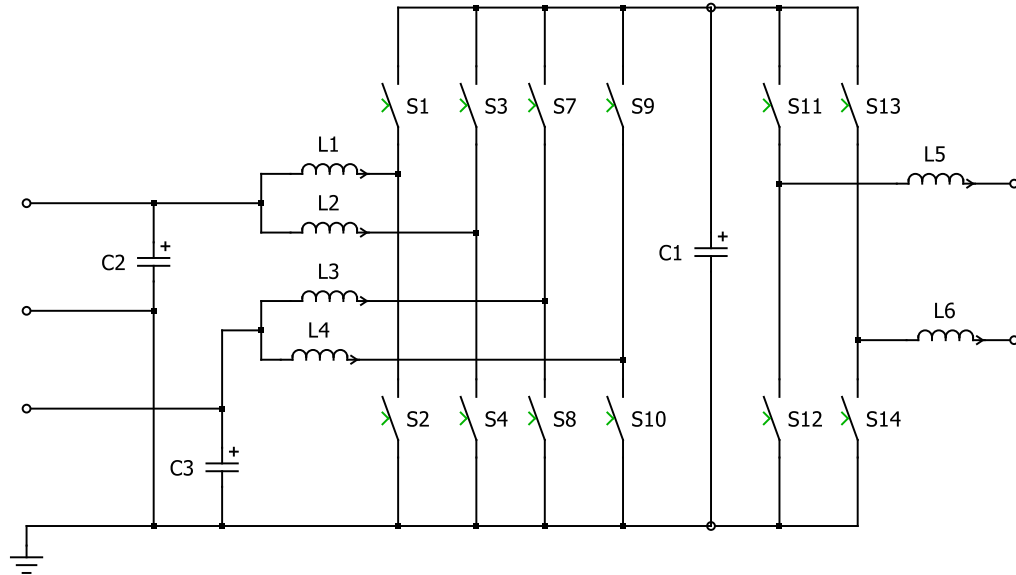
Figure 24 - Proposed energy storage schematics. Two DC-DC converter and one Inverter. Each converter is based on H-bridge topology. On left port connection to PV module and Storage and on right connection to AC-loads and grid.

phase only if the power is higher enough. Final inverter stage is based on a simple H-bridge to reduce system complexity. For the purpose of component cost reduction DC-DC converters are based on the same topology: every converter is realized with two phases. At low working power will work only one converter phase, than at high power interleaved option will be enabled. In future section will be shown design steps of every modules and components of converters.

DC-DC converters

The chosen approach, as a system cost reduction tool, is the symmetrical approach to design the two DCDC converters. At the end of the design steps only little changes will be perform to customize the converters. Below simplifying hypothesis are point out:

- Two multiphase DC-DC converters
- Two phases each converter
- PV converter is unidirectional

- Storage converter is bidirectional

- Every phase has half of the total power

Starting from this hypothesis it is only necessary to follow the boost converter steps design with few additional precautions. Selected topology constrains are:

- $V_{IN} = 100\ V$

- $V_{OUT} = 450\ V$

- $I_L = 25\ A$

FIG shows current and voltage waveforms of a boost converter operating in continuous conduction mode (CCM) that means that inductor current never reach zero, if inductor current reaches zero converter operates in discontinuous conduction mode (DCM).
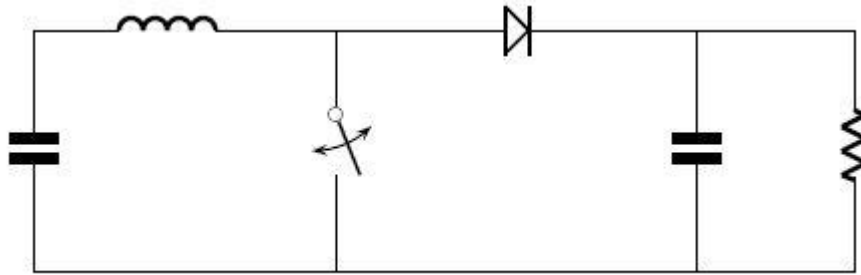
Figure 25 – Boost converter schematics. State ON when the switch is closed, state OFF when the switch is open.

During state ON the switch is closed:

$$V_i = L\frac{dI_L}{dt} \qquad\qquad (3.2.1)$$

$$\Delta I_{L,On} = \frac{1}{L} \cdot \int_0^{DT} V_i\, dt = \frac{DT}{L} V_i \qquad\qquad (3.2.2)$$

During state OFF the switch is open:

$$V_i - V_o = L\frac{dI_L}{dt} \qquad\qquad (3.2.3)$$

$$\Delta I_{L,Off} = \frac{1}{L} \cdot \int_{DT}^{T} (V_i - V_o)\, dt = \frac{(1-D) \cdot T}{L} \cdot (V_i - V_o) \qquad (\,3.2.4\,)$$

Because of the current variation during state ON is equal to state OFF:

$$\Delta I_{L,On} + \Delta I_{L,Off} = 0$$
$$= \frac{V_i \cdot D \cdot T}{L} + \frac{(V_i - V_o) \cdot (1-D) \cdot T}{L} \qquad (\,3.2.5\,)$$

This can be written as:

$$\frac{V_o}{V_i} = \frac{1}{1-D} \qquad (\,3.2.6\,)$$

That is the steady state relation between input and output voltage in a boost converter. With this is ideal relation, diode and switch losses are neglected, it is possible to calculate an indicative duty cycle value, D = 0.78. Modeling losses means a duty cycle a little bit higher.

In this application, it is not possible to ensure always CCM operation, PV power fluctuation and variable consumption, but it is possible to define a CCM minimum power. Defined a minimum power it is possible to calculate the required indictor
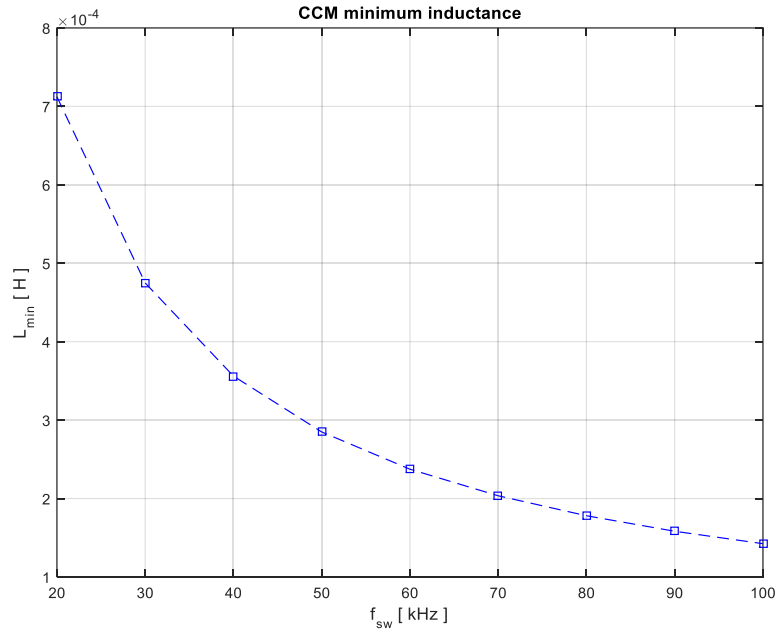
Figure 26 – Boost converter minimum inductance function of switching frequency. Minimum power is set at 500 W.

current ripple, equation (3.2.7). Inequality (3.2.8) is used to define the required minimum inductor value and in Figure 26 is shown its value function of switching frequency.

$$I_{ripple} = \frac{V_i \cdot D}{L \cdot f_{sw}}$$

(3.2.7)

$$L \geq \frac{V_i \cdot D}{I_{ripple} \cdot f_{sw}}$$

(3.2.8)

Increasing switching frequency it is possible to reduce inductor size, but it is necessary a little foresight to prevent its unfeasibility. Inductor core is a ferromagnetic material that with high current saturates, that means a reduction of the corresponding inductance. In addition, it is desirable to evaluate the fill factor in order to put all wire turn inside the inductor cavity, Figure 27.
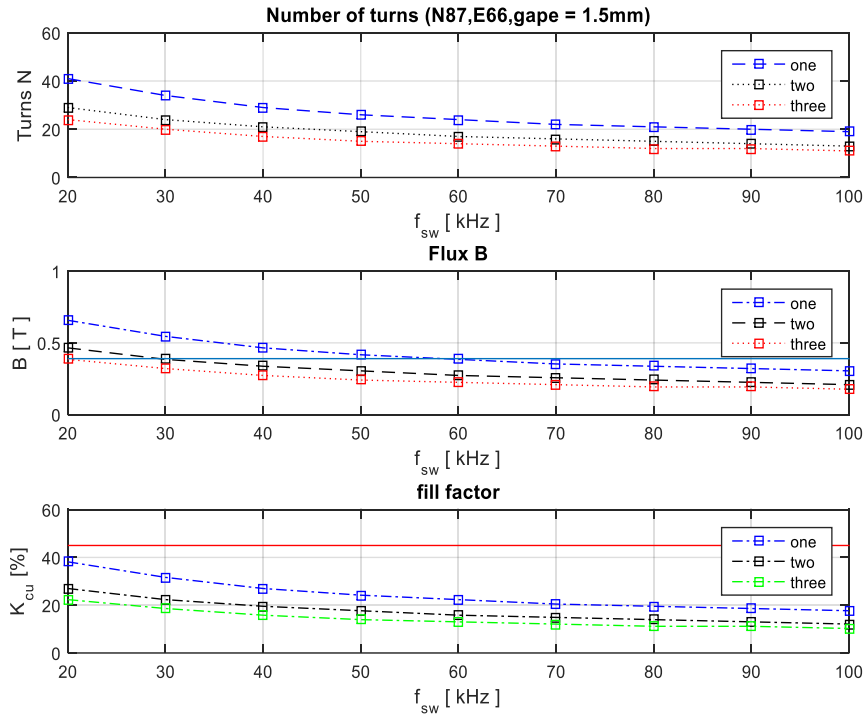
Figure 27 – Inductor parameters function of switching frequency with a particular core (E shape, material N87). Number of turns, magnetic flux density and fill factor.

Other consideration about inductor design in high flux operation will be shown in appendix and final designed value of the inductor will be presented after losses evaluation. In a simple boost output capacitor could be design with equation (3.2.9).

$$C_{out,min} = \frac{I_{o,max} \cdot D}{f_{sw} \cdot V_{o,ripple}}$$ (3.2.9)

With interleaved converter, capacitor could be little with equal voltage ripple, but its design will be examine in depth in future section, considering also inverter necessity.

Last useful information for the design is the converter transfer function. Equation (3.2.6) is the steady state relation between voltage input and output; with state space analysis, it is possible to derive transient relation. This argument is amply discussed in literature; in the follow are reported general and most important equation. State variable of this converter are:

$$x = \begin{bmatrix} i_L \\ v_o \end{bmatrix}$$ (3.2.10)

Performing a state space analysis, where D is the variable that express the switch state, we obtain:

$$\dot{x} = \begin{bmatrix} 0 & (D-1)/L \\ (1-D)/C & -1/RC \end{bmatrix} \cdot x + \begin{bmatrix} 1/L \\ 0 \end{bmatrix} \cdot v_{in}$$ (3.2.11)

Variables could be expressed as the sum of a 'bias' term plus a variation:

$$a = A + \hat{a}$$ (3.2.12)

Considering only variations of equation (3.2.12) and if we are in small signal condition it is possible to write:

$$\begin{cases} \dfrac{d}{dt}\hat{i}_L = -\dfrac{1-D}{L} \cdot \hat{v}_o + \dfrac{\hat{d}}{L} V_o + \dfrac{\hat{v}_{in}}{L} \\ \dfrac{d}{dt}\hat{v}_o = \dfrac{1-D}{C} \cdot \hat{i}_L + \dfrac{\hat{d}}{C} I_L + \dfrac{\hat{v}_o}{C} \end{cases}$$ (3.2.13)

Passing to Laplace domain it is possible to find out boost transfer functions. (3.2.14) is the relation between duty cycle and output voltage, while (3.2.15) is between duty cycle and inductor current. A resonance peak, due to LC stage, characterizes both transfer functions. Whereas current absorption from inverter as a component at 100 Hz it is recommended to design this resonance at a different frequency. Transfer function between duty cycle and output voltage is affected by a right zero function of load, this parameter is an implicit limitation of control loop band.

$$G_{d,v} = \frac{\hat{v}_o(s)}{\hat{d}(s)} = V_{in} \cdot \frac{1 - \dfrac{sL}{R(1-D)^2}}{(1-D)^2 + s\dfrac{L}{R} + s^2 LC} \qquad (\,3.2.14\,)$$

$$G_{d,i} = \frac{\hat{\imath}_L(s)}{\hat{d}(s)} = \frac{V_{in}}{1-D} \cdot \frac{2 + s\,RC}{R\,(1-D)^2 + s\,L + s^2 RLC} \qquad (\,3.2.15\,)$$
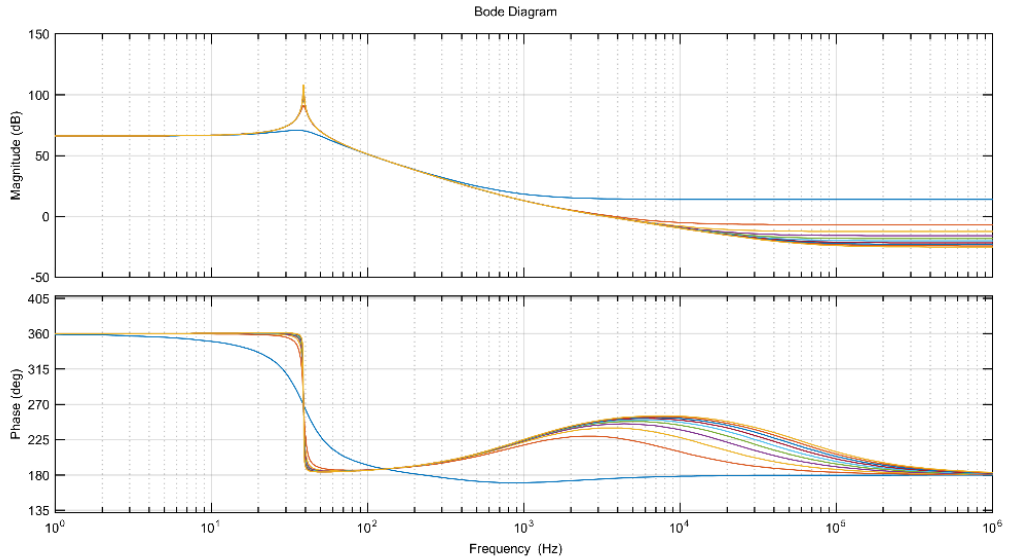
Figure 28 – Boost converter transfer function $G_{d,v}$ bode plot, magnitude and phase.

Inverter
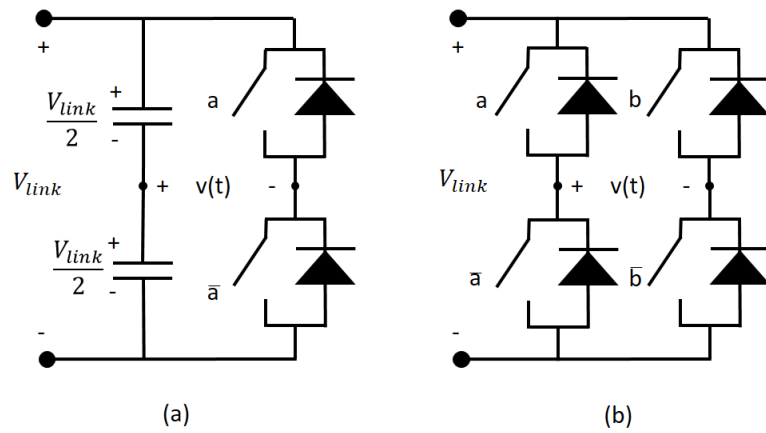
Figure 29 – Basic single phase inverter topologies: (a) half bridge (b) full bridge

The basic single-phase inverter topologies can be half-bridge and full-bridge (Figure 12.25). The main elements for a comparison are:

- The number of bidirectional switches (two for the half-bridge and four for the full-bridge).
- The switches voltages (double of the rated line voltage for the half-bridge and the rated line voltage for the full-bridge).
- The capacitor current, which also has a fundamental frequency component in the case of the half-bridge.
- The number of sensors (the half-bridge topology also needs one voltage sensor more to manage the balance between the two capacitor voltages).
- The algorithm complexity needed for the two converters (the half-bridge also needs a controller for the DC voltage balance).

In order to components cost reduction, full bridge topology is selected. Relation between input and output voltage is:

$$V_{\text{inv,mean}} = (2\delta - 1) \cdot V_{\text{dc}} \qquad (\,3.2.16\,)$$

Where δ is the inverter duty-cycle and it is possible to calculate its minimum and maximum value with (3.2.17) and (3.2.18).

36

$$\delta_{\max} = \left(\frac{V_{grid,pk}}{V_{dc}} + 1 \right) \cdot \frac{1}{2} \qquad (\,3.2.17\,)$$

$$\delta_{min} = \left(\frac{-V_{grid,pk}}{V_{dc}} + 1 \right) \cdot \frac{1}{2} \qquad (\,3.2.18\,)$$

Inverter root mean square current is calculated starting from minimum grid voltage (3.2.19).

$$I_{inv,rms,max} = \frac{P_{inv,max}}{V_{grid,rms,min}} \qquad (\,3.2.19\,)$$

C-link

This capacitor is the link between all converters: to define its value will be choose the most restrictive inequality. Equation derived from boost converter are shown before, now will be introduced inverter equations. DC-DC converter provides constant power, while the inverter draws a non-constant instantaneous power with mean value equal to the boost output power. Under some simplifying hypothesis link capacitor design is:

- Ideal inverter and output filter, efficiency equal to one.
- Neglect capacitor voltage ripple.
- Nominal conditions of the converter and the electricity network

$$\begin{aligned} P_{inv,out} \,(\,t\,) = \; & V_{grid}(t) \cdot I_{inv}(t) = X_{mean} - x_{variable} \\ = \; & V_{grid} \cdot I_{inv} - V_{grid} \cdot I_{inv} \qquad (\,3.2.20\,) \\ & \cdot cos(2w_{grid}t) \end{aligned}$$

$$I_{inv} = \frac{P_{out}}{V_{grid}} \qquad (\,3.2.21\,)$$

$$I_{boost} = \frac{P_{out}}{V_{dc}} \qquad\qquad (3.2.22)$$

$$i_C(t) = I_{boost} \cdot cos(2w_{grid}t) \qquad\qquad (3.2.23)$$

$$V_{dc,ripple} = V_{dc} \cdot 10\% = I_{boost} \cdot \frac{1}{w_{grid} \cdot C_{link}} \qquad\qquad (3.2.24)$$

$$V_{dc,max} = V_{dc} + \frac{V_{dc,ripple}}{2} \qquad\qquad (3.2.25)$$

$$C_{link} \geq \frac{I_{boost}}{w_{grid} \cdot V_{dc,ripple}} \qquad\qquad (3.2.26)$$

Inequality (3.2.27) is the most restrictive and electrolytic capacitor is, almost, an obligated technology choice, to reduce inductive passive component of the electrolytic capacitor it is possible to put in parallel smaller capacitors.

Output filter

The role of the output filter is twofold. On one side the output filter should have a dominant inductive behavior to guarantee the proper operation of the inverter if connected to a voltage source type system such as the electricity grid. In this sense grid converters replicate the well-known behavior of synchronous generators and of transmission lines where the control of active and reactive power exchange is related to the control of phase and magnitude of the electromagnetic force.

On the other side, inverter generate PWM carrier and side-band voltage harmonics. These voltages may lead to current flowing into the grid, which can disturb other sensitive loads and increase losses. Output filter made by a simple inductor is the simplest solution to comply with the two aforementioned.
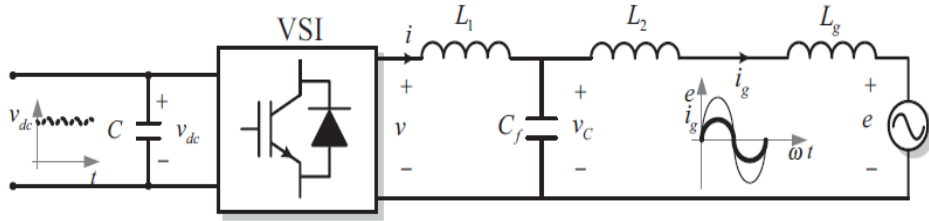
Figure 30 – Inverter LCL output filter scheme.

However, typically standards and grid codes recommend compliance with limitations that are very stringent for frequencies above a certain threshold. Hence a low-pass filter attenuation is needed and the preferred solution becomes the use of high-order filters like LCL, which provide 60 dB per decade attenuation for the PWM carrier and side-band voltage harmonics requirements.

In order to tune correctly the LCL filter the starting point is the current ripple on the converter side of the filter and the harmonic limit imposed on the grid current by standards, recommendations and utility codes.

The converter-side inductance is designed in order to limit the ripple of the converter–side current. Moreover, the inductor should be properly designed so as not to saturate and hence the correct inductor choice is a trade-off between ripple reduction and inductor cost. Accepting high values of the current ripple may lead to saturation problems in the core and consequently to the use of a core that could be used also for realizing higher value inductors.

On the other side of the filter the grid pollution is evaluated in terms of harmonics rather than in terms of ripple amplitude. Hence the LCL-filter effectiveness in reducing them should be evaluated using a frequency domain approach. In brief, a time domain analysis (ripple evaluation) drives the choice of the converter-side inductor while a frequency-domain analysis (harmonic evaluation) drives the choice of the LCL-filter resonance frequency

The last degree of freedom in the choice among couples of CL values that meet the resonance frequency requirement is used to minimize the installed reactive

power of the LCL filter. Have to be evaluated cost, weight and encumbrances of capacitor and inductors, the robustness of the LCL–filter attenuation capability with respect to the possible different grid impedance conditions.

Equations (3.2.28) define current ripple as a function of converter – side inductor:

$$\Delta I_{max} = \frac{V_{dc}}{n \cdot L_1 \cdot f} \qquad (3.2.27)$$

Where n is an index linked with used modulation. Solving for L_1, using unipolar modulation and limiting current ripple at 1% of the maximum current we obtain:

$$L_1 = \frac{V_{dc}}{200 \cdot f \cdot I_{max}} \qquad (3.2.28)$$

As next step it is evaluated the harmonic attenuation of the LCL filter and hence the choice of the resonance frequency value.

$$\frac{i_g(w)}{i(w)} = \frac{z_{LC}^2}{|z_{LC}^2 - w_{res}^2|} \qquad (3.2.29)$$

$$w_{res}^2 = \frac{z_{LC}^2 \cdot (L_1 + L_2 + L_g)}{L_1} \qquad (3.2.30)$$

$$z_{LC}^2 = \frac{1}{(L_g + L_2) \cdot C_f} \qquad (3.2.31)$$

3.3 Losses estimation

Losses estimation is an important design step used as key parameter. First different losses sources are classified and evaluated individually, and then they are compared to identify most significants. Main losses sources are:

- IGBT and diode;
- Link capacitor;
- Inductors;

IGBT and diode power losses, as well as power losses in any semiconductor component, can be divided in three groups:

a) Conduction losses

b) Switching losses

c) Blocking (leakage) losses, which are normally neglected.

Therefore, total IGBT and diode losses can be expressed as

$$P_{IGBT,Diode} = P_{cond} + P_{SW} + P_{block} \approx P_{cond} + P_{SW} \qquad (\,3.3.1\,)$$

Conduction losses can be calculated using an IGBT approximation with a series connection of DC voltage source (u_{CE0}) representing IGBT on-state zero-current collector-emitter voltage and a collector-emitter on-state resistance ($r_C = \frac{\Delta U_{CE}}{\Delta I_C}$).

$$u_{CE}(i_C) = u_{CE0} + r_C \cdot i_c \qquad (\,3.3.2\,)$$

The same approximation can be used for the anti-parallel diode, giving:

$$u_D(i_D) = u_{D0} + r_D \cdot i_D \qquad (\,3.3.3\,)$$
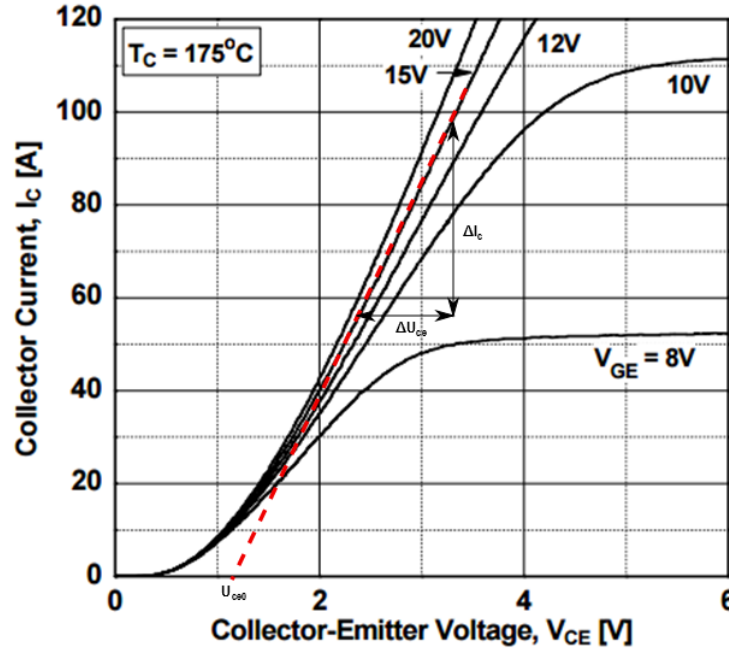
Figure 31 - IGBT output characteristics approximation

These parameters can be read directly from datasheet, Figure 31. In order to take the parameter variation into account, and thus to have a conservative calculation, the u_{CE0} and u_{D0} values read from the diagram have to be scaled with $(u_{CE,max}/u_{CE,typ})$ or $(u_{D,max}/u_{D,typ})$ values. Those exact values can be read from the datasheet tables, but for an engineering calculation a typical safety margin value of (1.1 - 1.2) can be used. The instantaneous value of the IGBT conduction losses is:

$$p_{IGBT,cond}(t) = \mathrm{u}_{CE}(t) \cdot i_C(t) = u_{CE0} \cdot i_C(t) + r_C \cdot i_C^2(t) \qquad (\,3.3.4\,)$$

If the average IGBT current value is $i_{C,avg}$, and the RMS value of IGBT current is $i_{C,RMS}$, then the average losses can be expressed as:

$$P_{IGBT,cond} = \frac{1}{T_{SW}} \int_0^{T_{SW}} p_{IGBT,cond}(t)dt \qquad (\,3.3.5\,)$$

Substituting (3.3.4) into (3.3.5), it is obtained:

$$P_{IGBT,cond} = u_{CE0} \cdot I_{C,avg} + r_C \cdot I_{C,RMS}^2 \qquad (\,3.3.6\,)$$

Similar calculation is done for diode conduction losses.

The turn-on energy losses in IGBT ($E_{IGBT,ON}$) can be calculated as the sum of the switch-on energy without taking the reverse recovery process into account ($E_{ON,Ti}$) and the switch-on energy caused by the reverserecovery of the free-wheeling diode ($E_{ON,Trr}$), equation (3.3.7). IGBT switch-off energy losses can be calculated in the similar manner, while diode switch-off energy losses are normally neglected.

$$E_{IGBT,ON} = \int_{t1}^{t2} \mathrm{u}_{CE}(t) \cdot i_C(t)dt = E_{ON,Ti} + E_{ON,Trr} \qquad (\,3.3.7\,)$$

IGBT and diode switching losses are the product of switching energies and the switching frequency:

$$P_{IGBT,SW} = \left(E_{ON,Ti} + E_{ON,Trr}\right) \cdot f_{SW} \qquad\qquad (\,3.3.8\,)$$

$$P_{Diode,SW} \approx E_{ON,Diode} \cdot f_{SW} \qquad\qquad (\,3.3.9\,)$$

The specification for the integration limits in IEC 60747-9 are:

- Turn-on: E_{ON}
  - $t1 : V_{GE} = 10\% \; of \; V_{G(ON)}$
  - $t2 : V_{GE} = 2\% \; of \; V_{CC}$
- Turn-off: E_{OFF}
  - $t3 : V_{GE} = 90\% \; of \; V_{G(ON)}$
  - $t4 : V_{GE} = 2\% \; of \; I_C$
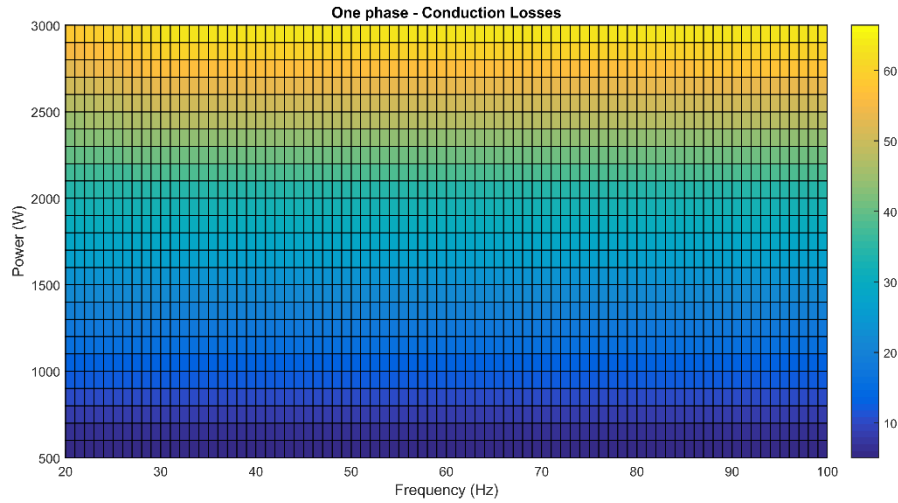
Figure 33 – One phase DC-DC converter conduction losses
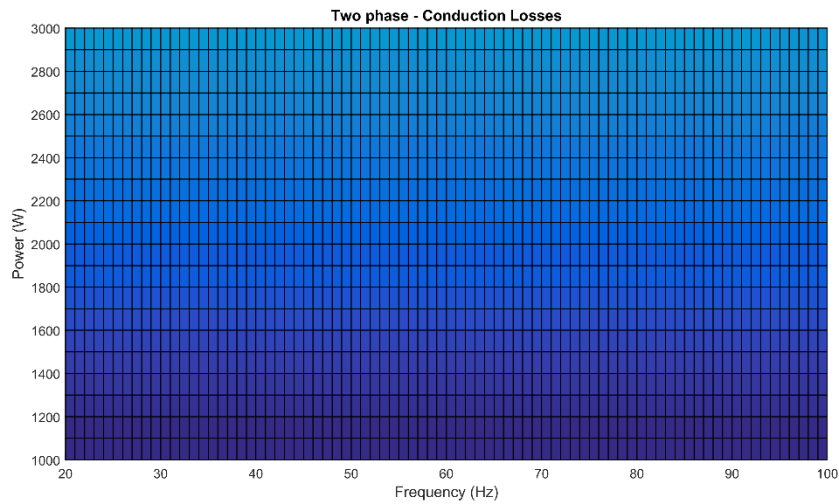
Figure 32 - Two phases DC-DC converter conduction losses

Figure 33 and Figure 32 show calculated conduction losses, Figure 34 and Figure 35 show switching losses in case of a single phase DC-DC converter or a two phases interleaved DC-DC converter as a function of output power a switching frequency.
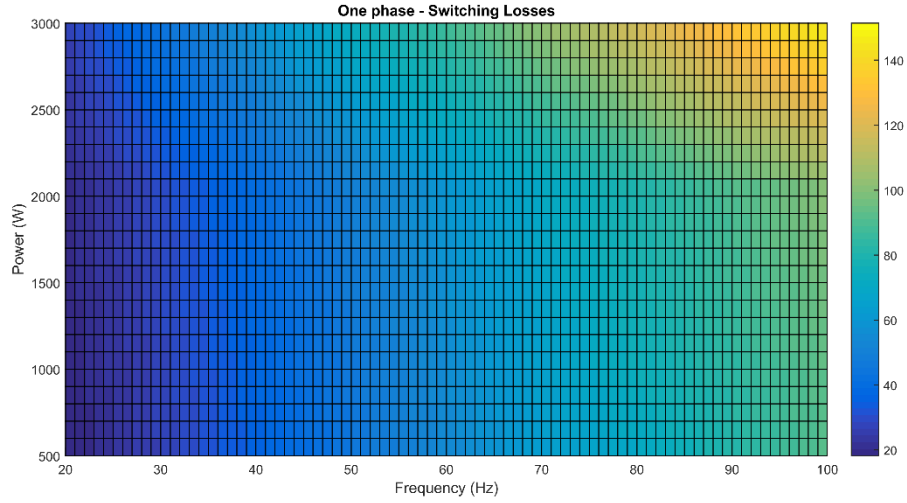
Figure 35 – One phase DC-DC converter switching losses
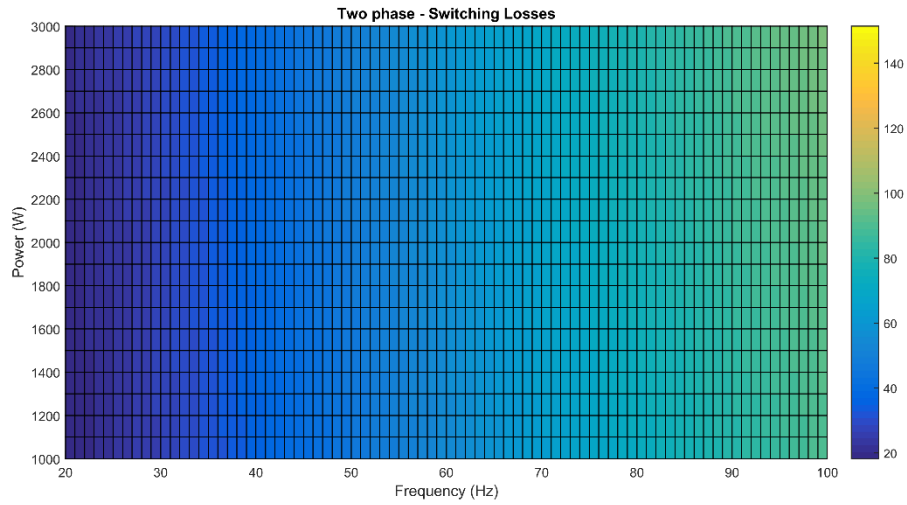
Figure 34 – Two phases DC-DC converter switching losses

Link capacitor losses could be estimated with (3.3.10)

$$P_{C,loss} = I_{C,RMS}^2 \cdot ESR \qquad\qquad (\,3.3.10\,)$$

where ESR is the capacitor series resistance and $I_{C,RMS}$ is the root mean square current circulating in the link capacitor.
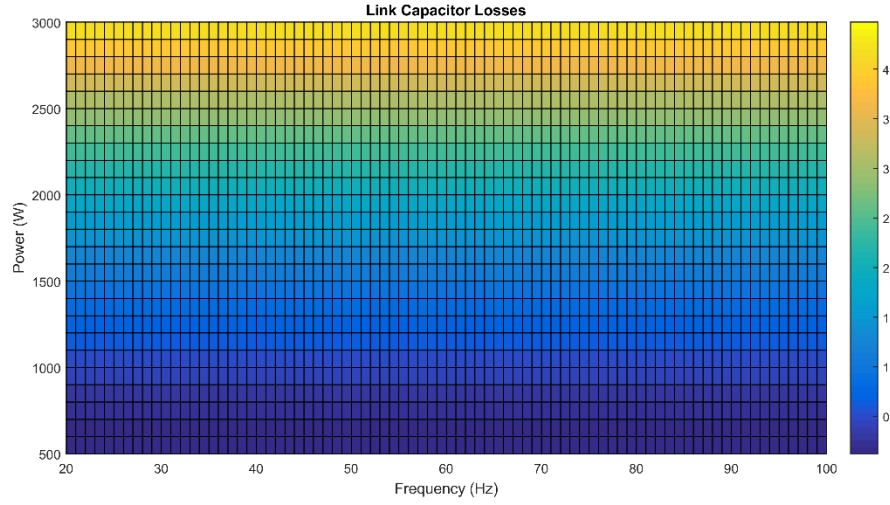
The evaluation of inductor losses is used as key parameter of the system switching frequency; it is necessary to distinguish two losses sources:

- Wire losses.
- Core losses

Wire losses can be calculated from the series resistance of the wire and the DC component of the current:

$$P_{cu,losses} = R_{cu} \cdot I_{DC}^2 \qquad (3.3.11)$$

Where the series resistance is calculated as:

$$R_{cu} = MLN \cdot N \cdot \frac{\rho}{A_{fe}} \qquad (3.3.12)$$

Where MLN is the approximated length of every turn, N is the number of turns, ρ is the resistivity of the material and A_{fe} is the area of the wire. It is possible to hone this equation evaluating the frequency effect, so called 'skin effect'[3]. There are different approach to evaluate this phenomenon, based of different approximations (equations (3.3.14) and (3.3.16))

---

[3] Skin effect is the tendency of an alternating electric current (AC) to become distributed within a conductor such that the current density is largest near the surface of the conductor, and decreases with greater depths in the conductor. The electric current flows mainly at the "skin" of the conductor, between the outer surface and a level called the skin depth. The skin effect causes the effective resistance of the conductor to increase at higher frequencies where the skin depth is smaller, thus reducing the effective cross-section of the conductor.

$$R_{ca} = R_{cc} \cdot \left[1 + \frac{1}{48}\left(\frac{r}{\delta}\right)^4\right] \qquad (3.3.13)$$

Where r is the wire radius and δ is the skin depth:

$$\delta = \sqrt{\frac{2 \cdot \rho}{\omega \cdot \mu}} \qquad (3.3.14)$$

Another approximation is based on the calculation of an effective area crossed by current:

$$A_{fe,eff} = \pi \cdot (2 \cdot r \cdot \rho - \rho^2) \qquad (3.3.15)$$

At analyzed frequency the phenomenon is negligible.

Core losses can be estimated, in first approximation, using Steinmetz's equation (3.2.19):

$$P_{core,losses} = k \cdot f^\alpha \cdot B^\beta \qquad (3.3.16)$$

where k, α and β are material parameters, generally found by curve fitting. Equation (3.3.17) is a simplified form that only works with a sinusoidal frequency and does not take into account factors such as DC offset. However, due to the fact that most electronics expose materials to non-sinusoidal flux waveforms, various improvements to Steinmetz's equation had been made. Appendix (A) provides a comprehensive review on this field. Figure 38 shows inductor losses estimation based on datasheet aAn improved generalized Steinmetz equation, often referred to as iGSE (3.2.20).

$$P_{core,loss} = \frac{1}{T}\int_0^T k_i \left|\frac{dB}{dt}\right|^\alpha \left(\Delta B^{\beta-\alpha}\right)dt \qquad (3.3.17)$$

where T is the considered period, ki is defined in (3.2.21)

$$k_i = \frac{k}{(2\pi)^{\alpha-1}\int_0^{2\pi}|\cos\theta|^\alpha \cdot 2^{\beta-\alpha}\,d\theta} \qquad (3.3.18)$$

where k, α and β are the same parameters used in the original equation. This equation can calculate losses with any flux waveform using only the parameters needed for the original equation, but it ignores the fact that the parameters, and therefore the losses, change under DC bias conditions. DC bias cannot be neglected without severely affecting results, but there is still not a practical physically-based model that takes both dynamic and nonlinear effects into account. However, this equation is still widely used because most other models require parameters that are not usually given by manufacturers and that engineers are not likely to take the time and resources to measure.

$$P_{core,loss} = V_e \frac{k'_i(\Delta B)^{\beta'-\alpha}}{T} \cdot$$
$$\cdot \left[\left| \frac{V_i - V_o}{N\,A_e} \right|^\alpha \cdot DT + \left| \frac{-V_o}{N\,A_e} \right|^\alpha \cdot (1-D)T \right]$$

(3.3.19)
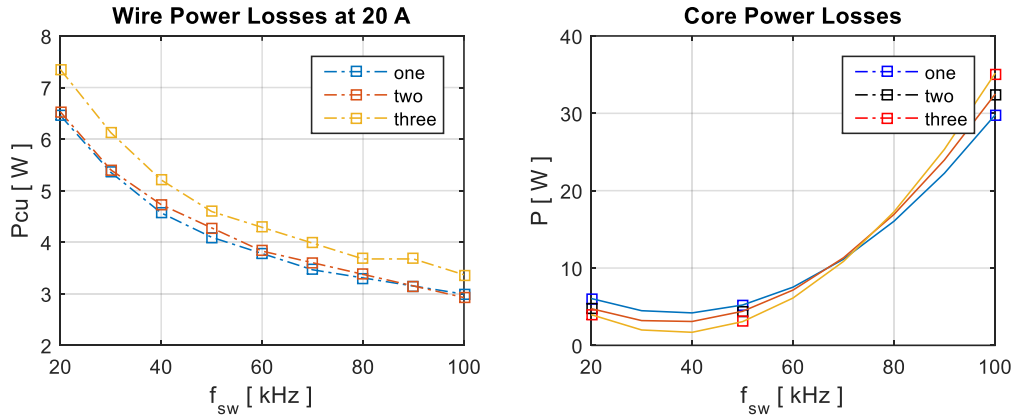
Figure 37 – Inductor wire losses and core losses function of frequency and number of parallel E core.
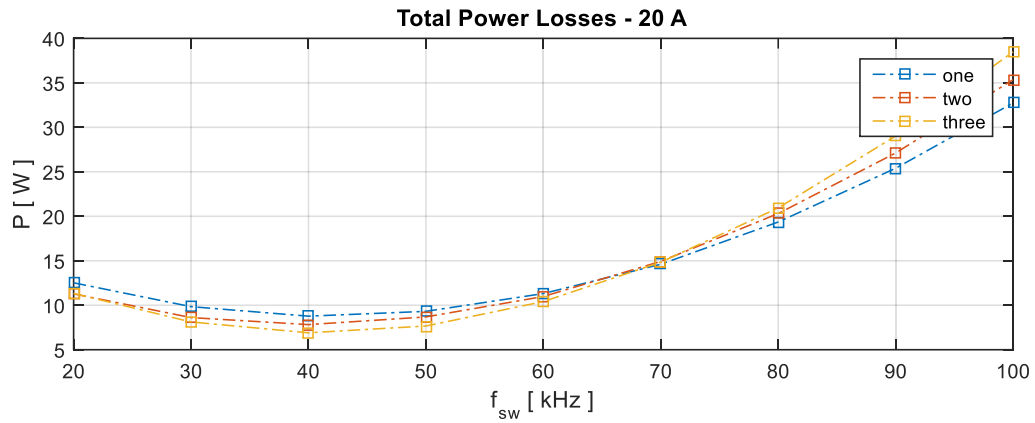
Figure 38 – Total inductor losses function of switching frequency and number of parallel E core.

Figure 39 shows total system estimated losses as sum of inductor losses, switch conduction losses, switch switching losses and link capacitor losses, in case of single phase communtation. Losses are presented as function of output power and switching frequency, colorbar is expressed in watt. At 40 kHz of switching frequency cosidered system losses give an efficiency among 90% at the maximum working power of 5 kilowatts.
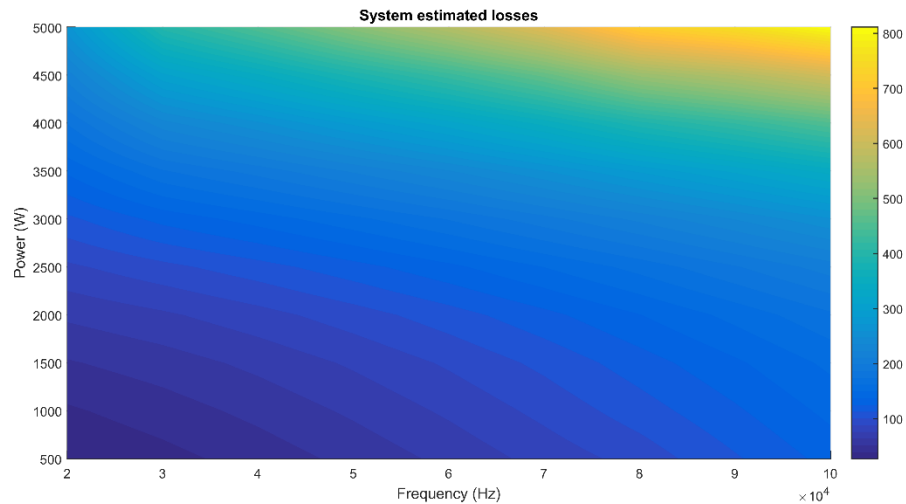
Figure 39 – System estimated losses. Single phase converter: inductor, switches and link capacitor losses. Inductor size change with frequency to fix

Chapter 4.   Software Architecture

In this chapter sofware architecture is described; all controls and communications protocols are implemented in a digital signal processor (DSP) that is described in the first section. The second section is adressed to used communication standard. Finally third section is adressed to control system despription: each module control system is shown and single block are described.

4.1 DSP-based control and communication system

Control and communication system are implemented using a Texas Instruments 32 Bit CPU, model TMS320C28335 of Delfino family. DSP fucntional diagram is shown in Figure 41 and in the following are pointed out its main features:

- 32-Bit CPU with Single-Precision Floating-Point Unit (FPU)

- Clock frequency up to 150 MHz

- Three 32-Bit CPU Timers

- Up to 18 PWM Outputs

- 88 Individually Programmable GPIO Pins

- Peripheral Interrupt Expansion (PIE) Block

- 2 x 8 Channels 12-Bit ADC

- 2 CAN Modules

- One SPI Module

- One Inter-Integrated-Circuit (I2C) Bus

- Operating Temperature: –40°C to 125°C

For each converter is implemented a finite state machine (FSM) with four states: Fault, Idle, Initialization, Running. In Figure 40 is shown the FSM flow chart. Starting from Fault state, if there are not fault signals (external harware signals) goes in Idle state. There are three type of possible fault signals:

- Over current

49

- Over voltage

- Over temperature

These controls are done at hardware level in order to ensure safety and preserve components. From Idle state, when it is received 'start' are initialized all control structures in Initalization state and finally it goes in Running state. In Running state are implemented different control systems according to the converter operations. In this way there are three FSM that work in parallel and it is possible to enable or disable independently, but due to hardware configuration there is a cross control on faults.Communication, HMI and control system will be shown in the follow.
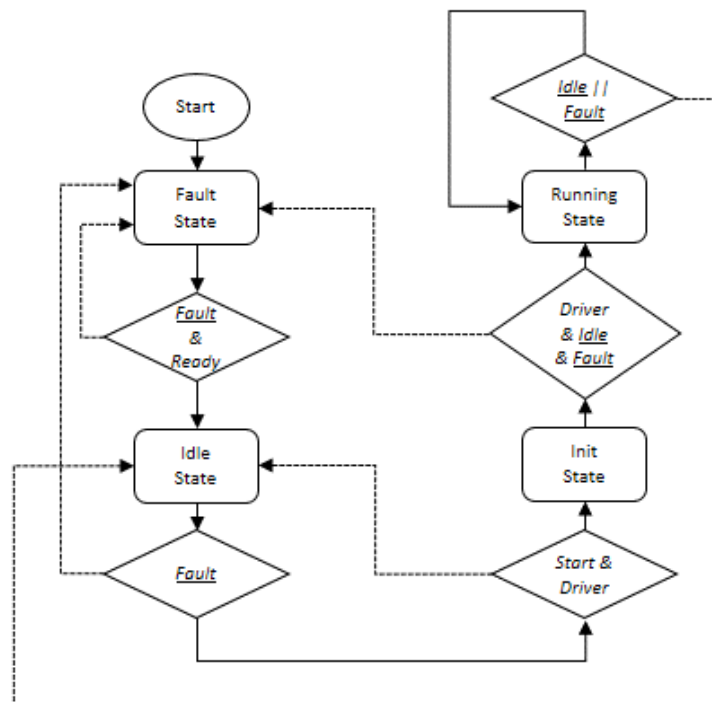
Figure 40 – Converter's finite state machine (FSM) flow chart
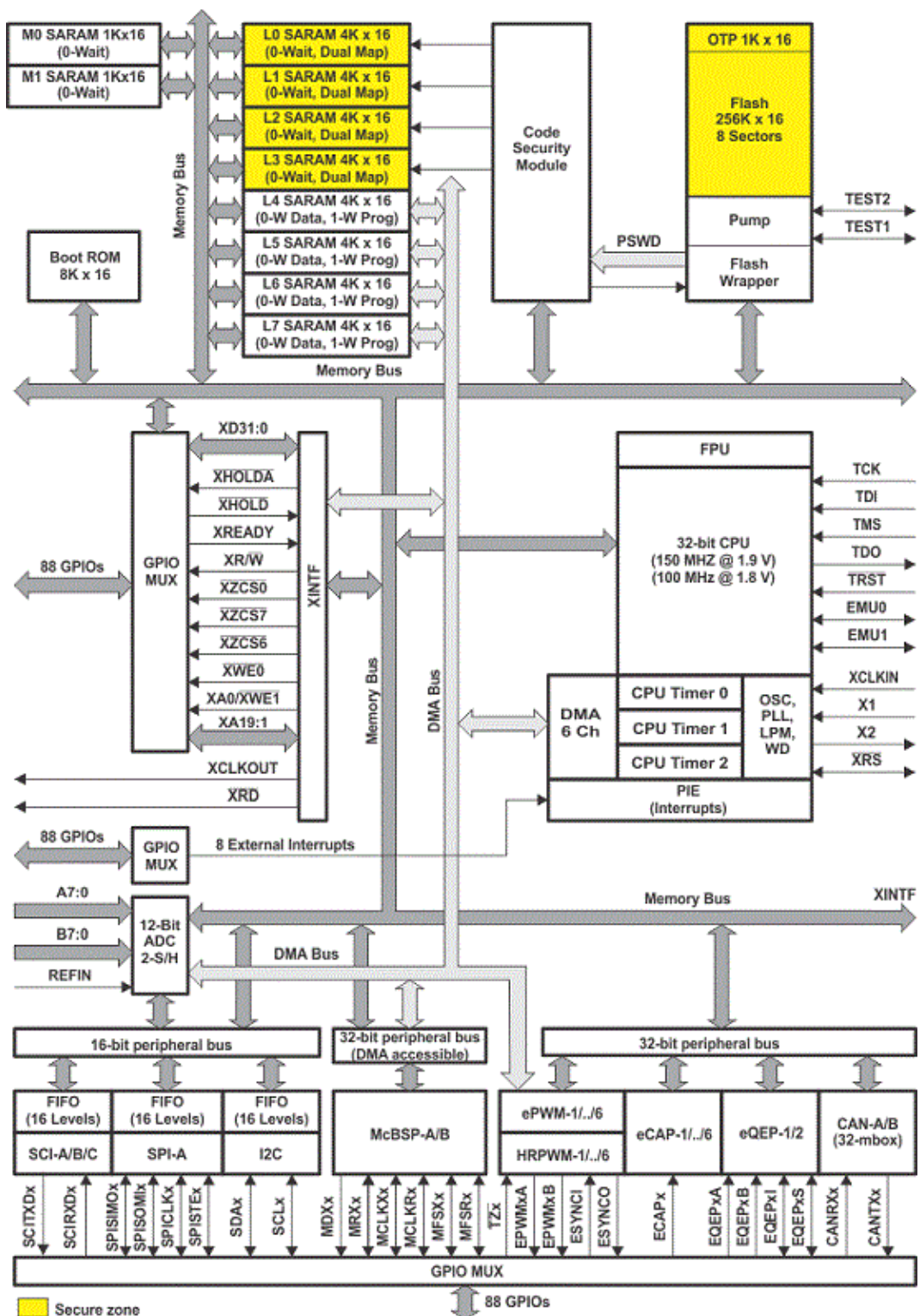
Figure 41 – TI DSP functional diagram

4.2 Communication systems

Requires of the communication system are fault tollerance and ability to connect multiple systems. CAN standard is the best option in order to reach these targets. Controller Area Network (CAN or CAN-bus) is a serial communications bus standard. Originally developed for the automotive industry to replace the complex wiring harness with a two-wire bus. The specification calls for high immunity to electrical interference and the ability to self-diagnose and repair data errors. These features have led to CAN's popularity in a variety of industries including building automation, medical, and manufacturing. The CAN communications protocol, ISO-11898: 2003, describes how information is passed between devices on a network and conforms to the Open Systems Interconnection (OSI) model that is defined in terms of layers. Actual communication between devices connected by the physical medium is defined by the physical layer of the model. The ISO 11898 architecture defines the lowest two layers of the seven layer OSI/ISO model as the data-link layer and physical layer, Figure 42.
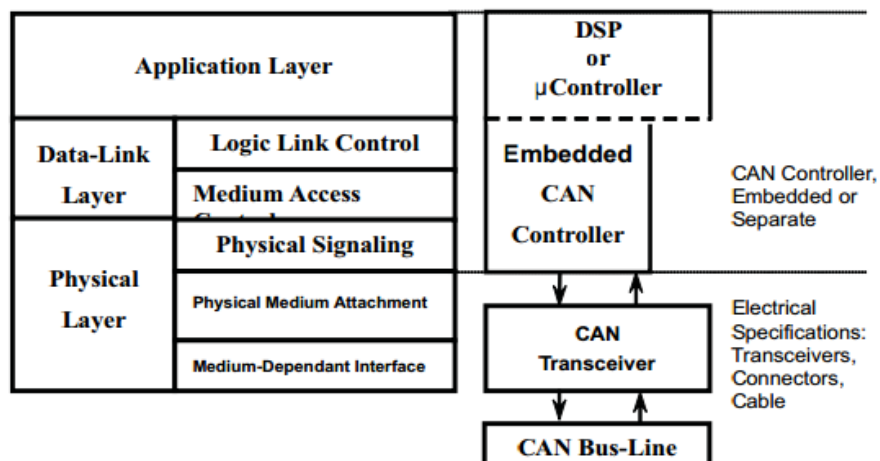
Figure 42 – The Layered ISO 11898 Standard Architecture

The data link and physical signaling layers of Figure 42, which are normally transparent to a system operator, are included in the integrated CAN controller. Connection to the physical medium is then implemented through a line transceiver to form a system node as shown in Figure 43.

Signaling is differential which is where CAN derives its robust noise immunity and fault tolerance. The High-Speed ISO 11898 Standard specifications are given for a maximum signaling rate of 1 Mbps with a bus length of 40 m with a maximum of 30 nodes. It is possible to increase bus length reducing bit rate.
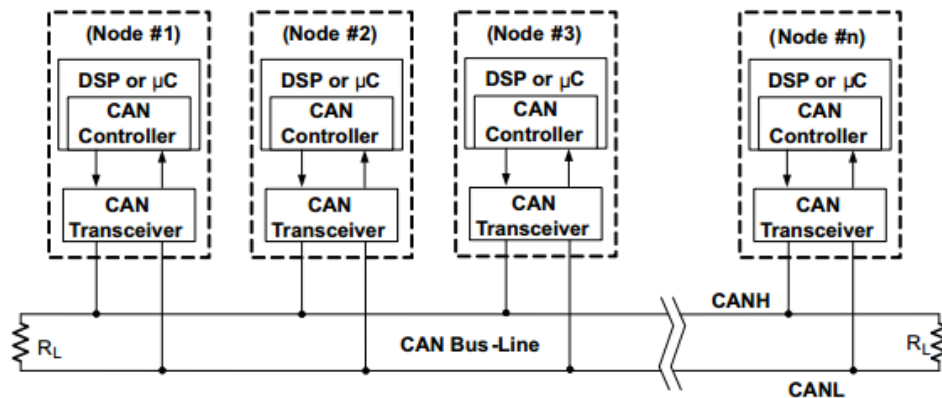
Figure 43 – Details of a CAN Bus

4.3 Digital control system

Proposed control system is composed of two main sections, one to for DC-DC converters and the other for inverter. Usually DC-DC converter are controlled in
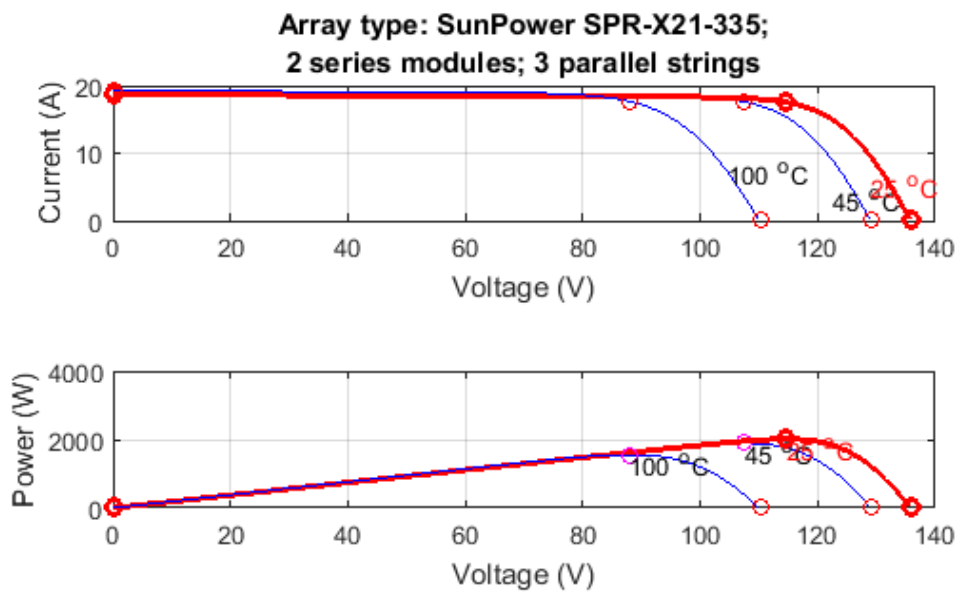
Figure 44 – Photovoltaic solar V-I curves function of temperature

order to set a constant output voltage and there are several methods to reach this target. [35] [36] [37] Different control algorithms has been developed for PV applications. PV panels parameters are function widely related to temperature (Figure 44) and irradiation (Figure 45), in order to maximize generated power it is necessary to use Maximum Power Point (MPP) algorithm to set converter's duty cycle. [38] [39] Usually, in grid connected PV system all generated power is sent to the grid while in case of stand alone applications different solution are implemented. [40, 41, 42]
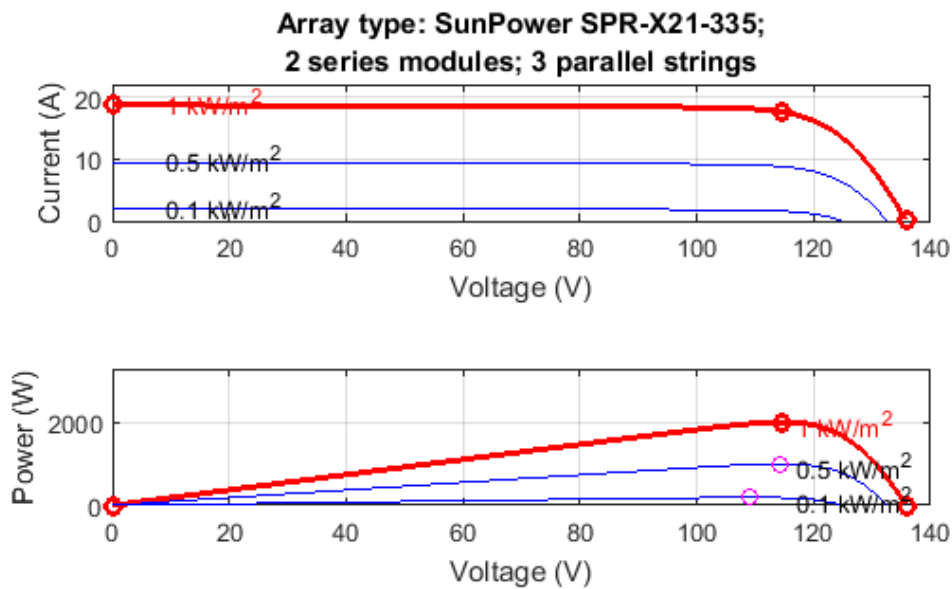
Figure 45 – Photovoltaic solar V-I curves function of irradiation

Figure 46 shows DC-DC converters control scheme. Converter connected to the battery is a bidirectional converter. It works as a boost converter when power flows from the battery to DC bus, while it is a buck converter when the battery is under charging. It is controlled with a dual loop, voltage and current control. This control is also called average current method. In order to charge the battery before send energy to the grid, the reference signal of the current loop has two components. The first one is the output of the voltage loop and the second is coming from the MPPT block of the PV converter. Finally, before the PWM block,

54

there is the Hysteretic Interleaved block where is enabled the converter second phase.

Converter connected to PV panels is unidirectional and works as a boost converter. Its first control stage is an MPPT block where is implemented the pertub and observe method. In this method the controller adjusts the voltage by a small amount from the array and measures power; if the power increases, further adjustments in that direction are tried until power no longer increases. Perturb and observe is the most commonly used MPPT method due to its ease of implementation. Pseudo code of Perturb and observe algorithm is:


```
IF (ΔP>0)
        IF (ΔV>0)       d += δ;
        ELSE            d -= δ
ELSE
        IF (ΔV>0)       d -= δ;
        ELSE            d += δ
```


Output of MPPT block is used as reference for a current control loop that used the inductors currets as feedback. Then, before PWM block, it is implemented an hysteretic interleaved block where, through a power computation, is enabled the second phase.

The aim of interleaved operation is to reduce current through components, inductors and switches, but as seen in Section 3.3 it is an efficient approach only at relative high powers. Because of PV generation and residential consumtpion are implicitly variable interleaved operation is enable only over a selected power threshold. Moreover to avoid oscillation of the second phase operation this threshold is different to enable or disable the second phase.
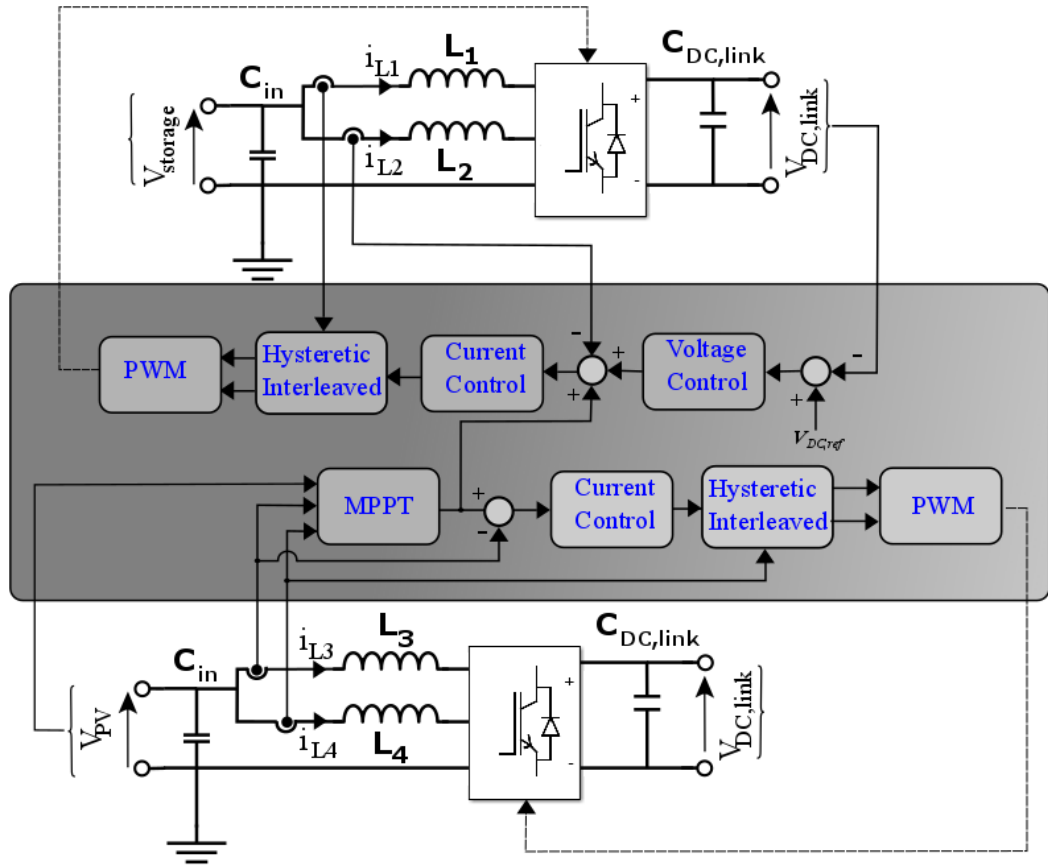
Figure 46 – Dc-Dc converters control scheme.

Figure 47 – Inverter control scheme shows inverter control scheme. Basically there is an inner current control, where the feedback is the inverter output current, and an outer voltage loop, where the feedback is the inverter output voltage. Voltage loop is necessary in case of stand alone operation, while it is useless in case of grid connected operation. In grid connected operation output voltage is measured in order to synchronize the system to electricity network voltage. Synchronism and flux control blocks will be analyzed in depth in follow sections.

The aim of synchronism block is to ensure that the system work correctly, from the phase point of view, both in case of stand alone or grid connected operation.

The aim of flux control block is to modify the reference of current loop in order to apply different energy management.

Output of current controller is the modulating signal of PWM module. Using a full bridge inverter topology it is possible to use different modulation that will be explained in the next section.
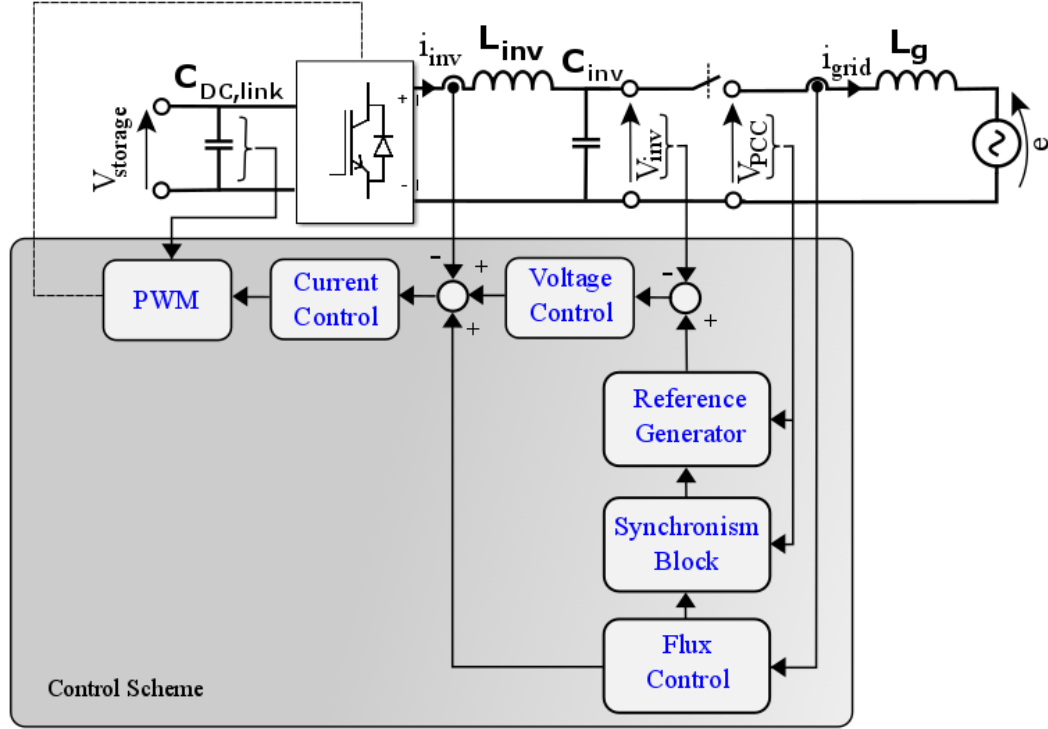
Figure 47 – Inverter control scheme

Inverter modulation

Half-bridge topology allows only a bipolar PWM modulation while the full-bridge allows a unipolar PWM with a better harmonic content, Figure 48. In the case of asymmetrical sampling (sampling of the modulating signal on both the carrier edges), the produced bipolar voltage is:

$$
v(t) = \frac{4\,V_{dc}}{\pi} \sum_{\substack{m=0 \\ m>0}}^{\infty} \sum_{\substack{\leftrightarrow n=1 \\ \leftrightarrow n=-\infty}}^{\infty} \frac{1}{q} J_n\left(q\frac{\pi}{2}M\right) \sin\left((m+n)\frac{\pi}{2}\right) \cos(m\omega_c t + n\omega_0 t) \cdot \qquad (\,4.3.1\,)
$$

where M is the amplitude modulation coefficient[4], ω_0 is the pulsation of the modulating signal, ω_c is the pulsation of the carrier signal, J_n is the Bessel function of order n and $q = m + n\,(\omega_0/\omega_c)$.

In the bipolar PWM signal reported in (4.2.1) the odd harmonic sideband components around the odd multiples of the carrier fundamental and even harmonic sideband components around even multiples of the carrier fundamental are completely eliminated as well as even low-ordered baseband harmonics.

In the case of the full-bridge it would be possible to modulate the two legs together to obtain a bipolar PWM signal or to adopt the unipolar modulation where the two legs of the bridge are modulated with opposite modulating signals. In the case of asymmetrical sampling, the produced voltage is:

$$v(t) = 2V_{dc}M\cos(\omega_0 t)\,\cdot$$

$$\cdot \sum_{m=1}^{\infty} \sum_{n=-\infty}^{\infty} \frac{1}{2m} J_{2n-1}(m\pi M)\cos\big((m+n-1)\pi\big)\,\cdot \qquad\qquad (\,4.3.2\,)$$

$$\cdot \cos(2m\omega_c t + (2n-1)\omega_0 t)$$

Due to the unipolar PWM the odd carrier and associated sideband harmonics are completely cancelled, leaving only odd sideband harmonics $(2n-1)$ terms and even $(2m)$ carrier groups.

Figure 48 shows the effect of bipolar or unipolar modulation on the voltage between output phases. Choose of modulation has a notable impact on output filter design. Considering a carrier signal frequency of 10 kHz, that means an inverter switching frequency of 10 kHz using a bipolar modulation it will be necessary to design a filter to remove the component at 10 kHz, while with an

---

[4] The amplitude modulation coefficient is the ratio between amplitudes of modulating and carrier waves.

unipolar modulation switching frequency is moved at 20 kHz. Hence unipolar modulation is used in order to reduce output filter size.
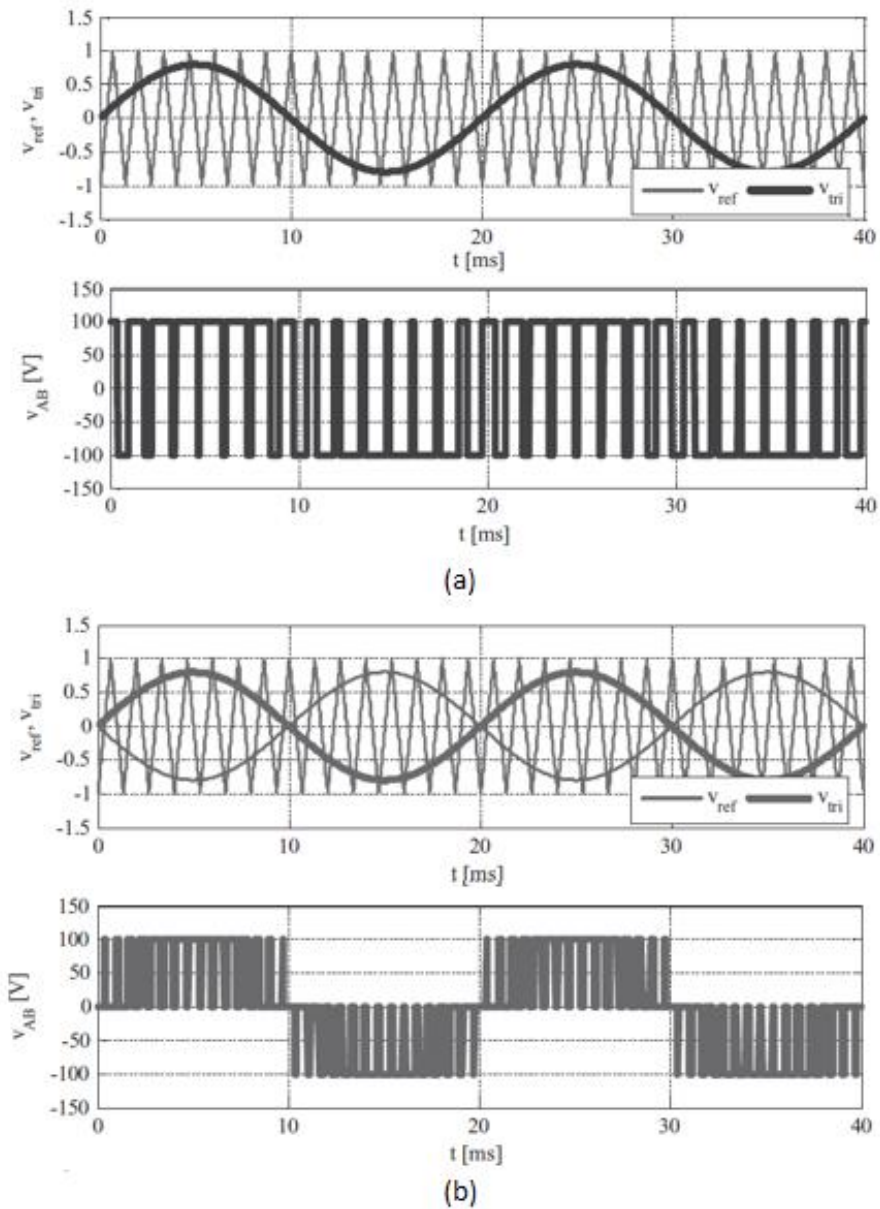
Figure 48 – Effect of different modulation on output frequency component: Bipolar PWM (a) and Unipolar PWM (b)

Synchronism algorithm

Figure 49 shows the flow chart of the synchronism block. There are three main state Stand Alone state, Synchronization state and Connected state. Passage through states is managed by the control signal called 'black out'. In Stand Alone state sinusoidal signal necessary to generate the SPWM is internally generated. When a grid connection is detected FSM goes in Synchronization state where start a phase-locked loop (PLL) and after correction of pulsation and delays goes in Connected state. In Connected state the PLL provide the syncronization signal. A phase-locked loop is a closed-loop system in which an internal oscillator is controlled to keep the time of some external periodical signal by using the feedback loop.
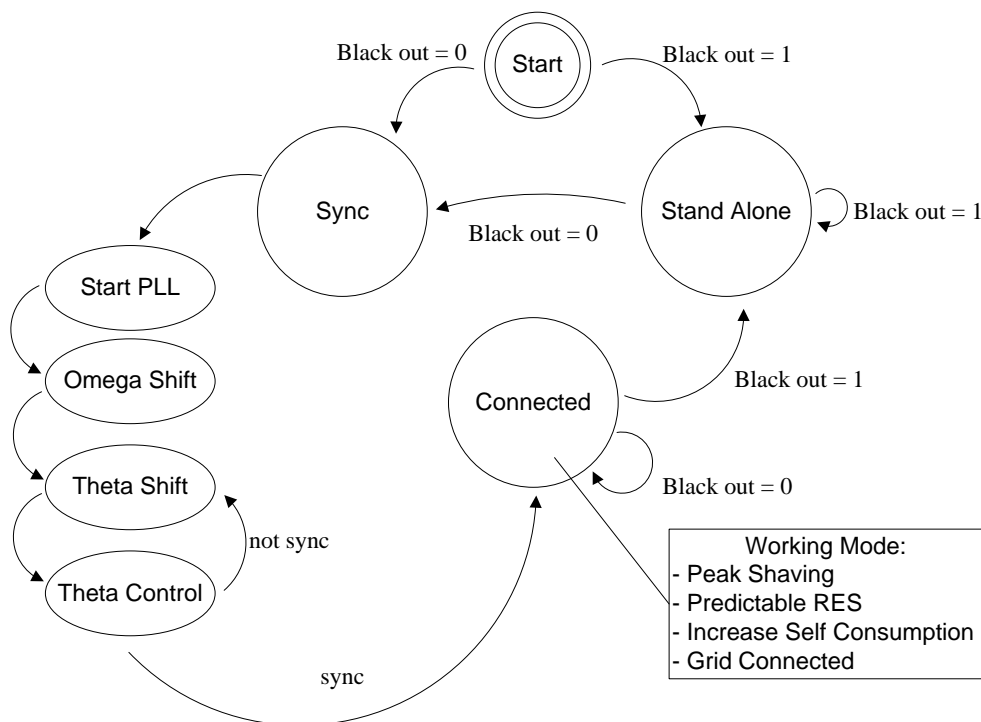
Figure 49 – Synchronism block Finite State Machine flow chart

PLL provides continuous information about the phase-angle and amplitude of the magnitude of interest, generally the fundamental grid voltage The first grid-
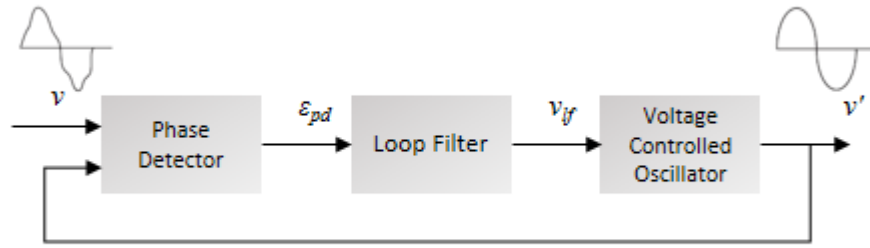
Figure 50 – Basic structure of a Phase-Locked Loop

connected power converters offered a low degree of control and were synchronized to the grid by detecting the zero-crossing of the grid voltage. This detection technique presents some drawbacks, such as inaccuracy and detection of multiple zero-crossings in the case of distorted grid voltage. Afterwards single phase PLL were adopted, but the bandwidth should be very low. To increase bandwidth were introduced quadrature PLL, Figure 51: the inquadrature error does not generate any steady-state oscillatory term, which allows the increase of PLL bandwidth. Inside block diagram of Figure 51 there is the Park transformation (4.2.3).
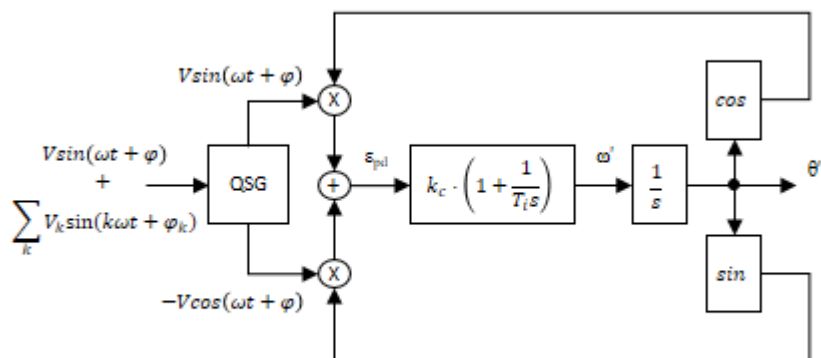
Figure 51 – Diagram of ideal QPLL. QSG is the ideal quadratur signal generator

61

$$\begin{bmatrix} v_d \\ v_q \end{bmatrix} = \begin{bmatrix} \cos(\Theta) & \sin(\Theta) \\ -\sin(\Theta) & \cos(\Theta) \end{bmatrix} \begin{bmatrix} v_\alpha \\ v_\beta \end{bmatrix}. \tag{4.3.3}$$

The real problem in single phase system is how to obtain the component β or rather how to realize the quadratur signal generator (QSG). In three-phase system it is relatively simple applying Clarke Transformation to phase voltages, but in single phase system one component is missing. The simple way to obtain the second component is to derive or insert a delay on the input signal. The implemented solution is based on use of inverse Park transformation. This approach entails the creation of a virtural component as output of inverse park transformation block used as input of the park transformation block. Angle theta obtained is finally used to generate the synchronization signal applied in the inverter PWM.
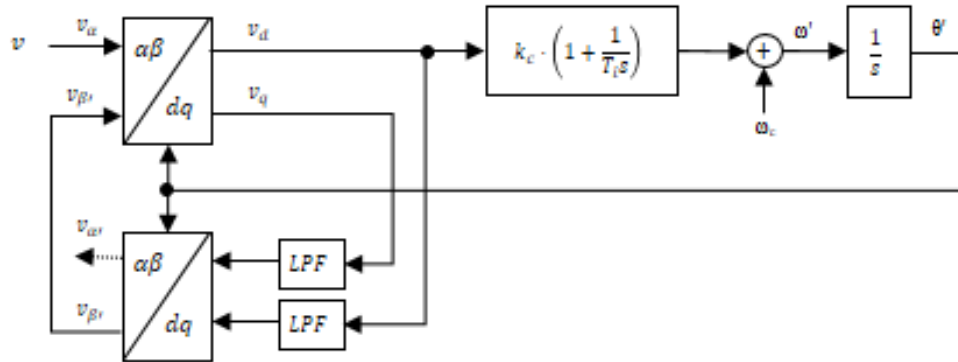
Figure 52 – PLL based on inverse Park transform

Grid interaction: power flux control

Into the flux control block is implemented algorithms dedicated to control the energy flux between household and the electriciy network. Algorithms can have different targets as maximization of self-consumption, improve electricity network stability or send energy to the grid only in high remunerative time slot. After an evaluation of measured signals, according to chosen target, the block output is a

current reference used as integration of the current control loop. Below are described three different algorithms of flux control considering power flow reduction, changing consumption profiles or changing production profiles.

- Grid zero control
- Consumption peak shaving control
- Limit generation peak control

The grid zero control objective aims to reduce unnecessary energy flows between the house and the grid. These unnecessary energy flows happen when locally generated energy is sent from the house to the grid that latter on is needed to be imported from the grid to the house. This objective is achieved by giving priority to store the generated energy locally prior to exporting it to the grid and, in complement, also giving priority to consuming the stored energy prior to importing it from the grid.

This implies that the generated energy not immediately consumed is sent to the storage system until it is full and the consumption that is not immediately satisfied by the local generation is supported by the storage system while it has not reached the minimum state of charge (SoC).
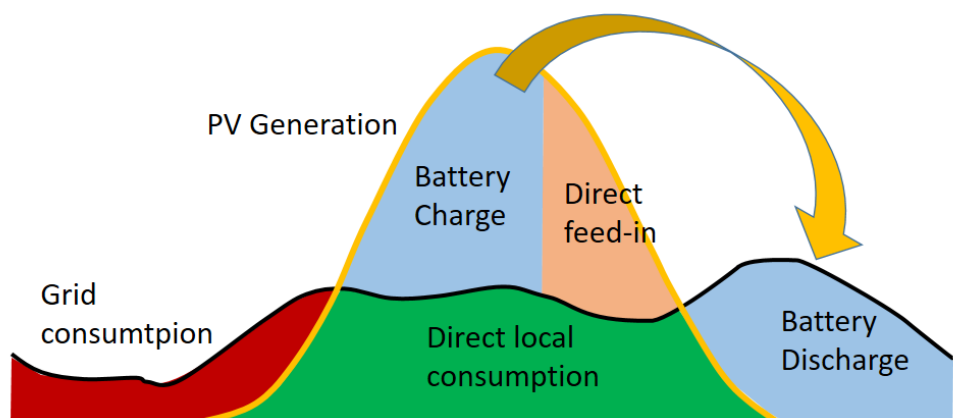
Figure 53 – Use of storage system to increase self consumption of energy generated by PV suorce, different destination of generated energy and sources to supply consumtpion

In consumption peak shaving control, energy storage objective aims to reduce the peaks of energy demand from the grid without affecting the consumption utilization. Within this objective, the house power demand from the grid is always limited to a desired value and all the consumption above that value is supported by the energy from the storage system.

The priority is given to the storage system having energy to support the consumption peaks, whenever needed. So the PV energy is only used to supply directly the consumption when it is above the desired peak and otherwise it is sent to the storage system. When no PV generation is available and extremely low state of charge, the storage system is also charged with energy from grid when the consumption is below the desired peak.

In limit generation peak control the storage system is used to guarantee that the power from PV generation sent to the grid is limited to a maximum value, thus avoiding the existence of export peaks. The existence of export peaks could become a problem for the grid management, since the PV generation peaks among all the houses in a distribution area are simultaneous.
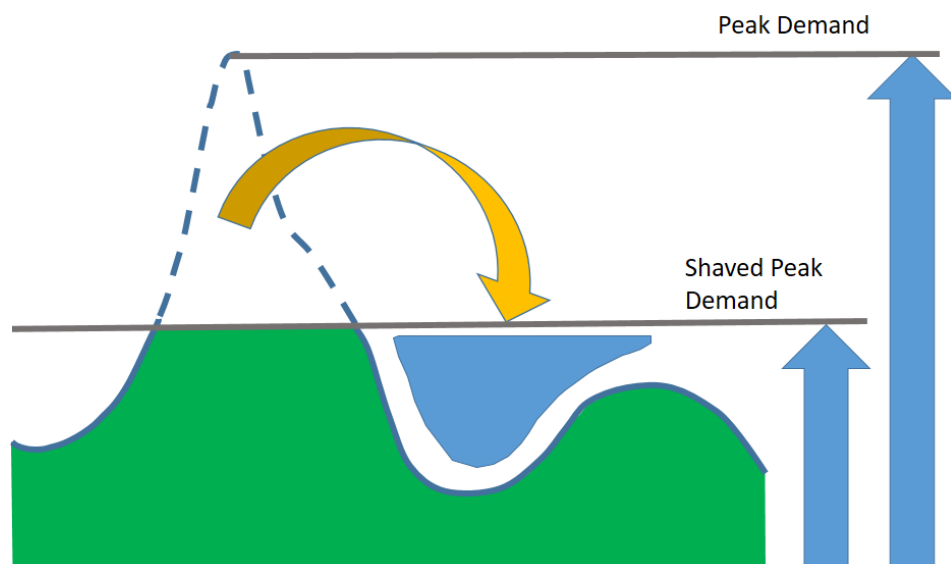
Figure 54 – Consumption peak shaving, general description diagram

The algorithm used for this objective uses the energy from the storage system whenever needed to supply the consumption, in order to keep the storage system at the minimum SoC, and sends energy to the storage system every time that the power from PV generation minus the actual consumption is above the export limit value desired.

The first two controls can be implemented through a power flow between the house and the grid feedback using an arbitrary reference value; in grid zero control the desidered vaule is zero, zero power flow between house and grid, instead in consumption peak shaving the reference is a positive value. The third control, limit generation peak, can be implemented using as feedback the inverter uotput power. In the next chapter, results of the described control algorithm will be provided.

Chapter 5.   Prototyping

In this chapter are reported a selection of the simulations done during the design step, components are listed structure and workbench implementation steps are shown. Workbench workability is preceded by sensorsors and components characterizations to identify parasitic effects and system delays; finally test done on the realized workbench are reported.

5.1 Simulation

Simulations are permformed in Matlab/Simulink environment using the Simscape/Simpower package: this package allow a good simulation quality of electrical behaviors and the possibility to implement complex digital control structures. It was impossible to simulate the system all at once due to high computational load; parallel simulations was performed combining system's modules using outputs from some simulations as input of the others. Block diagram showed in section 4.3 (Figure 46, Figure 47) can be used as reference of the simulations shown below.
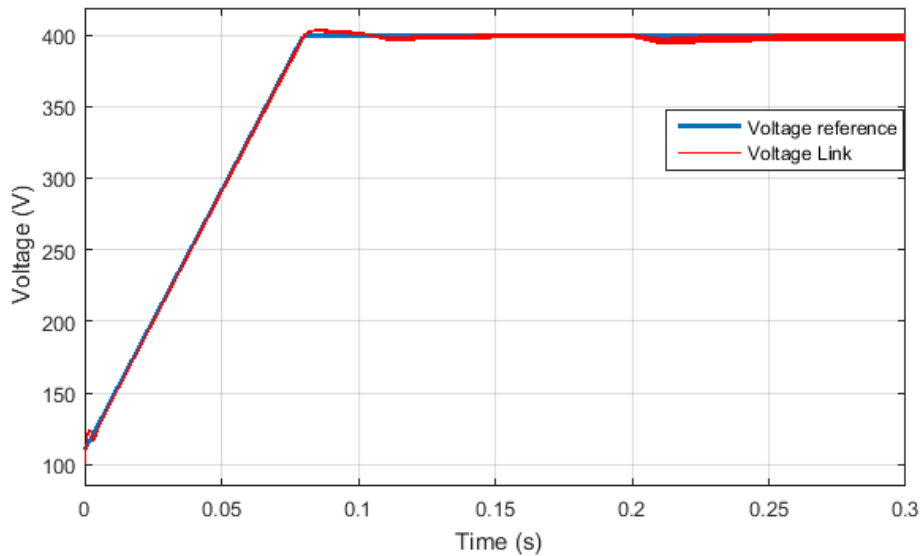
Figure 55 – DC-DC softstart control, reference voltage and measured voltage on link capacitor

Figure 55 shows the soft start control of DC DC converter: the blue line is the reference voltage of the voltage control loop, while red line is the output voltage on the link capacitors. The output of the external voltage loop is the current reference of the internal current loop. The current control works on the average value of the inductor current; Figure 56 shows DC-DC converter inductor current at a particular load: switching frequency is 40 kHz and current ripple is 5 A as designed in the previous section.
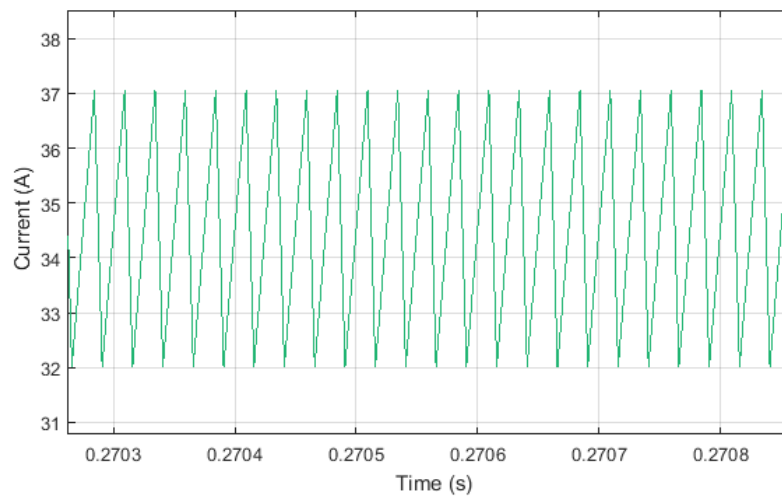
Figure 56 – Zoom in of battery DC-DC converter inductor current

The control band of the internal current loop must to be set at high frequency then, when the inner loop is correctly tuned, it is possible to tune the controller of the external voltage loop considering the loads dynamics. This method imply that the internal loop doesn't modify the behavior of the external one from magnitude and phase point of view.

The DC-DC converter load dynamincs is tied to inverter input current. The inverter works at 10 kHz and the output sinusoidal voltage is at 50 Hz. Figure 58 shows the current on the link capacitor when the inverter is working. It is possible to see the shape at 100 Hz, as a straighted sinusoid at 50 Hz, and the particular of the current shape at inverter switching frequency.
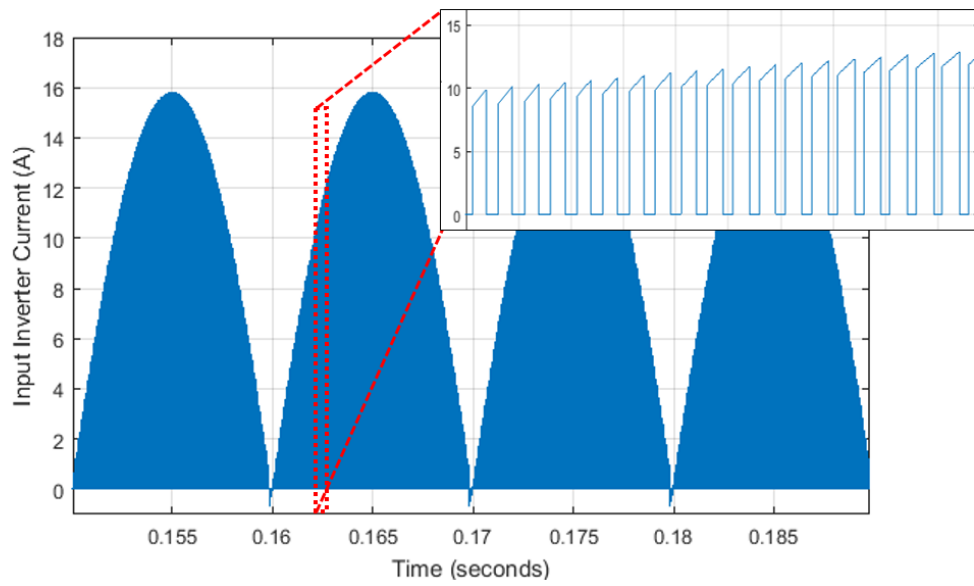
Figure 58 – Link capacitor current

Also the inverter control is based on a dual loop control structure: an internal current loop and an external power loop. Furthermore the reference of the internal loop is the combiantion of the power loop, which set the amplitude of the reference, and the synchronization block. Figure 57 shows the particular of the internal current loop. The reference signal change its amplitude and the current feedback, the inverter output current, follow the reference. Usually, in PV grid
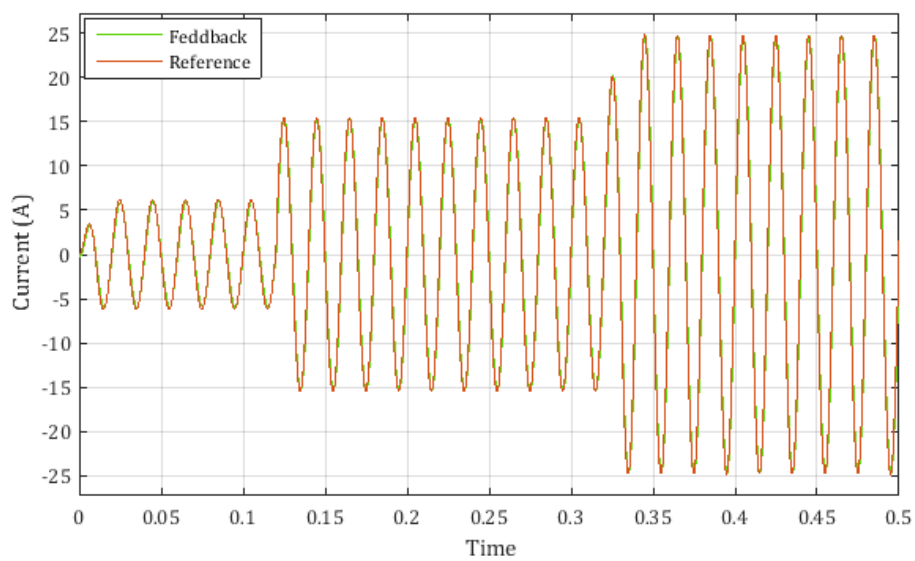
Figure 57 – Inverter current control loop of outtput current

connected inverter, the current reference is set to a fixed value: if the MPPT control is realized by converter near PV panel, the inverter follow the current reference with the limitation of not affecting the voltage on the link capacitor. In this case the current amplitude is variable in time and the voltage on the link capacitor is managed by the battery DC-DC converter. As deeply described in section 4.3 the external loop can have different target. In Figure 59 powers interaction it is shown in case of grid power limitation. This control algorithm can be realized usign as feedback signal the grid power: load is supply by inverter power while grid power is essentially constant. In this case the reference of the power control is set to an integer value, but it can be set to zero to obtained the grid zero control.
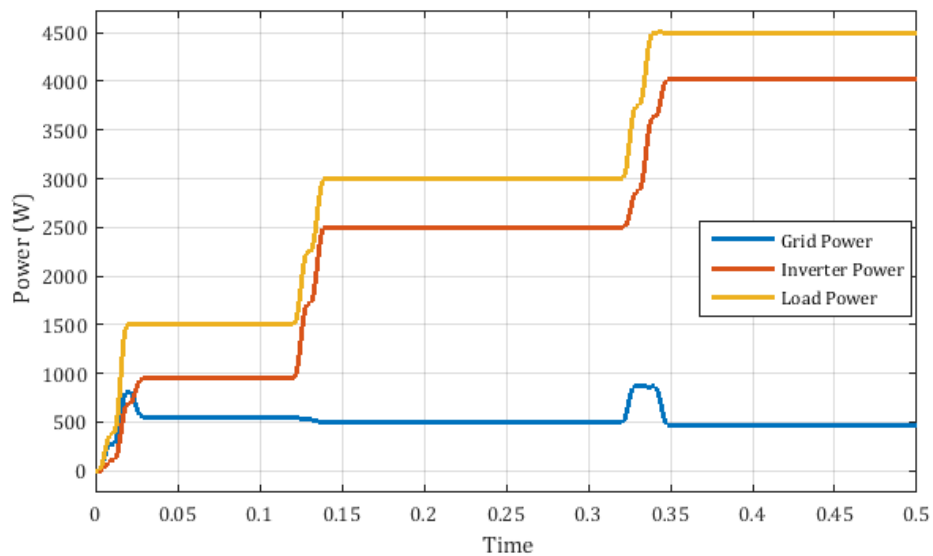
Figure 59 – Example of grid power control simulation

The phase reference of the internal current loop is given through a digital PLL. Figure 60 shows the comparison of two PLL in case of distorted reference signal. Both algorithms work using a virtual component shifted of 90° with the reference signal: in the first case the virtual component is realized with a deriving the reference, while the second case use an inverse Park transformation.
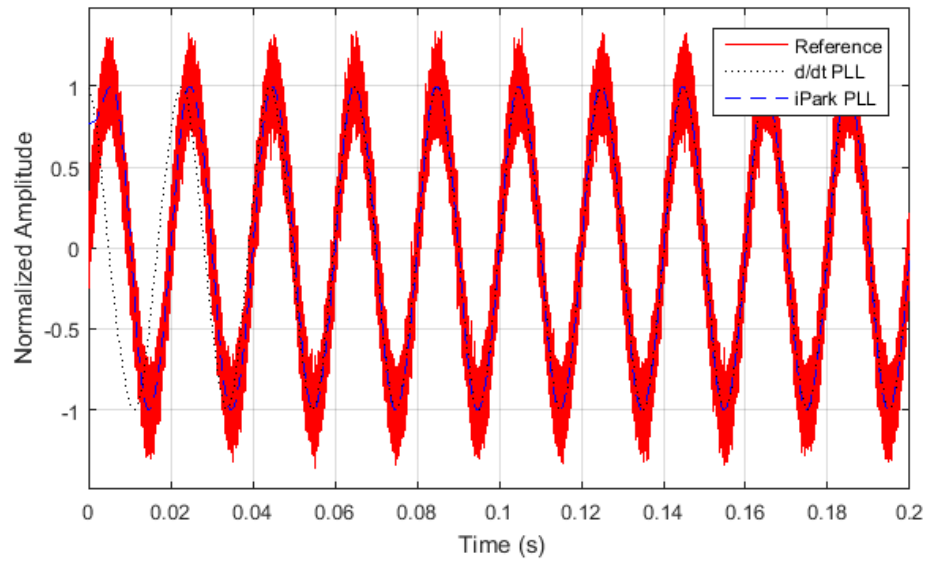
Figure 60 - Synchronization algorithms comparison in case of distorted reference signal

The Inverse Park approach follow the reference in the first period, while the derivative approach need two periods to reach the reference. Figure 61 shows the comparison of the angles calculated in both approaches. Manipolating the angles it is possible to correct delay introduced by passive components as the inverter output filter or to manage the power factor.
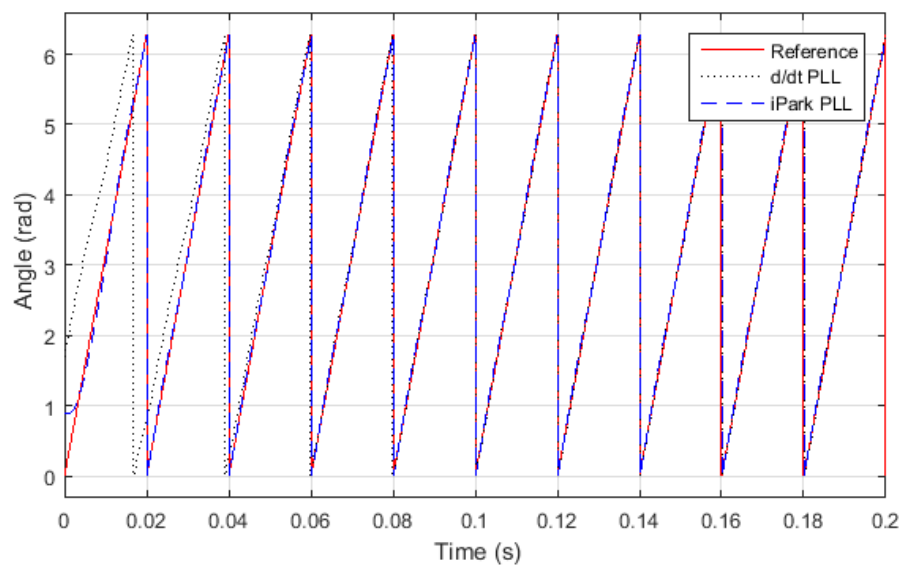
Figure 61 - Comparison of calculated angle of synchronization algorithms

5.2 Workbench
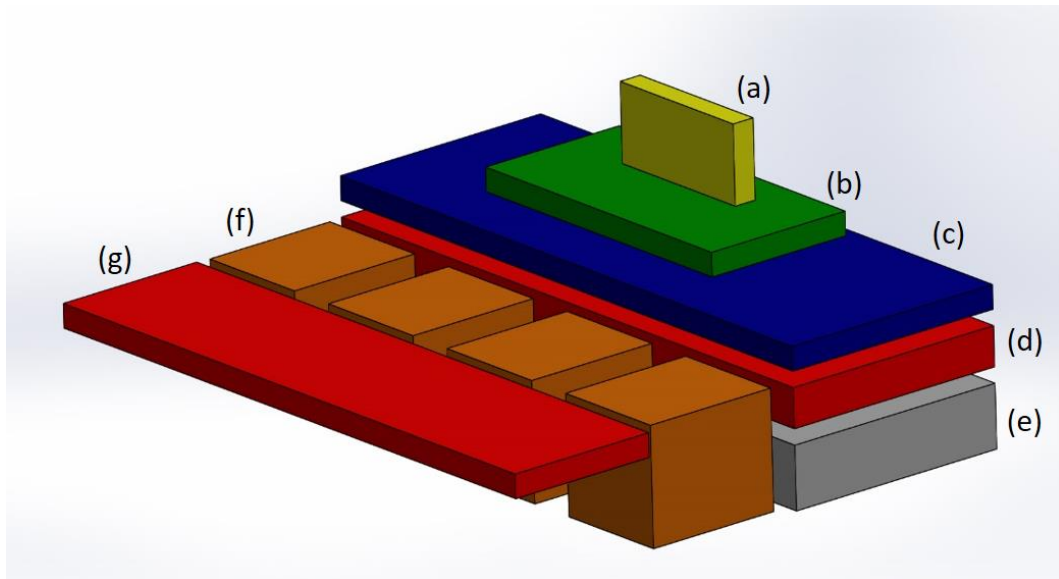
Figure 62 – Struture of the realized prototype. (a) control card, (b) carrier board, (c) driver board, (d) power board, (e) heat sink, (f) inductors, (g) sensor board.

Figure 62 shows the 3D structure of the prototype that is made up five boards (control card, carrier board, driver board, power board and sensor board), four inductors and the heat sink under the power board. Power input and output are all placed on the sensor board, that is dedicated as interface with the external envinment, while low power, control and logic input/output are placed on the carrier board.

Components and Characterization

Table 1 – List of Components

Component	Producer	Code	Max Voltage	Max Current	Max Temperature
IGBT	Fairchild	FGA40N65SMD	600 V	40 A	175 °C
Diode	Fairchild	RHRG5060	600 V	50 A	175 °C

Component	Producer	Code	Range	Note	Max Temperature
Current sensor	Allegro	ACS756	±50 A	Hall Effect	165 °C
Voltage sensor	Avago	ACPL-C87	0 ÷ 2 V	Optically Isolated	125 °C
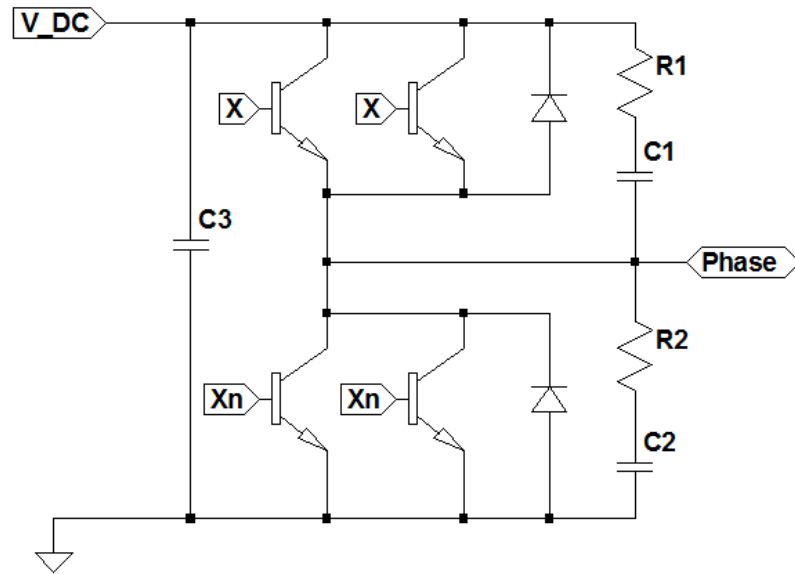
Figure 63 – Phase with passive snubber circuit schematic

In order to avoid current spikes when the switch is closing a little capacitance is placed near to switches between DC bus and ground, moreover two passive RC snubber circuit are placed alongside of switches to reduce oscillations during transitions, Figure 63.

Figure 64 shows the circuit schematic of voltagea sense. The component is optically isolated and require two isolated voltage sources. The first stage of measure is a voltage divider to be comply with the specific of input voltage, the outout stage is design to be comply with DSP and carrier board specifics.
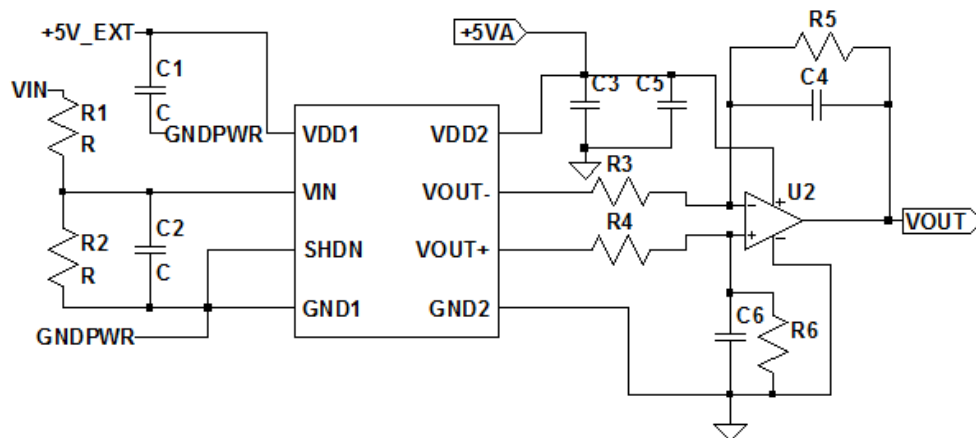
Figure 64 – Voltage sense circuit schematic using ACPL-C87

5.3 Results

In this section are reported oscilloscope acquisition of working converters. A programmable load it is used for this acquisition, whose maximum voltage is 400 V. Because of that the output voltage reference is set to a lower value.
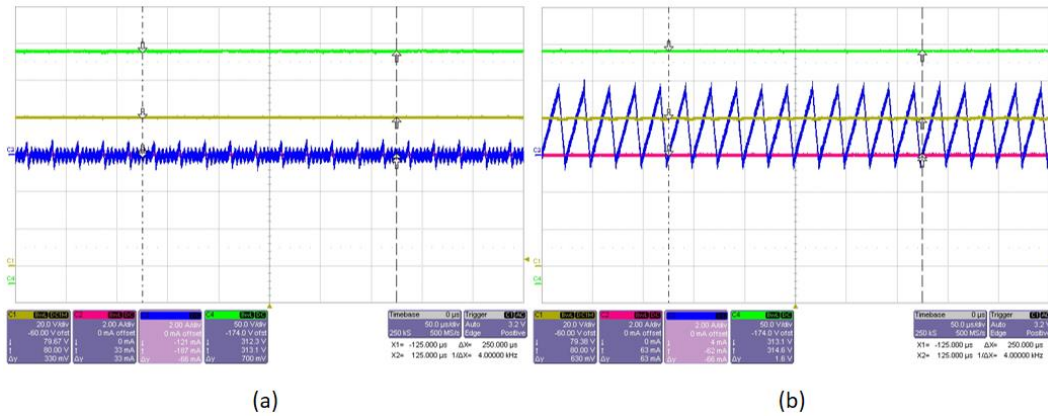
Figure 65 – Unidirectional DC-DC converter, one phase active, different operation mode.

Single phase operation of the unidirectional DC DC converter is shown in Figure 65, while Figure 66 shows the inteleaved operation of the same converter. Input voltage, output voltage and phase's currents are shown. Both DCM and CCM mode are shown. In case of DCM operation it is visible an oscillation due to an LC load used in during these tests. In case of two working phase switching commands are shifted of 180°; this shift is visible watching inductor currents.
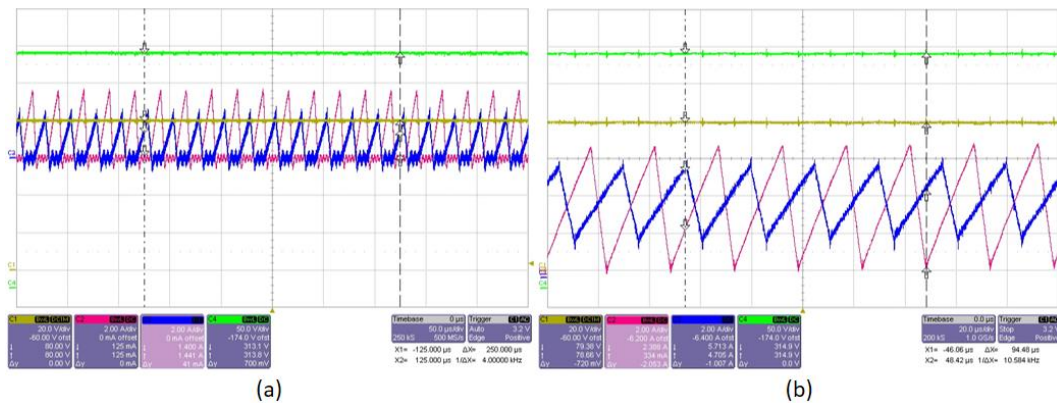
Figure 66 – Unidirectional DC-DC converter, two phase active, different operation mode.

(a)   (b)
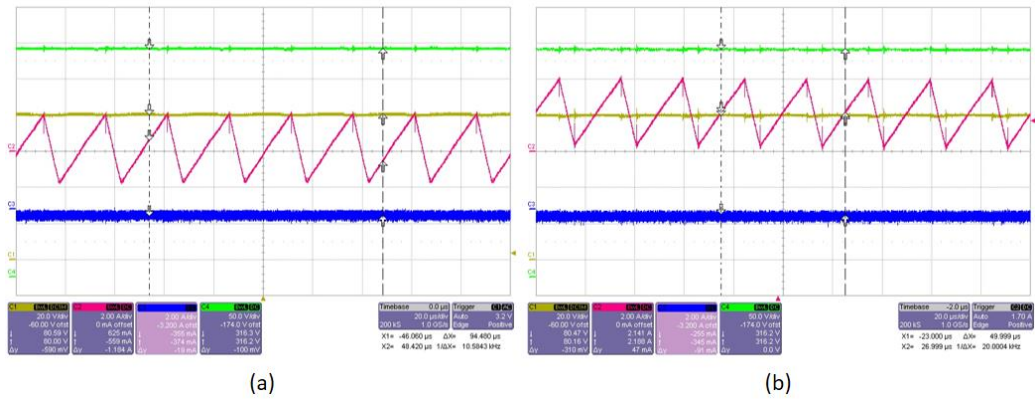
Figure 68 – Bidirectional DC-DC converter, one phase active, different operation mode

Figure 68 and Figure 67 report signals of the bidirectional DC-DC converter. Both DCM and CCM operation modes are shown. Due to the presence of the two switches, istead of one switch and one diode, during 'DCM' operation current can go under zero; the presence of the IGBT internal diode cause little current peak at commutation point. As in the case of the unidirection converter with two working phases the interleaved operation is used: phase command are shifted of 180°. In all test reported on DC-DC converters the output voltage is stable at different output power.

(a)   (b)
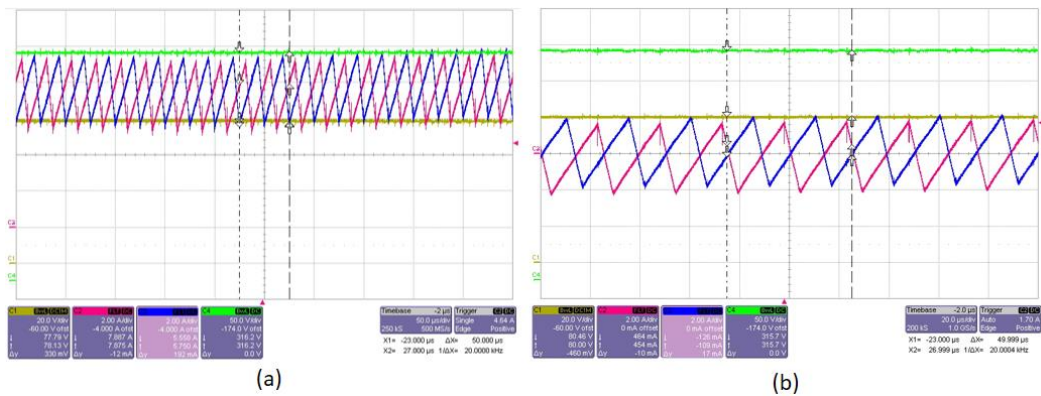
Figure 67 – Bidirectional DC-DC converter, two phase active, different operation mode

When two switches are working on the same phase, bidirectional DC-DC converter and inverter, it is important to set a dead time. In the follow are reported measurement of the dead time at different point of the control chain.
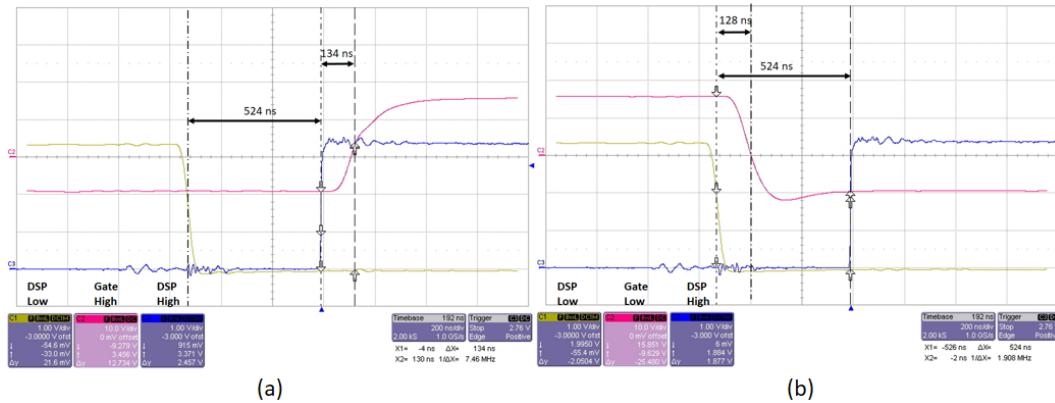
Figure 70 – Phase command chain; dead time at command level and driver delay. (a) IGBT high side (b) IGBT low side.

Figure 70 shows the dead time at the DSP output and the dealay introduced by the IGBT driver. Dead time has the same value during turn on and turn off, 524 ns. During turn on (a) driver delay is 134 ns, while during turn off (b) is 128 ns.
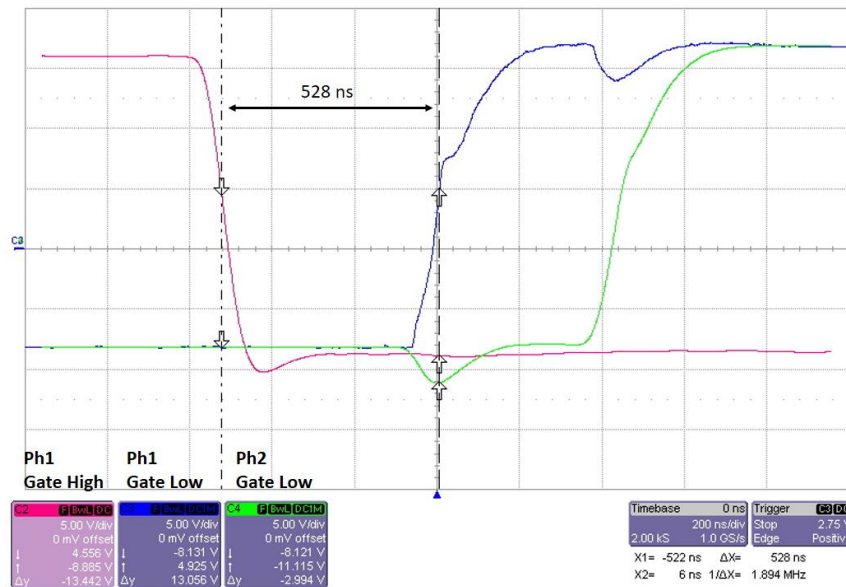
Figure 69 – Phase dead time at gate level, inverter acquisitions. (Red) Phase one high side gate; (Blue) Phase one low side gate; (Green) Phase two low side gate.

Figure 69 shows dead time at gate level, after IGBT drivers. To perform this measurement it is used one differential probe, on the high side gate, and two normal probe, on the low side (same ground level). Dead time measured on gates

is 528 ns. Looking at blue and green curves it is evident an interaction between gate voltages: during turn on phase there is a little fall on the other voltage.
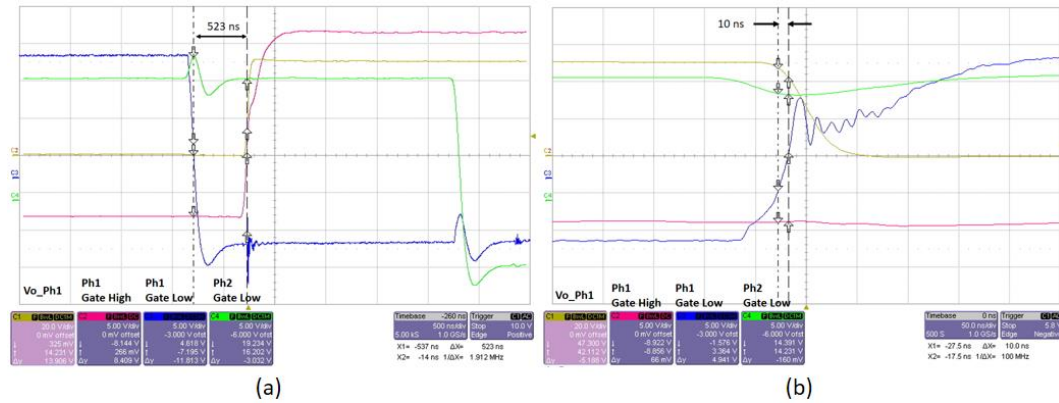
Figure 71 – Inverter dead time and diode conduction. (Yellow) Inverter phase one voltage; (Red) Phase one high side gate; (Blue) Phase one low side gate; (Green) Phase two low side gate

Figure 71 shows gates signals and the voltage on the phase (a). In (b) is measured internal diode conduction time, equal to 10 ns.

Moreover it is measured the system efficiency in open loop, Figure 72. Efficiency using one or two phases are compared with estimated switch losses calculated before.
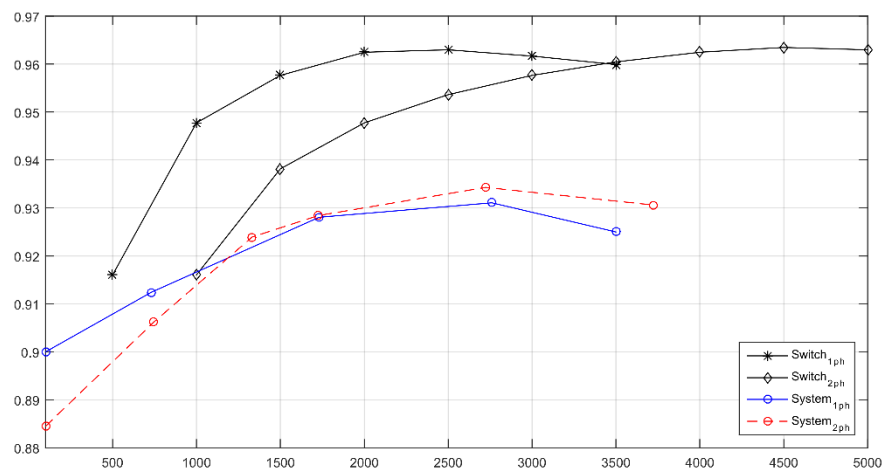
Figure 72 – Efficiencies comparison

Chapter 6.   Conclusion and future works

The motivation of this work thesis was the development of a feasible solution for a good and smart use of the energy. Trends of electricity generation from renewable sources show the need for new innovative solutions to reach the global target of CO_2 reduction and tackle climatic changes. Moreover distributed production, characterized by intermittent and unpredictable power profiles, has generated new issues for electricity network management. Energy storage are, always more, an interesting option to achieve these goals. They are becoming more popular together with the advent of electric vehicles and cost reduction of lithium – based accumulators. Energy storage systems use electronics converters that are characterized by faster dynamics than conventional power plants enabling them to balance fluctuations in the grid much more precisely and efficiently. This creates persuasive business cases. Energy storage systems provide a number of benefits and applications:

- Frequency regulation
- Voltage control
- Black start capability
- Short circuit capability
- Renewable energy integration (modeling of power gradients and stabilization of feed-in)
- Peak shaving
- Price arbitrage
- Can be used as an alternative or compliment to grid expansion

There are several companies that, during the last few years, added first storage systems in the company's portfolio to ride the wave of the moment (e.g. Kyocera, Panasonic, SMA, Tesla, Enetelus, Storelio), other companies base all their business on this applications as Younicos or Stem, but there are many others.

In this work thesis a modular energy storage system for residential applications was realized; the proposed system combine a renewable generator, an accumulator and the user or the electricity network. Electricity generation from renewable sources and residential consumptions are intermittent and variable, the chosen power stage topology allow to maximize system efficiency according to required powers. Modules are based on the duplication of H – bridge structure, in order to components system cost reduction, and multiphase operation. High gain interleaved converters and high current inductors were studied during the design and the workbench available maximum AC power is 5 kW.

It was implemented a DSP – based control structure to manage all converters with a single control unit. Implemented control algorithms allow a good power flow management and the integration in the electricity network or stand alone application. Acting on priority calls and control loops band it is created a multilayer control structure to guarantee safety and allow the different working modes.

System modularity and scalability was a key factor of all the design from a hardware and software point of view. Thanks to this approach it is possible to put in parallel more systems in order to increase maximum available power or connect additional sources or accumulators; moreover it is possible to change generators types (eolic turbines/hydraulic pumps) or storage technologies (flywheels/supercapacitors) using the same control structure and minor changes.

Keeping constant the actual configuration the realized workbench is an optimum candidate to test converters' control loops and their influence on a complex system. A natural evolution of this study is to thoroughly investigate benefits of energy storage in industrial applications, e.g. avoid peak power absorption during starting phases or particular processes. A fascinating future work is the virtualization of control unit higher layers in order to allow the implementation of more complex control algorithms. To the same extent, switches wilde bandgap technology must be taken into account in order to increase system efficiency.

Appendix

A. High current ferrite core losses

This appendix is dedicated to core losses estimation in case of direct current magnetization. There are two common methods for calculating core loss:

1. Hysteresis model
2. Empirical equations

Hysteresis models often introduce an intermediate step of calculating B-H loop. In the follow is reported a state of the art of main empirical equations method contributions. Emperical equation are often in the form of Steinmetz equation (A.1).
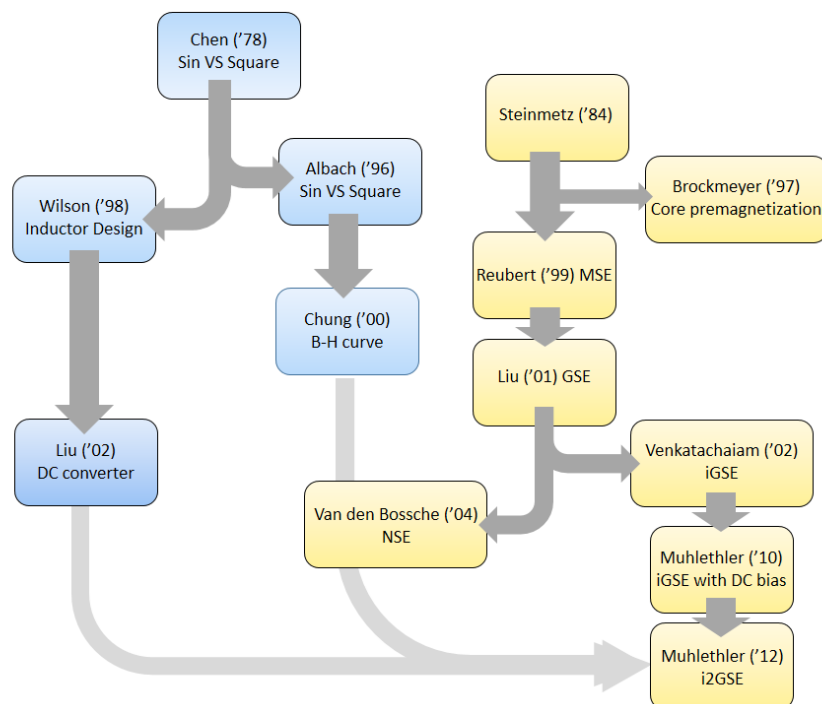
Figure 73 – Core losses estimation chronicle

1	Chen	*Comparison of the High Frequency Magnetic Core Losses under two different Driving Conditions: A Sinusoid Voltage and a Squarewave Voltage*	1978
2	Steinmetz	*On the law of hysteresis*	1984
3	Albach, Durbaum, Brockmeyer	*Calculating core losses in transformers for arbitrary magnetizing currents a comparison of different approaches*	1996
4	Brockmeyer, Neues	Frequency Dependence of the Ferrite-Loss Increase Caused by Premagnetization	1997
5	Wilson, Wilson, Owen	*Coupling of magnetic design choices to DC-DC converter electrical performance*	1998
6	Reinert, Brockmeyer, De Doncker	*Calculation of losses in ferro and ferrimagnetic materials based on the modified Steinmetz equation*	1999
7	Chung, Poon, Liu, Pong	*Analysis of Buck-Boost converter inductor loss using a simple online B-H curve tracer*	2000
8	Li, Abdallah, Sullivan	*Improved calculation of core loss with nonsinusoidal waveforms*	2001
9	Liu, Wilson, Wong	*A method for inductor core loss estimation in power factor correction application*	2002
10	Venkatachalam, Sullivan, Abdallah, Tacca	*Accurate prediction of ferrite core loss with nonsinusoidal waveforms using only Steinmetz parameters*	2002
11	Van den Bossche, Valchev, Georgiev	*Measurement and loss model of ferrites with non-sinusoidal waveforms*	2004
12	Mühlethaler, Biela, Kolar, Ecklebe	*Core losses under DC bias condition based on Steinmetz parameters*	2010
13	Mühlethaler, Biela, Kolar, Ecklebe	*Improved core loss calculation for magnetic components employed in power electronic systems*	2012

$$P_{core,losses} = k \cdot f^{\alpha} \cdot B^{\beta} \qquad\qquad (A.1)$$

where k, α and β are material dependent, namely Steinmetz parameters, and B is the magnetic flux density. These parameters are given in most datasheets for sinusoidal exitation, but they are not valid in case of non sinusoidal exitation.

In 1978 Chen compare magnetic core losses in case of different exitation (sinusoidal and squarewave), claims results experimentally confirmed by Albach in 1996. In the follow of Chen research fisrt Wilson and then Liu calculate core losses in case of DC-DC converter applications without consindering Steinmetz equations.

Others tried to generalize Steinmetz equation. Reinert, in 1999, with the Modified Steinmetz equation (MSE), then Li in 2001 with Generalized Steinmetz Equation (GSE), during Venkatachalam in 2002 with Improved Generalized Steinmetz
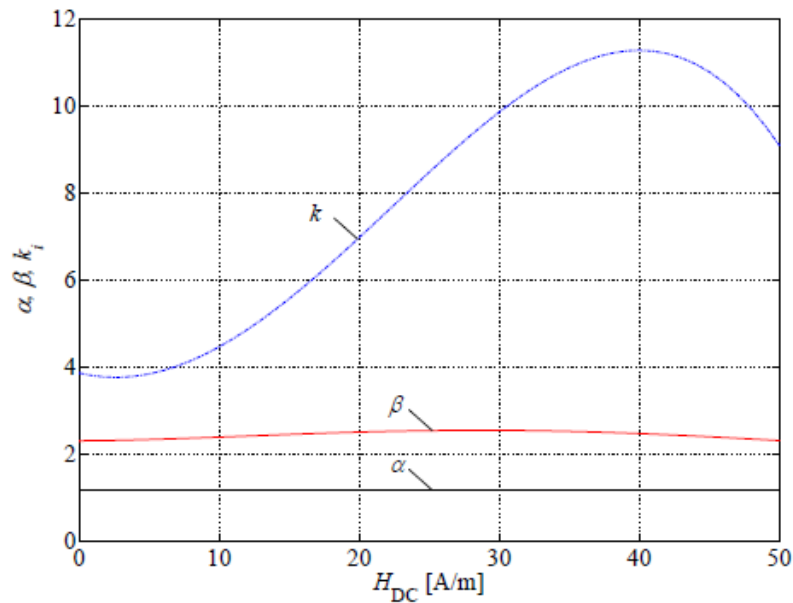
Figure 74 – Steinmetz parameters under DC bias conditions

Equation (iGSE) and Van den Bossche independently develop the Natural Steinmetz Equation (NSE) that maching exately the iGSE. Mühlethaler in 2010

shows that Steinmetz parameters α is independent from DC bias current, while parameters k and β change as a function of magnetic field intesity, (A.2).

$$H_{DC} = N \cdot \frac{I_{DC}}{l_{fe}}$$
(A.2)

In our case design the magnetic field intesity is extremely high also out of the analysis made in this paper. Finally Mühlethaler in 2012 present the improved-improved generalized Steinmetz equation (i²GSE) that have a better fitting of losses in case of low duty cycle.
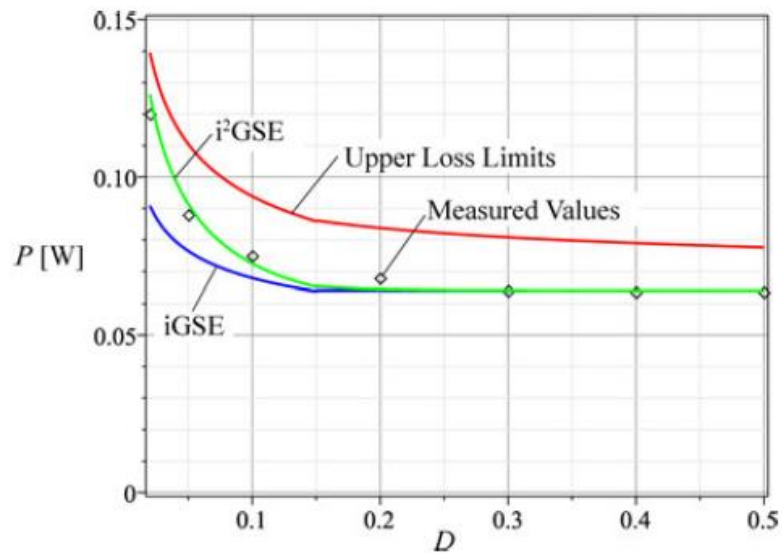
Figure 75 – Comparison between different core losses equations

B. Super efficient DC appliances

The U.S. ENERGY STAR program[5] collects the most efficient appliances of the U.S. market. The first television of the list is a LED 16 inches screen, with a declared annual consumption of 19 kWh (value related to an use of 5 hours per day). A super-efficient DC solution has four times lower consumption. Below some of the Global competition LEAP Awards 2014 winners are shown: the products featured in the Global LEAP Awards are among the best off-grid LED room lighting appliances and TVs in the World. TVs of the list have consume from 5 W to 10 W and LED lights of the list have consumption in the range 3 – 5 W.

Table 2 - Winners of Global LEAP Awards outstanding off-grid LED room lighting appliance competitions 2014. Global LEAP Award is a Clean Energy Ministerial initiative.

Model	LED-DC12V	SLL-L1903D	T5 Tube
Power	5 W	3 W	5 W
Category	LED Bulb	LED Indoor Fixture	LED Indoor Fixture
Rated Luminance	425 lm	310 lm	400 lm
CRI	82	70	82
Operating Voltage	12 V	8-18 V	12 V

Table 3 - Winners of Global LEAP Awards outstanding off-grid televisions competitions 2014. Global LEAP Award is a Clean Energy Ministerial initiative.

Model	SO16M	SO19M	UA23HG4060AR
Power	6 W	8 W	10 W
Category	Small TV	Medium TV	Large TV
Screen Size	671 cm^2	995 cm^2	1458 cm^2
Functional Voltage Range (Rated)	12-18 V	12-20 V	10.5-14.6 V

Thermal comfort is one of the most important service that electricity access could improve. In rural area, particularly in hot-humid climate, the thermal comfort could be improved by use of ceiling fan, in [43] is presented a general adaptation

---

[5] ENERGY STAR is a U.S. Environmental Protection Agency (EPA) voluntary program that helps businesses and individuals save money and protect our climate through superior energy efficiency. http://www.energystar.gov/about

method. Nevertheless, ceiling fans contribute significantly to residential electricity consumption. For example, in India, ceiling fan alone accounted for approximately 6% of residential energy use in 2000: this figure is expected to grow to 9% in 2020 [44]. In [45] is presented an analysis of the potential for improvement of ceiling fan components to reduce global energy consumption and greenhouse gas (GHG) emissions. Improved blade design, the increased use of brushless DC (BLDC) motors are identified as cost effective options to improve the efficiency of ceiling fans, with a potential power consumption saving of more than 50%. In [46] are listed the most efficient appliances, divided by category, specifying the best of research stage and of the market. Considering the best ceiling fan available on the market, it consumes 2W to achieve 19.3 m^3/min/W. The fan, with a diameter of 1.3 m, has different operating speed: minimum 49 rpm consuming 1.49 W, up to a maximum of 178 rpm consuming 14.81 W.

Another essential household service is the possibility to conserve foods. Among all refrigerators, available on market, it is possible to find efficient DC solutions. These appliances use variable speed drive (VSD) to eliminate periodic servicing and they are equipped with BLDC motor. The declared annual consumption can be less than 100 kWh. Obviously, refrigerator consumption is related to external ambient temperature and its usage (number of times that the door is open and duration). Below are shown different typical consumptions at different ambient temperatures.

Table 4 - Refrigerator daily consumption at different ambient temperature.

Ambient Temperature	Daily consumption
21 °C	168 Wh
32 °C	276 Wh
43 °C	432 Wh

Annual consumption at 21°C is 61 kWh, while it is 158 kWh with an ambient temperature of 43°C; the mean value between these two scenarios is 110 kWh/year.

C. Electricity consumption in rural areas

In [31] is reported that, for those that have electricity access in sub-Saharan Africa, average residential electricity consumption per capita per year is 317 kWh, 225 kWh excluding South Africa. Consumption per capita is significantly lower in rural areas, typically in the range of 50 to 100 kWh per year.

There is no single internationally accepted and adopted definition of household minimum electricity level of electricity. In [31] it is considered and initial threshold level of electricity consumption for rural household as 250 kWh, different is the threshold of [47] that assumes 120 kWh per person (600 kWh per household, assuming five people per household). While the Energy Sector Management Assistance Program (ESMAP) has led the development of a framework that categorizes household electricity access into six tiers based on supply levels (tier 0 being no electricity, tiers 4 and 5 being greater than 3 kW) and different attributes of supply. [48] In this analysis, first of all, is given a set of energy services using high efficient appliances, then it is obtained the household electricity consumption.

According to [49] the most important appliances in a rural area are:

- Lights;
- Mobile charger;
- Television;
- Refrigerator;
- Fan;

Table 5 summarized the used essential energy services, daily use and consumption; under the assumption of profiles similar to European consumption behavior, it is extracted from [50] the consumption profiles and in Figure 76 is represented the profile of a village with 200 households. Most of the energy

consumption is due to refrigerators and village peak consumption is reached in the evening with a value of 3.5 kWh.

Table 5 - User's energy services. First column energy services of the house, second appliances general information, third time of utilization and finally daily consumption of each appliances.

Energy Service	General info	Daily Use	Daily consumption
Lighting	2 x 300 lm	4 hours	12 Wh
Refrigerator	38.7 liters	24 hours	270 Wh
Television	15.6''	4 hours	22 Wh
Ceiling Fan	19.3 m^3/min/W	8 hours	16 Wh
Mobile phone charger	2600 mAh	One charge per day	12 Wh
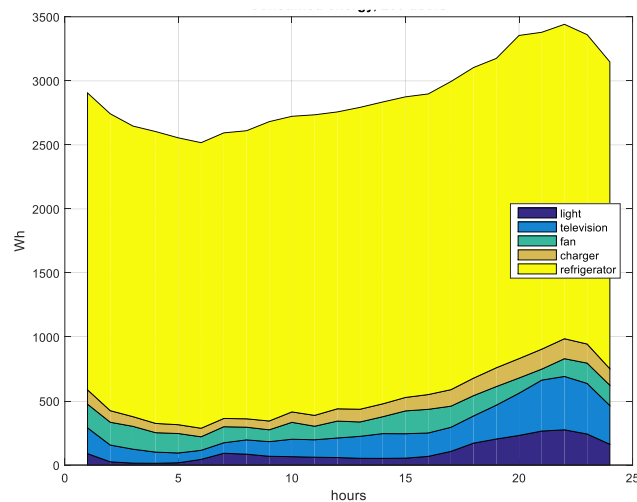
Figure 76 - Consumption breakdown of a village with a limited set of appliances, 200 users.

Daily consumption, for a single house, is 340 Wh, whose 270 Wh due to refrigerator. Annual total consumption is 124 kWh and refrigerator, alone, consumes 100 kWh: 80% of consumption is caused by refrigerator. These values will be used in next sections as parameters to optimize solar power system and storage.

D. Energy storage system optimization for rural area application

Use of renewable energy sources to increase electricity access require an evaluation based on the available natural resources. Solar resource needs to be taken into account in the precise location of the new microgrid. There are several database[6], in particular, NREL dataset is made up hourly data of all days of the year. For a limited number of location, irradiation data are related to ambient temperature. Figure 77 shows a post-processing of the dataset: irradiance daily values are shown. Each graph represent one month. Johannesburg is the selected location of the analysis.
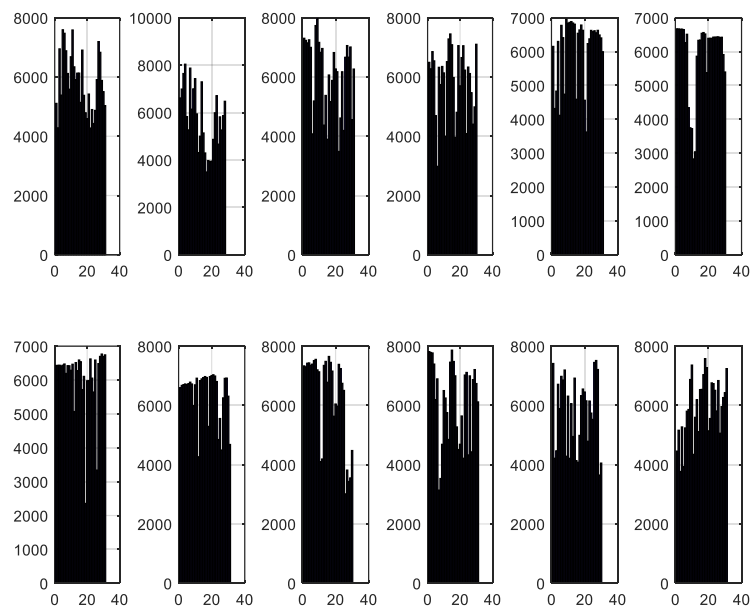
Figure 77 - Johannesburg, daily irradiance, all days of the year clustered in months (elaboration from NREL database).

In Figure 78 maximum, minimum, median and average values calculated based on monthly data, for each month, are shown. The daily absolute minimum irradiance

---

[6] NASA SSE, HelioClim-1, NCEP/NCAR, World Radiation Data Centre, NREL/USA, SWERA, SOLEMI, Meteonorm, SolarGIS, SRRI, PVGIS, Climate-SAF PVGIS

is in July, 2.3 kWh/m^2, while the absolute maximum is in February, 8 kWh/m^2. The average irradiance is around 6 kWh/m^2/day.
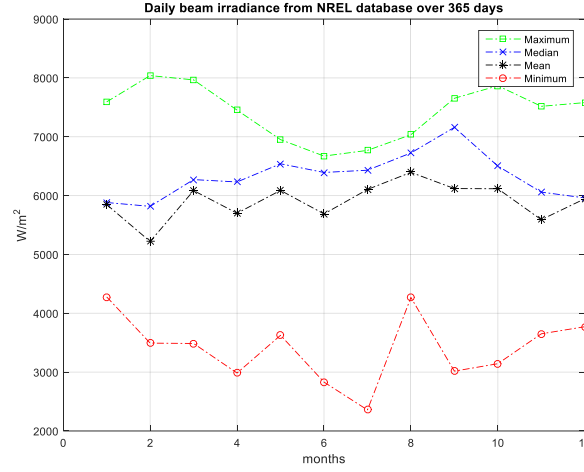
Figure 78 - Johannesburg, daily irradiance. For each month are calculated maximum, median, average and minimum values.

These data values are necessary to design PV system nominal power, but they are not sufficient. In order to correctly design a solar home system, the production/consumption mismatch must be taken into consideration, particularly in the periods of the year with less solar radiation. With poor design black-out events can occur. Figure 79 shows the suggest power system block diagram.. Equation (D.1) defines solar plant nominal power and in (D.2) is defined variable 'μ_{tot}', that is the total daily efficiency, as function of simultaneous production and consumption percentage 'd'.

$$P_N \geq \ E_{consumption} \cdot G_{STC} \cdot \mu_{tot} \ /G \tag{D.1}$$

$$\mu_{tot} = \left(\frac{d}{\mu_{drt}} + \frac{1-d}{\mu_{drt} \cdot \mu_{stg}} \right) \tag{D.2}$$

where 'G' is daily irradiance, 'G_{STC}' is irradiance in standard test condition (STC)[7] and '$E_{consumption}$' is the daily energy consumption. 'μ_{drt}' is the system efficiency

---

[7] G_{STC} is 1000 Wh/m^2
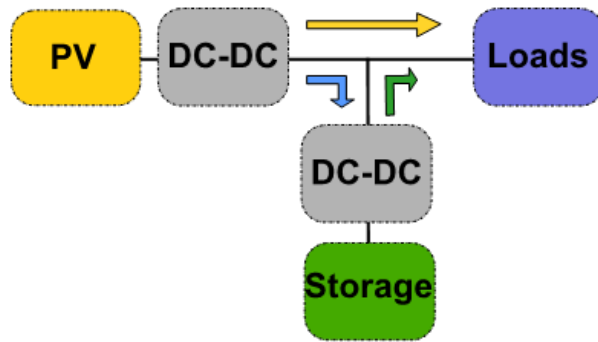
Figure 79 - Power system block diagram

in case of simultaneous production and consumption and 'μ_{stg}' is the storage round-trip efficiency, including its own converter.

In Table 6 assumed efficiencies are reported. Temperature efficiency, that models the reduction of generated power introduced by high ambient temperature, is an average value calculated from temperature profiles of NREL database. Table 7 shows the variation of daily total efficiency, when changing simultaneous production/consumption percentage according to equation (D.2). This percentage change with user's consumption behavior.

Table 6 – Estimated System's efficiencies

Efficiency	
Temperature	0.98
MPPT	0.99
PV converter	0.97
Wire & Connections	0.95
Storage	0.95
Storage Round trip	0.90
Storage converter	0.96

Table 7 - Equivalent total efficiency variation with different direct consumption percentage

d	μ_{tot}
10%	0.7939
20%	0.8050
30%	0.8161
40%	0.8273
50%	0.8384

Table 78 shows solar PV nominal power, calculated according to (D.1), changing daily irradiance and simultaneous production/consumption percentage. Using as irradiance the absolute daily minimum, in column two, the largest nominal power is obtained: this approach is the most conservative, leading to an oversizing of the solar power plant. Almost all days of the year, there is an energy over production, which is in excess of household consumption

Table 8 - Minimum nominal power of solar PV changing percentage of direct consumption and daily irradiance. Abs max G is the absolute maximum irradiance, Abs min G is the minimum absolute irradiance, Avg G is the average irradiance.

$P_N(d,G)$	Abs max G 8 kWh/m^2	Abs min G 2.4 kWh/m^2	Avg G 6.3 kWh/m^2
d = 0.1	53 W	178 W	67 W
d = 0.2	52 W	176 W	66 W
d = 0.3	51 W	174 W	65 W
d = 0.4	51 W	171 W	64 W
d = 0.5	50 W	169 W	63 W

Equation (D.3) is used to find the minimum energy of the storage, where 'DOD' is the depth of discharge, which is necessary to avoid safety problem and increase battery lifetime. Energy consumption profiles is taken from Appendix (C). In order to increase reliability it is performed an analysis over a whole year. Figure 80 shows daily overproduction (total production minus household consumption considering efficiencies) for each month and day of a year. System's parameters are 95 W of PV nominal power and a storage capacity of 300 Wh, calculated by (D.3) Values under zero are black out events.

$$E_{storage} \geq E_{consumption} \cdot (1 - d) \cdot [1 + \min(DOD)] \qquad \text{(D.3)}$$
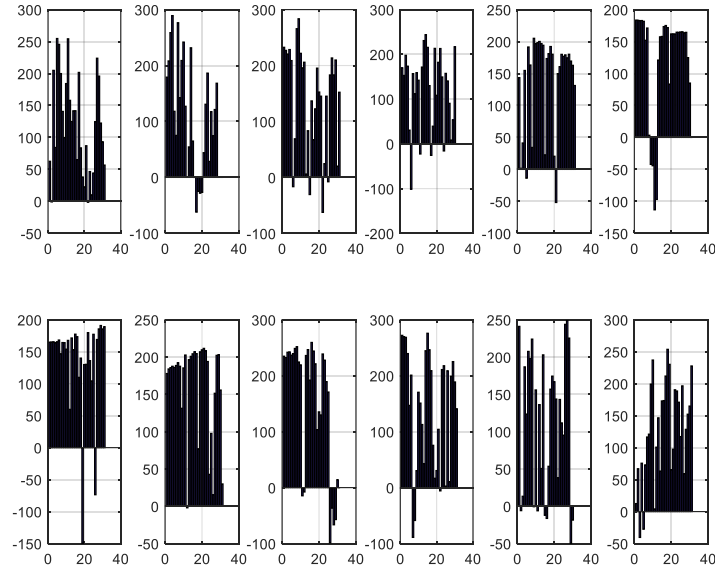
Figure 80 - Energy overproduction with 95 W of PV nominal power and 300 Wh of storage, in Johannesburg.

Black-out events occurs because equation (D.3) is true only in case of PV nominal power calculated using the absolute minimum irradiance, column two of Table 8 . In order to design a storage system with other PV nominal powers and avoid black-out events it is necessary to add a correction factor, equation (D.4)

$$E_{storage} \geq E_{consumption} \cdot (1 - d) \cdot [1 + \min(DOD)] + \max(\sum E_{blackout}) \qquad \text{(D.4)}$$
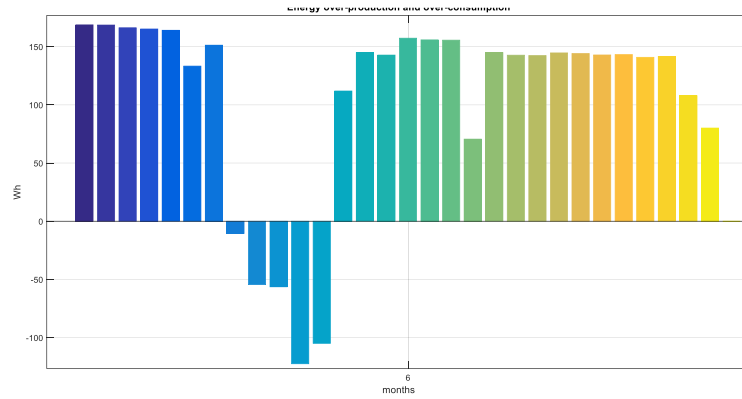
Figure 81 - Greatest event of consecutive blackouts of the year. PV nomial power 95 W, storage size 300 Wh. Each bar represents a day of June.

'$E_{blackout}$' is the daily missing energy. Over the year the maximum missing energy of consecutive days is taken. In this particular simulation, the worst case is in June, Figure 81. The sum of consecutive missing energy daily values, in June, is 350 Wh. With an adequately designed battery, it is possible to store energy over produced in days before the critical period, and then use it in low irradiance days. In case of the storage is completely charged, it is possible to use the energy excess to supply ancillary services as water pumps and water purification systems

Figure 82 shows the relation between solar PV nominal power, storage size and monthly cost of energy. Energy cost is the amortization of system considering life time. Included costs are PV module [11], storage [8] and power electronics equipment (converters, balancer, installation) as a percentage of module and storage costs. The estimated lifetime of all system is conservatively assumed to be
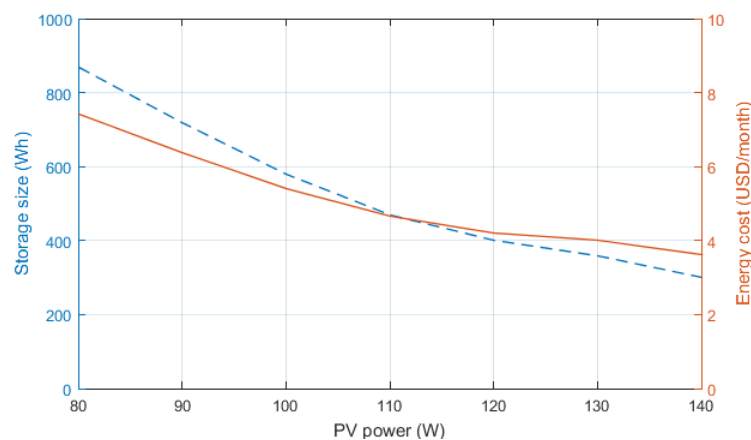
Figure 82 – Storage size and monthly system cost function of PV nominal power.

10 years. Designing solar power systems in such a way to minimize storage size is the most cost effective solution. Monthly cost of energy is in all design options lower than 8 USD, values under 5 USD can be affordable cost also for households in poor areas.

E. Pay Back of Energy Storage: Italian case

The aim of this appendix is to quantify the profit margin derivating by the use of an energy storage system. The analysis is based on Enel tariffs.[8] Tariff for residential costumers two-rate time of day tariff are reported in Table 9, with a contractual peak power up to 3 kW, and **Errore. L'origine riferimento non è stata trovata.**, with a contractual peak power over 3 kW. The tariff has two main parts energy matter (a) and network services (a) and different categories inside each one. collect similar costs.

Table 9 – Enel Energy cost drawback in case of contractual peak power up to 3 kW

|				Transport and meter management	System burden
(a)	Fixed part		€/month	2.365300	
	Energy part	F1	€/kWh	0.065010	
		F23	€/kWh	0.058290	
		< 1800 kWh	€/kWh	0.001640	
		< 2640 kWh	€/kWh	0.009760	
		< 4400 kWh	€/kWh	0.021340	
		> 4400 kWh	€/kWh	0.021340	
(b)	Fixed part		€/month	1.200100	0
	Power part		€/kW/month	0.838000	0
	Energy part	< 1800 kWh	€/kWh	0.007160	0.039402
		< 2640 kWh	€/kWh	0.032660	0.057802
		< 4400 kWh	€/kWh	0.069080	0.082592
		> 4400 kWh	€/kWh	0.069080	0.082592

Table 10 - Enel Energy cost drawback in case of contractual peak power over 3 kW

				Transport and meter management	System burden
(a)	Fixed part		€/month	3,418600	
	Energy part	F1	€/kWh	0,065010	
		F23	€/kWh	0,058290	
(b)	Fixed part		€/month	1,609100	0,000000
	Power part		€/kW/month	1,807500	0,000000

---

[8] https://www.enelservizioelettrico.it/it-IT/tariffe/uso-domestico (13/04/2016)

		< 1800 kWh	€/kWh	0,026170	0,082592
	Energy part	< 2640 kWh	€/kWh	0,042590	0,082592
		< 4400 kWh	€/kWh	0,042590	0,082592
		> 4400 kWh	€/kWh	0,042590	0,082592

Table 11 shows the comparison between yearly tariff in case of peak power of 3 kW or 4.5 kW and four consumption. Total yearly cost will be function of which time slot energy is consumed, Figure 83.

Table 11 – Tariff comparison of different contractual peak power

		3 kW	4.5 kW
Fixed	€/month	6,079400	13,161450
F1		0,065010	0,065010
F23		0,058290	0,058290
1800 kWh	€/kWh	0,048202	0,108762
2640 kW		0,100222	0,125182
4400 kW		0,173012	0,125182
6500 kW		0,173012	0,125182
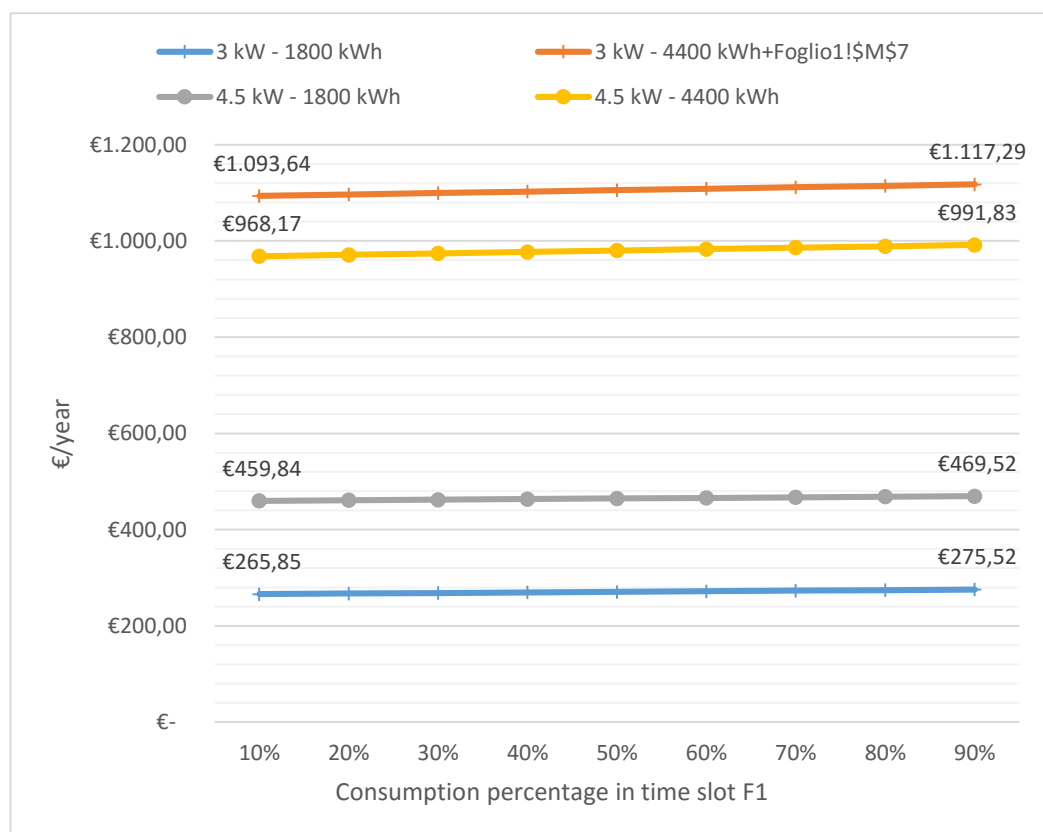
Figure 83 – Energy cost function of time slot. Comparison of different peak power.

Installing an energy storage system it is possible to shift residential consumtion from F1, higher cost, to F23, lower cost. Considering fixed the yearly consumption (no change of habits) saved money are only 9.68 €/year, with an annual consumtpion of 1800 kWh, and 34.94 €/year, with an annual consumption of 6500 kWh. This profit margin is too little to justify an investement.

In case of 1800 kWh yearly consumtpion passing from a peak power of 4.5 kW to 3 kW save among 200 €, while with 6500 kWh of yearly consumption it is possible to save among 200 € passing from 3 kW to 4.5 kW.

Greatest profit margin it is reached, more than 650 €/year, in case of:

- Consumption reduction (or using own supply)
- Changing peak power
- Load shifting

Acknowledgement

Firstly, I would like to express my sincere gratitude to my parents, Marco e Marina, and all my family to always believe, motivate and support me. I thank all the Mechatronics Laboratory staff; Mirko, Diego and Luca with whom I worked on this project, senior members that helped me so much answering to all my doubts and questions and my fellow labmates for the stimulating discussions and for all the fun we have had in the last three years. My sincere thanks also goes to FLAG-MS staff. I would like to thank all the staff of Istitute of Systems and Robotics in particular the person of the director, professor Anibal T. de Almeida, for his guidance during my period abroad and Mahmoud Tavakoli that has welcome me in the university, in his family and show me the amazing Coimbra. Last but not the least, an enormous thanks to my beautiful wife Silvia that support and endure me throughout writing this thesis and to my son Giovanni that completely changed my mind. My work is for both of you.

List of References

[1] T. B. Reddy and D. Linden, Linden's Handbook of Batteries, Fourth ed., New York: The McGrau-Hill, 2011.

[2] B. Sorensen, Renewable Energy Conversion, Transmission and Storage, Elsevier, 2007.

[3] R. Faria, P. Marques, R. Garcia, P. Moura, F. Freire, J. Delgado and A. T. de Almeida, "Primary and secondary use of electric mobility batteries from a life cycle perspective," *Journal of Power Sources,* vol. 262, pp. 169-177, 15 Semptember 2014.

[4] J. Neubauer and A. Pesaran, "The ability of battery second use strategies to impact plug-in vehicle prices and serve utility energy storage applications," *Hournal of Power Sources,* vol. 192, no. 23, pp. 10351-10358, 2011.

[5] G. Lacey, G. Putrus and A. Salim, "The use of second life electric vehicle batteries for grid support," in *EUROCON, 2013 IEEE*, Zagreb, 2013.

[6] J. Makansi and J. Abbound, "Energy storage: the missing link in the electricity value chain," ESC, 2002.

[7] D. Boero, D. Gandini, M. Chiaberge and M. De Giuseppe, "Energy storage system for domestic peak shaving," in *Power electrinics EE2013*, Novi Sad, 2013.

[8] A. K. Srivastava, R. Zamora and D. Bowman, "Impact of distributed generation with storage on electric grid stability," in *Power and energy society general meeting*, San Diego, 2011.

[9] M. Beaudin, H. Zareipour, A. Schellenberglabe and W. Rosehart, "Energy storage for mitigating the variability of renewable electricity sources: an updated review," *Energy for sustainable development,* vol. 14, no. 4, pp. 302-314, 2010.

[10] Energy commision of California, "220 strategic analysis of energy storage in California," Tech. Rep. CEC, 2011.

[11] Zpryme research & coulsulting, "Energy storage: Asian system & apps," 2012.

[12] J. Eyer and G. Corey, "Energy storage for the electricity grid: benefits and market potential assessment guide," Tech. Rep. Sandia National Laboratories, 2010.

[13] P. Denholm and R. M. Margolis, "Evaluating the limits of solar photovoltaics (PV) in electric power systems utilizing energy storage and other enabling technologies," *Energy Policy,* vol. 35, no. 9, pp. 4424-4433, 2007.

[14] G. Mulder, F. De Ridder and D. Six, "Electricity storage for grid-connected household dwellings with PV panels," *Solar Energy,* vol. 84, no. 7, pp. 1284-1293, 2010.

[15] R. Dufo-Lopez and J. L. Berna-Augustin, "Techno-economic analysis of grid-connected battery storage," *Energy Conversion and Management,* vol. 91, pp. 394-404, 2015.

[16] R. Dufo-Lopez and J. L. Bernal-Augustin, "Techno-economic analysis of grid-connected battery storage," *Energy Conversion and Management,* vol. 91, pp. 394-404, 2015.

[17] A. Zeh, M. Rau and R. Witzmann, "Comparison of decentralised and centralised grid-compatible battery storage systems in distribution grids with high PV penetration," *Progress in photovoltaics,* vol. 24, no. 4, pp. 496-506, 2016.

[18] R. Luthander, J. Widén, D. Nilsson and J. Palm, "Photovoltaic self-consumption in buildings: A review," *Applied Energy,* vol. 142, pp. 80-94, 2015.

[19] J. Moshovel, K.-P. Kairies, D. Magnor, M. Leuthold, M. Bost, S. Gahrs, E. Szczechowicz, M. Cramer and D. U. Sauer, "Analysis of the maximal possible grid relief from PV-peak-power impacts by using storage systems for increased self-consumption," *Applied Energy,* vol. 137, pp. 567-575, 2015.

[20] P. Bronski, J. Creyts, M. Crowdis, S. Doig, J. Glassmire, L. Guccione, P. Lilienthal, J. Mandel, B. Rader, D. Seif, H. Tocco and H. Touati, "The economics of load defection," Techinical Report Rocky Mountain Institute, 2015.

[21] C. Liu, J. Kan, Y. Zhi, W. Li, J. Sun, G. Cai and J. Wang, "Reliable transformerless batteru energy storage system based on cascade dual-boost/buck converters," *IET Power Electronics,* vol. 8, no. 9, pp. 1681-1689, 2015.

[22] E. Babaei and O. Abbasi, "Structure for multi-input multi-output dc-dc boost converter," *IET Power Electronics,* vol. 9, no. 1, pp. 9-19, 2015.

[23] G. Deepak, M. J. B. Reddy and D. Mohanta, "Hardware Implementation of Grid Connected PV System with Energy Management Scheme," in *Environment and Electrical Engineering (EEEIC)*, Wroclaw, 2013.

[24] V. Scarpa and P. Cortes Lopez, "Marching Circuit Topologies and Power Semiconductors for Energy Storage in Photovoltaic Systems," *Bodo's Power System,* pp. 60-62, September 2014.

[25] B. S. Borowy, L. F. Casey, G. H. Davis and J. Rajda, "Advanced Semiconductor Impact on Distributed Generation, Energy Storage and the Utility Grid," in *Power Engineering Society Genral Meeting*, Tampa, 2007.

[26] N. C. Sintamarean, E. P. Eni, F. Blaabjerg, R. Teodorescu and H. Wang, "Wide-Band Gap Devices in PV System - opportunities and challenges," in *International Power Electronics Conference*, Hiroshima, 2014.

[27] S. Jahdi, O. Alatise and P. A. Mawby, "The impact of silicon carbide technology on grid-connected Distributed Energy resources," in *IEEE PES ISGT Europe 2013*, Lyngby, 2013.

[28] U. Schwarzer, S. Buschhorn and K. Vogel, "System Benefits for Solar Inverters using SiC Semiconductor Modules," in *PCIM Europe 2014; International Exhibition and Conference for Power Electronics, Intelligent Motion, Renewable Energy and Energy Management; Proceedings of*, Nuremberg, 2014.

[29] S. Ugarte, J. Larkin and B. v. d. REE, "Energy storage: which market designs and regulatory incentives are needed?," Policy Department A: Economic and Scientific Policy, 2015.

[30] IEA, "World Energy Outlook," 2014.

[31] IEA, "Africa Energy Outlook," 2014.

[32] World Health Organization (WHO), "World Helth statics," 2014.

[33] D. Schnitzer, D. S. Lounsbury, J. P. Carvallo, R. Deshmukh, J. Apt and D. M. Kammen, ", Microgrids for rural electrification, United Nations Foundation, February 2014," United Nations Foundation, February 2014.

[34] D. Gandini, *Design and Simulation of an Energy Storage System for Residential Application,* Torino, 2013.

[35] W. Tang, F. C. Lee and R. B. Ridley, "Small-Signal Modeling of Average Current-Mode Control," *Transaction on Power Electronics,* vol. 8, no. 2, pp. 112-119, 1993.

[36] P. Mattavelli, "Digital Control of dc-dc Boost Converters with Inductor Current Estimation," *Applied Power Electronics Conference and Exposition, 2004. APEC '04. Nineteenth Annual IEEE,* vol. 1, pp. 74-80, 2004.

[37] D. Wu, G. Calderon-Lopez and A. J. Forsyth, "Discontinuous conduction/current mode analysis of dual interleaved buck and boost converters with interphase transformer," *IET Power Electronics,* vol. 9, no. 1, pp. 31-41, 2016.

[38] G. Escobar, S. Pettersson, C. Ho, M. Karppanen and T. Pulli, "PV current sensorless MPPT for single-phase PV inverter," in *37th Annual Conference on IEEE Industrial Electronics Society*, Melbourne, 2011.

[39] B. Subudhi and R. Pradhan, "A Comparative Study on Maximum Power Point Tracking Techniques for Photovoltaic Power Systems," *IEEE Transactions on Sustainable Energy,* vol. 4, no. 1, pp. 89-98, 2013.

[40] M. Ciobotaru, R. Teodorescu and F. Blaabjerg, "Control of single-stage single-phase PV inverter," in *Power Electronics and Applications*, Dresden, 2005.

[41] S. W. G. L. a. G. T. Z. Qi, "Integrated Control of Energy Management for Stand-Alone PV System," in *Power and Energy Engineering Conference*, Wuhan, 2009.

[42] M. D. a. V. Agarwal, "A novel control strategy for stand-alone solar PV systems with enhanced battery life," in *Applied Power Electronics Conference and Exposition (APEC)*, Fort Worth, 2014 .

[43] R. L. Hwang, M. J. Cheng, T. P. Lin and M. C. Ho, "Thermal perceptions, general adaptation methods and occupant's idea about the trade-off

between thermal confort and enegy saving in hot-humid regions," *Build and Environment,* 2009.

[44] S. de la Rue du Can, V. E. Letschert, M. A. McNeil, N. Zhou and J. A. Sathaye, "Residential and Transport Energy Use in India: Past Trend and Future Outlook," Berkeley CA: Lawrence Berkeley National Laboratory, 2009.

[45] N. Shah, N. Sathaye, A. Phadke and V. Letschert, "Cost and benefits of efficiency improvement in ceiling fans," in *EEDAL*, 2013.

[46] L. Desroches and K. Garbesi, "Max Tech and Beyond: Maximizing appliance and equipment efficiency by design," LBNL, 2011.

[47] T. Sanchez, The Hidden Energy Crisis: How policies are failing the world's poor, London: Practical Action Publishing, 2010.

[48] ESMAP, "Beyond connections - Energy Access redefined," The world bank group, Washington DC, 2015.

[49] Global LEAP, "Off-Grid appliance market survey," 2015.

[50] A. de Almeida, P. Fonseca, N. Feiberg and B. Schlomann, "Characterization of the household electricity consumption in the EU, potential energy savings and specific policy recommendations," *Energy and Building,* vol. 43, no. 8, pp. pages 1884-1894, August 2011.

[51] A. Phadke, A. Jacobson, W. Y. Park, G. R. Lee, P. Alstone and A. Khare, "Powering a home with just 25 Watts of solar PV," Berkeley Lab, April 2015.

[52] B. Decourt and R. Debarre, "Electricity storage," SBC Energy Insiture, Paris, 2013.

[53] IEA, "Thermal Energy Storage Today," in *IEA Energy Storage Technology Roadmap Stakeholder Engagement Workshop*, Paris, 2014.